A mass-conservative method for the integration of the two-dimensional groundwater (Boussinesq) equation

E. Cordano, and R. Rigon

E. Cordano, Dynamics in the Agro-ecosystems technological platform Sustainable Agro-Ecosystems anb Bioresources Department , CRI Research and Innovation Centre - Fondazione Edmund Mach,Via E. Mach 1,San Michele all'Adige (Trento), 38010, Italy (emanuele.cordano@gmail.com)

R. Rigon, Dipartimento di Ingegneria Civile e Ambientale/ CUDAM, Università di Trento, Via Mesiano, 77, 38123, Trento (riccardo.rigon@ing.unitn.it)

Abstract.

This work presents a new conservative finite-volume numerical solution for the two-dimensional groundwater flow (Boussinesq) equation, which can be used for investigations of hillslope subsurface flow processes and simulations of catchment hydrology. The Boussinesq Equation, which is integrated for each grid element , can take account of the local variations of topography and soil properties within the individual elements. The numerical method allows for wetting and drying of the water-table, without "ad hoc assumptions". The stability and convergence of the method is shown to be guaranteed *a priori* by the properties of the solver itself, even with respect to the boundary conditions, an aspect which has been neglected in previous literature. The numeric solutions are validated against some approximate analytical solutions, and compared to those of another (1D) numerical solver of the Boussinesq equation. The solver capabilities are further explored with simulations of the Panola experimental hillslope where the bedrock topography, which is accurately known, causes complex wetting and drying patterns; in this situation the importance of a two-dimensional description of subsurface flows to obtain properly simulated discharges becomes clear. Finally, a comparison is made between the results of the presented algorithm and the output of the GEOtop hydrological distributed model, which simulates variably saturated soils; the findings of the comparison are discussed.

1. Introduction

Subsurface water flows play a fundamental role in determining the partition between surface and subsurface water flows. In the past, parametrizations of groundwater flows in hillslope and catchment hydrology were often developed on the basis of conceptualized approaches [*Beven and Kirkby*, 1979; *Barling et al.*, 1994; *Troch et al.*, 2003, 2004; *Akylas and Koussis*, 2007; *Harman and Sivapalan*, 2009, and references therein] which were mainly aimed at the identification of runoff source areas and the estimation of discharge at the hillslope toe. In these studies, steady state approaches were often used, but they have proven to be insufficient for many purposes, especially revealing the real patterns of soil moisture distribution [*Western and Grayson*, 1998]. Therefore, in subsequent researches these have been modified to introduce more dynamic conditions [e.g. *Barling et al.*, 1994; *Chirico et al.*, 2003] and/or effects due to the downslope topography [e.g. *Hjerdt et al.* 2004; *Lanni et al.* 2011]. Eventually, these latter studies also proved to be of interest in determining hillslope stability [e.g. *Dietrich and Montgomery*, 1994; *Iverson*, 2000; *D'Odorico et al.*, 2005] by coupling the simplified hydrology with geomechanics.

In the more traditional contexts of groundwater analysis, analytical solutions for unconfined groundwater flow have been produced for suitably simplified conditions and simple geometries, [*Hantush*, 1967; *Barenblatt et al.*, 1990; *Fan and Bras*, 1998; *Lockington et al.*, 2000; *Parlange et al.*, 2000; *Kim and Ann*, 2001; *Rai et al.*, 2006; *Song et al.*, 2007; *Telyakovskiy et al.*, 2010]. These studies have been a valuable reference in understanding the processes dynamics, however, they have been less useful in exploiting the information generated by the growing knowledge of catchment topography.

Very rarely do hillslope hydrologists use complete three-dimensional numerical models [e.g. as those in *Harbaugh et al.*, 2000a; *Panday and Huyakorn*, 2004], developed in mainstream groundwater studies, and they have always have looked for the greatest algorithmic simplicity. In hillslope literature, the search for conceptualized or analytical methods has been justified by the avoiding the computational burden of solving the complete three-dimensional form of the groundwater equations, which seemed too great, but also by the perception that hillslopes water table dynamics has different characteristics than in aquifers, and, therefore, requires a special care.In facts, soils can more frequently dry than large scale aquifers, and the presence of rugged bedrocks and shallow perched water tables, can bring to disconnected patterns of soil moisture *Tromp-van Meerveld and McDonnell* [2006]. This is called wetting-and-drying phenomenon and has been studied thoroughly in surface water literature [*Stelling and Duynmeyer*, 2003]. However, it has been less investigated in groundwater literature, and, for instance MODFLOW [*Harbaugh et al.*, 2000b] has been shown to fail to in modelling it [*Doherty*, 2001; *Werner et al.*, 2006; *Sokrut et al.*, 2007; *Painter et al.*, 2008].

Overall, considering the various approaches, it can be verified that there is a gap in literature: there are many three-dimensional solvers for the scopes of groundwater analysis, which possibly unsuitable to model hillslope problems; there are contributions that investigate the one-dimensional version of the groundwater equation, in which the lateral width of a hillslope is appropriately parametrized [e.g *Troch et al.*, 2003, 2004 and references therein]. But much fewer, and much more recent, are the two-dimensional solvers [*Rocha et al.*, 2007; *Harman and Sivapalan*, 2009; *Cayar and Kavvas*, 2009; *Dehotin et al.*, 2011].

This paper tries to support the statement that a two-dimensional simplification of groundwater flow, based on a new numerical method, can answer the needs of spatial information for hillslope hydrology (in relation to hillslope-toe discharge and soil saturation patterns - therefore contributing also to some hillslope stability problems) and of for modern catchment hydrology.

To obtain this result, the paper implements a new and clean numerical method which merges the achievements of *Brugnano and Casulli* [2008] and *Casulli* [2009], and, in particular, extends the latter (which deals with free surface waters) to the case of Darcian flow.

The paper is organized as follows: in Section 2 the form of the Boussinesq equation and its terms are discussed; in Section 3 the equation is discretized according to the new conservative scheme; in Section 4 the effect of boundary conditions on the structure of the solver is presented; in Section 5 the model is validated against appropriate analytical and numerical solutions and the model is applied to the Panola experimental site to confirm its behavior at the presence of rugged terrain.

2. The Boussinesq's groundwater equation

The governing equation for groundwater flow used in this paper has been derived from the hydraulic theory of unconfined, saturated, groundwater flow in a sloping aquifer. It is based on Darcy's Law and the continuity equation (soil water and groundwater budget). It was first introduced by *Boussinesq* [1877] and it will be referred throughout the paper as BEq. It has been applied by many authors in studies of free aquifers and pumping [e.g. *Manglik and Rai*, 2000; *Don et al.*, 2005; *Rai et al.*, 2006], and in the study of recession curves of a hillslope draining into a surface water body [e.g. *Childs*, 1971; *Brutsaert*, 1994;

Troch et al., 2003 and others]. The integration of the BEq is finally gaining increased interest in relation to coupled surface/subsurface models [e.g. *Pruess et al.*, 1999; *Panday and Huyakorn*, 2004; *Kollet and Maxwell*, 2006; *Rigon et al.*, 2006].

Recently, *Hilberts et al.* [2005, 2007] generalized the BEq, including unsaturated groundwater flow, using the concept of *drainable porosity*, which can be applied to studies of hillslope hydrology, runoff production and landsliding; *Cordano and Rigon* [2008] were able to derive it from simplifications of comprehensive three-dimensional Richards Equation.

The BEq applied to a generic hillslope has the following two-dimensional form:

$$\frac{\partial h_w(\eta, x, y)}{\partial t} = \nabla \cdot \left[K_S(x, y, z)\, h(\eta, x, y)\, \vec{\nabla}\eta \right] + Q(x, y) \tag{1}$$

where η [L] is the unknown piezometric head (water-table elevation); x, y are planimetric Cartesian coordinates; t is time; $h_w(x, y, \eta)$ is the total water volume stored in a soil column per planimetric unit area; $h(\eta, x, y)$ is the thickness of the aquifer, which is a function of η and space since it is defined as $h := \max(0, \eta - z_b(x, y))$ where $z_b(x, y)$ is the bedrock elevation; $\nabla\cdot$ [L^{-1}] is the divergence operator; $\vec{\nabla}$ [L^{-1}] is the gradient operator; Q [$\mathrm{L\ T}^{-1}$] is a source term, which also accounts for boundary conditions (as explained in the next sections); and K_S [$\mathrm{L\ T}^{-1}$] is the saturated hydraulic conductivity. Multiplying $h_w(x, y, \eta)$ [L] by the domain area gives the total volume of water stored. As shown in *Cordano and Rigon* [2008], $h_w(x, y, \eta)$ can be calculated as the integral of volumetric water content over the vertical depth, assuming a vertical hydrostatic distribution of soil water pressure:

$$h_w(\eta, x, y) = \int_{-\infty}^{z_s} \theta_w(x, y, z, \eta - z) dz \tag{2}$$

where the z axis is positive upward, z_s is the elevation of the terrain surface, and $\theta_w(x, y, z, \psi)$ is the volumetric soil water content, variable in space. Then, the drainable porosity [dimensionless] is calculated by deriving $h_w(\eta, x, y)$ with respect to η:

$$s(x, y) = \frac{\partial h_w(\eta, x, y)}{\partial \eta} \tag{3}$$

Remarkably, while $h_w(\eta, x, y)$ and $h(\eta, x, y)$ are always positive quantities, $\eta(x, y)$ can be lower than bedrock elevation and even assume negative values, when a water table does not exist over the bedrock. This fact is crucial in modelling the wetting-and-drying phenomenon, and, when not recognized, implies the introduction of tricks to adjust the numerical solution [for instance fixing a minimum low water level, as in *Painter et al.*, 2008].

Equation (1) is written in *conservative* form, i.e. the time derivative is with respect to the volume of total stored water per unit area, which is the conserved quantity, and the second addendum of the equation contains the divergence of mass fluxes. By applying definition (3) and the derivation chain rule to the left-hand side of (1), BEq can be rewritten in the form usually found in papers and manuals [e.g. *Bear*, 1972; *Harbaugh et al.*, 2000a; *Painter et al.*, 2008]:

$$s(x, y) \frac{\partial \eta}{\partial t} = \nabla \cdot \left[K_S(x, y, z)\, h(\eta, x, y)\, \vec{\nabla} \eta \right] + Q(x, y) \tag{4}$$

However, writing of the equation in either form (4) or (1) is not the same thing in terms of numerical resolution [*Celia et al.*, 1990]. In fact, at the edge of the wet zones the water level $\eta(x, y)$ is not a smooth function and the two equations are, therefore, not equivalent [e.g. *Leveque*, 2002]. In practice, in order to conserve mass in presence of wetting and drying other authors usually introduce "ad hoc" iteration procedures for control (called outer iteration procedure, a "type of damping or under-relaxation", in *Painter et al.*, 2008) which are unnecessary.

Actually, other Authors [*Dehotin et al.*, 2011, and literature cited therein], even use a different "Boussinesq" equation, where the coefficient within square brackets, i.e. $K_S(x, y, z)\, h(\eta, x, y)$, the water-table transmissivity, is set not dependent on z, i.e. on the water table level η, and no mention of the concept of "drainable porosity" or "specific yield" is made.The latter case, even if it seems to reproduce standard groundwater case studies in a fairly reasonable manner, cannot account properly for wetting and drying because of non vanishing transmissivity in dry cells. To solve a generic *free-surface hydrodynamic problem*, i.e. the Shallow Water Equation (SWEq) or the BEq, *Brugnano and Casulli* [2008] found a rigorous numerical method. Such a method is conservative, can simulate wetting or drying fronts, and is the one used in the following sections. This paper, in fact, also extends *Casulli* [2009]'s method to the case of using equation (1), in order to account for sub-grid heterogeneity of topography and hydraulic conductivity.

3. Application of a mass-conservative scheme to the Boussinesq Equation

In this section we show that equation (1) can be cast as a system of the form:

$$\vec{V}\left(\vec{\zeta}\right) + \mathbf{T}\cdot\vec{\zeta} = \vec{b} \tag{5}$$

where $\vec{\zeta} = \left[\zeta_1, \ldots, \zeta_i, \ldots, \zeta_{N_p}\right]^T$ is the array of the unknown quantities (one for each of the N_p grid cells), $\vec{b} = \left[b_1, \ldots, b_i, \ldots, b_{N_p}\right]^T$ is the array of known parameters, and $\vec{V}\left(\vec{\zeta}\right) = \left[V_1(\zeta_1), \ldots, V_i(\zeta_i), \ldots, V_{N_p}(\zeta_{N_p})\right]^T$ are the values of the field conserved quantity, i.e. the water volume stored in the i-th cell, a non-linear function of η. All these "vectors" are denoted by the symbol $\vec{\cdot}$, or *harpoon*, to distinguish them from space vectors, denoted by $\vec{\cdot}$. In this section we also show that the discretisations adopted endow the matrix $\mathbf{T}$ the properties, further specified in Appendix A, that make the system numerically solvable with the use of a Newton method [e.g. *Kelley*, 2003] and the conjugate gradient algorithm [e.g. *Schewchuk*, 1994] having convergence to solutions guaranteed a priori [*Brugnano and Casulli*, 2008].

The discretization of (1) requires three steps:

- definition of the grid;
- integration of (1) over the i-th cell (in space);
- choosing a time marching technique (discretization in time).

3.1. Properties of the grid

The integration domain of (1) needs to be divided into N_p convex, non-overlapping polygons (grid elements), delimited by a total number of N_l sides (or edges), joining in N_v vertices (such that $N_p + N_v = N_l + 1$). In the example in Figure 1, there are four polygons, twelve sides, and nine vertices.

In order to simplify the estimation of fluxes between cells, the polygons are organized in

an *orthogonal grid* [*Casulli and Walters*, 2000]. Such a grid is drawn so that the segment joining the centers of two adjacent polygons and the edge common to them both have a non-empty intersection and are orthogonal to each other.

The topological connection of these geometric elements can be described through the use of an *adjacency matrix* of dimensions $N_p \times N_l$, composed by as many rows as there are polygons in the grid and as many columns as there are sides [e.g. *Cormen et al.*, 2001, Section 22.1: Representations of graphs, pp. 527−531], such that:

$$\mathcal{A}_{ij} = \begin{cases} 1 & \text{if the } j-\text{th edge is part of the } i-\text{th polygon} \\ 0 & \text{elsewhere} \end{cases} \tag{6}$$

$\mathcal{A}_{ij}$ is a sparse matrix and it is usually implemented as a data structure in the form of an *adjacency list* that can be represented in a very compact way, only occupying the necessary contiguous space in computer memory [e.g. *Davis*, 2006 and references therein]. The sum of each row of the adjacency matrix gives the number of sides of each polygon. The sum of each column gives at most two, since an edge is shared by two polygons at most. The edges of the i-th polygon can then be grouped into the following subset:

$$\mathcal{F}_i = \{j \,\text{such that}\, \mathcal{A}_{ij} = 1\} \tag{7}$$

In practice, all the edges and all the polygons are progressively numbered and ordered into two arrays with N_l and N_p elements respectively. Each polygon has, as an attribute, a vector containing the indexes of its edges, i.e. the elements of $\mathcal{F}_i$.

It is also necessary to assess the correspondences between two adjacent polygons and their shared edge, i.e. given the polygon i and the edge $j \in \mathcal{F}_i$, what is the index r so that

$\mathcal{A}_{rj} = 1$ when $\mathcal{A}_{ij} = 1$. Since $\mathcal{A}$ has at most two non-zero entries per column, the polygon r, if it exists, is unique. Thus, a function between (i, j) and r, such that $r = \rho(i, j)$ can be found by inspecting the following $N_p \times N_l$ matrix:

$$\varrho_{ij} = \begin{cases} r & \text{if } \mathcal{A}_{ij} = 1 \text{ and } \mathcal{A}_{rj} = 1 \\ 0 & \text{otherwise} \end{cases} \tag{8}$$

Since ϱ_{ij} is a sparse matrix with few non-zero entries, only the non-null elements of ϱ are saved in the actual implementations. Each polygon contains, as an attribute, an array with the values of $r = \varrho_{ij}$ related to each $j \in \mathcal{F}_i$. If $\mathcal{A}_{ij} = 1$ and $\varrho_{ij} = 0$, the j-th edge belongs to the boundary. For the next computations it is useful for each i-th polygon to define the subset $\hat{\mathcal{F}}_i \subset \mathcal{F}_i$ as the subset of the edges which are not part of the boundary:

$$\hat{\mathcal{F}}_i = \{j \text{ if } \mathcal{A}_{ij} = 1 \text{ and } \varrho_{ij} \neq 0\} \tag{9}$$

The subset $\hat{\mathcal{F}}_i$ will be used later for the discretization of the divergence term in (1).

3.2. Spatial Discretization

Integrating (1) over the i-th polygon, one obtains:

$$\int_{p_i} \frac{\partial h_w(\eta, x, y)}{\partial t}\, dx\, dy = \int_{p_i} \nabla \cdot \left[K_S(x, y, h)\, h(\eta, x, y)\, \vec{\nabla}\eta\right] dx\, dy + \int_{p_i} Q(x, y) dx\, dy \tag{10}$$

where p_i is the planimetric area of the cell. Therefore, observing that the volume of stored water in the i-th cell is:

$$V_i(\eta_i) = \int_{p_i} h_w(\eta_i, x, y)\; dx\, dy \tag{11}$$

given that h_w is the water volume per unit area between the bedrock and the free surface level (η) as defined by (2), and then applying the divergence theorem, the following integrated form of the BEq is obtained:

$$\frac{\partial V_i}{\partial t} = \sum_{j \in \hat{\mathcal{F}}_i} \int_{\lambda_j} K_S(x,y,h)\, h(\eta(x,y)) \left(\vec{\nabla}\eta \cdot \vec{n}_j\right)\, d\lambda_j + \int_{p_i} Q(x,y)\, dx\, dy \tag{12}$$

where λ_j is the length of j-th edge, $d\lambda_j$ is the differential along the j-th edge, $\vec{n}_j$ is the outcoming versor orthogonal to the j-th edge, and $\vec{\nabla}\eta \cdot \vec{n}_j$ is the derivative (gradient) of η, estimated at the j-th edge and orthogonal to it. Remarkably, it can be noticed from (11) that the total stored volume is dependent on the spatial variability of h_w within the cell and, therefore, on the sub-grid variability of the drainable porosity, the bedrock and surface elevation. Due to the orthogonality of the grid, the spatial gradient component can be approximated with the finite difference:

$$\vec{\nabla}\eta \cdot \vec{n}_j \approx \frac{\eta_{\varrho(i,j)} - \eta_i}{\delta_j} \tag{13}$$

where δ_j [L] is the distance between the centers of the i-th and $\varrho(i,j)$-th polygons. Thus (12) is transformed into:

$$\frac{\partial V_i(\eta_i)}{\partial t} = \sum_{j \in \hat{\mathcal{F}}_i} \hat{\mathcal{T}}_j(\eta_i, \eta_{\varrho(i,j)}) \cdot \frac{\eta_{\varrho(i,j)} - \eta_i}{\delta j} + \int_{p_i} Q(x,y)\, dxdy \tag{14}$$

where $\hat{\mathcal{T}}_j(\eta_i, \eta_{\varrho(i,j)})$ is a transport coefficient [L ^{3}T^{-1}] along the j-th edge estimated with an upstream weighting scheme as follows [e.g. *Painter et al.*, 2008]:

$$\hat{\mathcal{T}}_j(\eta_i, \eta_{\varrho(i,j)}) := \max\left\{\int_{\lambda_j} \left[K_S(x,y)\, h(\eta_i, x, y)\right] d\lambda_j, \int_{\lambda_j} \left[K_S(x,y,h)\, h(\eta_{\varrho(i,j)}, x, y)\right] d\lambda_j\right\} \tag{15}$$

The main advantage of this upstream weighting estimator, $\hat{\mathcal{T}}_j$, is that it prevents water from leaving a nearly dry cell and allows water to flow to initially dry cells during a flooding [e.g. *Painter et al.*, 2008]. However, it can also be easily modified on the basis of knowledge of the local variability of hydraulic transmissivity (the integrand) in the volumes under consideration. It is remarkable that $\hat{\mathcal{T}}_j$ is a property of the j-th edge and is symmetric with respect to the level of η in adjacent cells, i.e. $\hat{\mathcal{T}}_j(\eta_i, \eta_{\varrho(i,j)}) = \hat{\mathcal{T}}_j(\eta_{\varrho(i,j)}, \eta_i)$. If the variations of hydraulic conductivity and porosity in space are known, for instance with a stochastic theory of the medium [e.g. *Dagan*, 1989], the above integral can be estimated when the cells are big enough to ensure ergodicity with a Monte-Carlo method.

3.2.1. Time Discretization

Each term in Equation (14) depends on time (which has been left implicit so far), and it can be discretized in a semi-implicit way as follows:

$$V_i(\eta_i^{n+1}) = V_i(\eta_i^n) + \Delta t \sum_{j \in \hat{\mathcal{F}}_i} \hat{\mathcal{T}}_j^n \frac{\eta_{\varrho(i,j)}^{n+1} - \eta_i^{n+1}}{\delta j} + \Delta t \, p_i \, \hat{Q}_i^n \tag{16}$$

where Δt is the time step and all the superscripts indicate the time instant. The transport coefficient $\hat{\mathcal{T}}_j$ is estimated at time n (and is therefore known), as is Q_i^n [$\mathrm{L}^2\mathrm{T}^{-1}$], the water-table recharge (or a sink) averaged over the whole i-th polygon. The gradient is treated implicitly and the solution of (16) must be sought by solving an algebraic non-linear system:

$$V_i(\eta_i^{n+1}) - \Delta t \sum_{j \in \hat{\mathcal{F}}_i} \hat{\mathcal{T}}_j^n \frac{\eta_{\varrho(i,j)}^{n+1} - \eta_i}{\delta j}^{n+1} = V_i(\eta_i^n) + \Delta t \, p_i \, \hat{Q}_i^n \tag{17}$$

for $i = 1$ to N_p. The system in (17) is a particular case of (5) where ζ_i is replaced with η_i^{n+1} and the following equalities are taken:

$$\left[\mathbf{T}\cdot \overrightarrow{\eta^{n+1}}\right]_i = -\Delta t \sum_{j\in\hat{\mathcal{F}}_i} \hat{\mathcal{T}}_j^n \frac{\eta_{\varrho(i,j)}^{n+1} - \eta_i}{\delta j}^{n+1} \tag{18}$$

and

$$b_i = V_i(\eta_i^n) + \Delta t\, p_i\, \hat{Q}_i^n \tag{19}$$

From (18), $\mathbf{T}$ results to be a symmetric and positive semidefinite matrix, which satisfies the **T2** property, defined in the Appendix, with diagonal entries:

$$T_{ii} = \Delta t \sum_{j\in\hat{\mathcal{F}}_i} \frac{\hat{\mathcal{T}}_j^n}{\delta j} \tag{20}$$

and off-diagonal entries:

$$T_{ir} = -\Delta t\, \frac{\hat{\mathcal{T}}_j^n}{\delta j}\, \delta_{r,\rho(i,j)} \qquad i \neq r \tag{21}$$

where $\delta_{r,\rho(i,j)}$ is the Kronecker delta symbol. It can be shown that, in each row of $\mathbf{T}$, the sum of the entries is zero:

$$\sum_{r=1}^{N_p} T_{ir} = 0 \tag{22}$$

Finally, Equation (17) is rewritten with the index notation as follows:

$$V_i(\eta_i^{n+1}) + \sum_{j=1}^{N_p} T_{ij}\eta_j^{n+1} = b_i \tag{23}$$

From (18) it follows that the unit vector, $[1..1]^T$, is the eigenvector of $\mathbf{T}$ associated to the null eigenvalue. This happens when the hydraulic head is uniformly distributed and, according to Darcy's law, there is no flux.

The stability and convergence to the exact solution is verified according to the conditions (A9) or (A10) (see Appendix A).

However, it can happen that $\mathbf{T}$ is reducible (and then $T_{ii} = 0$ for a certain value of i and $T_{il} = 0$ for certain adjacent cells i and l). In this case, no water flux occurs through the sides of some cells and there is a disconnected "wet" domain. Consequently, the matrix $\mathbf{T}$ has as many eigenvectors $\overline{v}$ corresponding to the zero eigenvalue as there are wet domains, i.e. groups of connected cells. The condition for each group of connected cells (to be compared with (A9)) becomes:

$$\sum_{i\in\Omega_d} V_i(\eta_i^n) + \Delta t \sum_{i\in\Omega_d} p_i \hat{Q}_i^n > 0 \qquad 1 \le d \le N_{sd} \tag{24}$$

where d is the index of the group of connected cells Ω_d.

4. Boundary Conditions

Equation (17), which represents the water balance of a generic cell, is solved by coupling with boundary conditions which can be either flux boundary conditions (Neumann type) or head boundary conditions (Dirichlet type). In the following we analyze how each choice of boundary condition modifies the integration properties of the system and, in particular, requires the modification of (17).

4.1. Flux-Based Boundary Condition (Neumann)

Neumann boundary conditions assess a positive or negative water flux along a certain part of the boundary. It consists in the introduction of a further source/sink term for the cells that are adjacent to the boundary of the integration domain, and can be accounted for with the following reformulation of the known term b_i :

$$b_i = V_i(\eta_i^n) + \Delta t\, p_i\, \hat{Q}_i^n - \Delta t \sum_{j \in \mathcal{F}_i/\hat{\mathcal{F}}_i} \int_{\lambda_j} q_L(\eta_i^n, x, y)\, h(\eta_i^n, x, y)\; d\lambda_j \tag{25}$$

where $\mathcal{F}_i/\hat{\mathcal{F}}_i$ is the subset of the edges of the i-th polygon belonging to the boundary and $q_L(\eta_i^n, x, y)$ is the outgoing water flux (water discharge per unit vertical area) [L T^{-1}] normal to the boundary. The new source/sink term affects the numerical stability of the method, therefore, (24) needs to be modified to account for the outgoing water flux as follows:

$$\sum_{i \in \Omega_d} V_i(\eta_i^n) + \Delta t \sum_{i \in \Omega_d} p_i\, \hat{Q}_i^n - \Delta t \sum_{i \in \Omega_d} \sum_{j \in \mathcal{F}_i/\hat{\mathcal{F}}_i} \int_{\lambda_j} q_L(\eta_i^n, x, y)\, h(\eta_i^n, x, y) d\lambda_j > 0 \qquad 1 \le d \le N_{sd} \tag{26}$$

4.2. Head-Based Boundary Conditions (Dirichlet)

Dirichlet boundary conditions assign the time-variable value for η at some boundary or internal cells according to a known function. Therefore, for any i cell belonging to the boundary:

$$\eta_i^{n+1} = \hat{\eta}_i(t^{n+1}) \tag{27}$$

where $\hat{\eta}_i(t)$ is an external forcing known *a priori*. Such i cells are called "Dirichlet Cells" (DC) in this paper. In this case, the nonlinear system to be solved is formed by (27) for the "Dirichlet cells" and by (23) for the other cells. Therefore, such a system has a nonlinear part similar to (5), i.e. one resulting in a monotonic function of η but also having a linear part which is not symmetric. In fact, for a cell adjacent to a Dirichlet cell, the left-hand side of (23) depends on values from the DC. On the contrary, (27) does not contain any unknown values from neighboring cells. Because this asymmetry makes the new algebraic equation system different from (5), the procedure described in Appendix A to solve it may not work correctly.

It is possible to avoid this problem by splitting the matrix $\mathbf{T}$, defined by (18), into two components:

$$\mathbf{T} = \mathbf{T^{ND}} + \mathbf{T^{D}} \tag{28}$$

where $\mathbf{T^{ND}}$ and $\mathbf{T^{D}}$ are both symmetric matrices constructed as follows:

$$T_{ij}^{ND} = \begin{cases} T_{ij} & \text{if neither } i-\text{th nor } j-\text{th cells are DC} \\ 0 & \text{elsewhere} \end{cases} \tag{29}$$

and

$$T_{ij}^{D} = \begin{cases} T_{ij} & \text{if either } i-\text{th or } j-\text{th cells are DC} \\ 0 & \text{elsewhere} \end{cases} \tag{30}$$

The matrix $\mathbf{T^{ND}}$ contains information about the connection between cells not belonging to the boundary, whereas $\mathbf{T^{D}}$ assumes non-zero values only in correspondence of Dirichlet cells. Then, (23) becomes:

$$V_i(\eta_i^{n+1}) + \sum_{i=1}^{N_p} T_{ij}^{ND} \eta_j^{n+1} + \sum_{i=1}^{N_p} T_{ij}^{D} \eta_j^{n+1} = b_i \tag{31}$$

Equation (31) is applied to non-Dirichlet cell i; however T_{ij}^D can assume non-null values only if j refers to a Dirichlet cell, therefore (31) can be re-arranged, using (27), as:

$$V_i(\eta_i^{n+1}) + \sum_{i=1}^{N_p} T_{ij}^{ND} \eta_j^{n+1} = b_i - \sum_{i=1}^{N_p} T_{ij}^{D} \hat{\eta}_j(t^{n+1}) \tag{32}$$

where $\hat{\eta}_j^{n+1}$, related to DC domain, moves to the right-hand side because it is known. The final solver of the Boussinesq Equation is represented by the system (32) for all the non-Dirichlet cells. The matrix $\mathbf{T^{ND}}$ satisfies the appropriate **T1** or **T2** properties defined in Appendix A and then (32) is solved with the procedure described in Appendix A.

5. Test cases

Analytical solutions of the general non-linear Boussineq Equation do not exist. Existing solutions are either approximated, usually obtained through a linearization of the flux term [e.g. *Brutsaert*, 1994; *Troch et al.*, 2004], which corresponds to assuming a suitably constant value of the hydraulic transmissivity $K_S\, h$, or they are related to particular cases. For instance, in the case of one-dimensional wetting processes, a non-linear analytic solution exists based on similarity analysis [*Barenblatt et al.*, 1990; *Lockington et al.*, 2000] and power series expansion [*Song et al.*, 2007]. An implementation of these analytical solutions is available as an R package [*Cordano*, 2011]. There are also two-dimensional analytical solutions for the linearized Boussinesq Equation, obtained according to *Hantush*'s approximation, which considers water table dynamics in a two-dimensional rectangular domain

with horizontal bedrock and pumping and/or bottom leakage processes [*Manglik and Rai*, 2000; *Rai et al.*, 2006].

However, in order to assess the performance of our solver, we have chosen: (i) a one-dimensional time variable analytical solution of the linearized equation on planar horizontal topography with a sudden increase of water head at the boundary together with the exact steady-state solution relative to the same problem [e.g. *Bear*, 1972, exercise 7.27] ; (ii) a one-dimensional solution on planar topography developed by *Song et al.* [2007] that derives from a similarity assumption and that refers to the fully non-linear wetting process; (iii) the one-dimensional width-averaged numerical solution proposed by *Troch et al.* [2004] known as the "Hillslope storage Boussinesq" model (HsB) [*Troch et al.*, 2003], applied to a simple planar hillslope (the HsB itself was, in turn, tested against solutions provided by Richards equations [*Paniconi et al.*, 2003]). Then, an application of the general non-linear Boussineq Equation to the Panola hilllslope [*Lanni et al.*, 2011; *Hopp and McDonnell*, 2009; *Tromp-van Meerveld and McDonnell*, 2006] in which wetting and drying patterns over an irregular topography bedrock are perfomed and compared with the hydrological response of a planar hillslope. A further comparison between the results of the Boussinesq Equation with those of a 3D variably saturated water flow model, e.g. the GEOtop hydrological distributed model [*Rigon et al.*, 2006], is finally discussed.

5.1. Comparison with an Analytical Linearized Solution with planar topography

In this example, a horizontal one-dimensional aquifer is analyzed with two head (Dirichlet) boundary conditions applied to the two borders in contact with two reservoirs (Fig. 1). At one border the pressure is assumed to increase suddenly to a constant value η_1,

generating a wave which moves to the opposite border where the water surface remains at height $\eta_2 < \eta_1$. If the physical parameters allow the linearization of Equation (4), the solution can be found analytically by following the examples illustrated in *Rozier-Cannon* [1984]. The mathematical problem is then reduced to solving:

$$\frac{\partial}{\partial x}\left[K_S\, h \frac{\partial \eta}{\partial x}\right] = s\frac{\partial \eta}{\partial t} \tag{33}$$

with the following boundary conditions:

$$\eta = \eta_1 \text{ at } \quad x = 0 \tag{34}$$

$$\eta = \eta_2 \text{ at } \quad x = L \tag{35}$$

and the initial condition:

$$\eta(x) = \eta_2 \tag{36}$$

As anticipated, assuming K_S and s to be spatially uniform (i. e. constant), the analytical solution can either be (a) exact at steady state, obtaining an asymptotic solution, or (b) approximate using a linearization during the trasient regime as shown in Figure 3.

The asymptotic solution is easily found. In fact, the asymptotic equation, for $t \to \infty$, is:

$$\frac{K_S}{2}\frac{\partial^2 \eta^2}{\partial x^2} = 0 \tag{37}$$

which can be easily integrated, resulting in:

$$\eta = (\beta_1 x + \beta_0)^{0.5} \tag{38}$$

where β_1 and β_0 are coefficients determined by satisfying the boundary conditions, resulting in:

$$\beta_0 = \eta_1^2 \tag{39}$$

$$\beta_1 = \frac{\eta_2^2 - \eta_1^2}{L} \tag{40}$$

During the transient time, Equation (33) can be linearized as follows:

$$\frac{\partial}{\partial x}\left[K_S \eta_M \frac{\partial \eta}{\partial x}\right] = s\frac{\partial \eta}{\partial t} \tag{41}$$

where η_M is a constant value of the height of the water surface, which must be contained between η_2 and η_1 and is therefore estimated with a weighted average:

$$\eta_M = p\,\eta_1 + (1-p)\,\eta_2 \qquad 0 \leq p \leq 1 \tag{42}$$

where p is normally estimated empirically. Equation (41) is formally equivalent to the one-dimensional *heat* equation [*Rozier-Cannon*, 1984] and is analytically solved using a Fourier series expansion. The detailed mathematical derivation and the explicit form of the solution are reported in Appendix B.

The comparison of the above solutions with BEq is shown, at different times and for different values of the hydraulic conductivity, in Figure 3. In these experiments, we set the boundary conditions η_1=2 m, η_2=1 m; the length of the domain, L= 1000 m; and the cell

size of side 1 m. The porosity was set to $s = 0.4$, whereas four different values of saturated hydraulic conductivity were tested: $K_S = 10^{-4}$ m/s; $K_S = 10^{-3}$ m/s; $K_S = 10^{-2}$ m/s; and $K_S = 10^{-1}$ m/s. This last value has little real physical relevance but it was used to allow the system to reach asymptotic conditions in a reasonable time. The numerical time step used was 3600 s (one hour). The water surface profiles are illustrated at 1,5,10 and 20 days. Figure 3 also shows the analytic solution (of the linearized equation) obtained with different estimates of p (p=0, p=0.5 and p=1). The steady state solution (38) is always the furthest right in the panels of Fig. 3. For the lowest hydraulic conductivities stationarity is not reached and the right boundary condition (at $x = L$) has no effect on the solution. As expected, the numerical solution provided by the BEq is located between the analytical solutions of the linearized equation for $p = 0$ and $p = 1$. In fact, if $p = 0$, the hydraulic transmissivity is underestimated being evaluated according to η_2, and corresponding to the transmissivity value of the undisturbed zone of the water table profile. The water table level obtained by our BEq solver converges to the one obtained with the linearized solution for $p = 0$ and then tends to η_2 when $x \to L$, as expected.

On the other hand, for $p = 1$ the numerical solution fits well with the linearized solution near the left boundary (at $x = 0$) where the transmissivity can be approximated by considering η_1 as water table level, despite the numerical solution presenting non-linear effects due to strong gradients of the water table surface. The same behavior can be observed more clearly in the cases of $K_S = 10^{-2}$ m/s (represented with red lines) and $K_S = 10^{-1}$ m/s (black lines) one day after the beginning of the simulation ($t = 0$), as illustrated at the top left of the figures. In the case of $K_S = 10^{-1}$ m/s the hydraulic transmissivity is large enough for the solution to reach stationarity after 20 days, but the

linearized solution does not fit the numerical solution even partially, tending towards a linear profile. However, the numerical solution is coincident with the exact steady solution given by (38).

5.2. Comparison with an Analytical Non-linear Solution with planar topography

The second test is a limit case of the previous one, defined by (33), including its boundary conditions, (34) and (35), and the initial condition, (36). In this test, the water surface level at the left boundary ($x = 0$) suddenly increases to η_1 value whereas the other boundary is initially dry and domain is indefinitely long , i.e. $\eta_2 = 0$ and $L \to \infty$ (see Fig. 2).

In this case, Equation (33) cannot be solved approximately with a linearization because of the cohexistence of "wet" and "dry" zones. In order to obtain the solution, *Song et al.* [2007] and *Lockington et al.* [2000] defined a new spatial-temporal coordinate:

$$\xi = x \left(\frac{2\, s}{\eta_1\, K_s\, t} \right)^{1/2} \tag{43}$$

With this coordinate, the analytic solution obtained with Equation (10) of *Song et al.*'s paper becomes:

$$\eta = \begin{cases} \eta_1 \sum_{n=0}^{\infty} a_n \left(1 - \frac{\xi}{\xi_0}\right)^n & \xi < \xi_0 \\ 0 & \xi \geq \xi_0 \end{cases} \tag{44}$$

where a_n is an infinite sequence of real numbers with the following properties:

$$a_0 = 0 \tag{45}$$

and

$$\sum_{n=0}^{\infty} a_n = 1 \tag{46}$$

and the values of a_n are calculated with the following recursive form:

$$\frac{(n+1)(n+2)}{\xi_0^2} \sum_{k=0}^{n+2} a_k \, a_{n+2-k} - \frac{n+1}{2} \, a_{n+1} + \frac{n}{2} \, a_n = 0 \tag{47}$$

and ξ_0 is a constant, related to the displacement of the wetting front, which is estimated such that (46) is verified. Equation (47) corresponds to Equation (16) of *Song et al.*'s paper. *Song et al.* [2007] gave an explicit form of (47) and fully described how to get the numerical values of the ξ_0 and a_n terms.

Fig. 4 illustrates the fit between *Song et al.*'s analytical solution and the numerical solution obtained with the BEq code. As in the previous case, the saturated hydraulic conductivities were set to $K_S = 10^{-4}$ m/s, $K_S = 10^{-3}$ m/s , $K_S = 10^{-2}$ m/s and $K_S = 10^{-1}$ m/s; the porosity was set to $s = 0.4$ in each of the four sub-cases; the water surface elevation, η_1, at the left boundary ($x = 0$) was set at 1 m; and analogously to the previous experiment, results were plotted at times of 1, 5, 10 and 20 days since the initial instant. The cell size used is 1 m, the numerical time step used is 3600 s for the lower conductivities (blue and red), whereas in the other two cases (red and black) the time step used is ten times smaller, i.e. 360 s. In fact, according to our numerical scheme, the wetting front can advance into one initially dry cell no more than once per time step and, therefore, if the time step is relatively long, the displacement of the wetting front could be underestimated. For this reason, disagreements between numerical and exact analytical solution may occur

in earlier time-steps. If the time-step is not sufficiently short, the analytical wetting front anticipates the numerical one, however for long times the lag between the two solutions is reduced and tends to be zero. In Fig. 4 this lag is significant, about 20 m, only in the case of $K_S = 10^{-1}$ m/s (an unrealistically high conductivity chosen to test a limit case) after one day (86400 s). In all the other cases, the numerical and analytical solutions fit quite well after 5 and 10 days (432000 s and 864000 s respectively). After 20 days (1728000 s), there is also a quasi-perfect agreement except for $K_S = 10^{-1}$ m/s when the wetting front reaches the right-hand side end of the numerical domain: in fact, while the numerical solution has the zero Dirichlet boundary condition (35) at $x = L$, the *Song et al.* analytical solution represents the movement of a wetting front over a semi-infinite planar dry bedrock and does not have any right-hand boundary condition. Therefore, the small disagreement is due to lateral right-hand boundary effects.

5.3. Comparison with HsB numerical solution

The BEq code was compared with an existing one-dimensional code, produced by *Troch et al.* [2004]. The test was conducted on virtual hillslopes of variable sizes, similarly to what was presented in *Troch et al.* [2003]. Three artificial, 100 m long, planar hillslopes were setup with different shapes:

- hillslope A, with a uniform width of 7 m ;
- hillslope B, (convergent) with an exponentially variable width from 50 m (at the top) to 7 m (at the toe); and
- hillslope C, (divergent) with an exponentially variable width from 7 m (at the top) to 50 m (at the toe).

In A, B, and C the slope is 0.05, the drainable porosity is uniformly distributed and equal to $s(x, y, z) = 0.3$, the saturated hydraulic conductivity is uniformly distributed and equal to $K_S(x, y, z) = 2.78 \cdot 10^{-4}$ m/s (1 meter per hour), and the initial soil water-table thickness is equal to $h(x, y) = 0.4$ m [*Troch et al.*, 2003].

A water-table recharge of 10 mm/day is applied to each of the three hillslopes.

The following boundary conditions are applied (Experiment 1) :

- a Dirichlet condition ($\eta = 0$) at the toe according to *Troch et al.* [2003];
- a no-flux condition at the top of the hillslope and at the lateral boundary.

In this experiment the time step used is 3600 s for our model and 180 s for the HsB model. These were chosen in order to have comparable computational times for both solvers, and we sacrificed time accuracy for increased spatial information. Both models work with a resolution of 1 m (but while the response of the BEq code is given pixel by pixel, the HsB model returns the mean level of the water table at each given distance along the transects, drawn in red in Fig. 5).

Fig. 6 shows the water-table thickness along the principal direction of the hillslopes at different times.

- In hillslope A the water-table thickness tends to be uniform in the middle part of the hillslope and have relevant gradients at the top and at the toe. After 5 and 20 days the thickness h increases with a peak at about 20 m, as expected.
- In hillslope B the behavior is initially similar to hillslope A. The peak of h after 20 days is greater than in hillslope A exceeding it by 1 m.
- In the hillslope C, after 1 day, h has a profile similar to that of hillslope A, then decreases in the upper part of the hillslope and increases a little in the lower part.

The results of our model confirm the results of the HsB model. The fit of the two solvers is relatively good. Few differences can be seen for convergent and divergent hillslopes. The HsB model is one-dimensional and assumes a uniform profile of h along the width. In the case of the convergent hillslope, our model underestimates the values predicted by HsB. On the contrary, in divergent hillslopes it overestimates them. These differences are relatively small and due to a non-uniform profile of the water table along the hillslopes' cross sections. In our case the water table depth in the middle part of the hillslope is greater for the convergent case or lower for the divergent case than close to the lateral boundary, a situation that obviously cannot be reproduced by a one dimensional model.

5.4. Application to the Panola hillslope with wetting and drying patterns

The capabilities of the model go beyond the description of hydrological responses of simple virtual hillslopes. Indeed, it was designed to be able to deal with complex topographies, as already shown in *Lanni et al.* [2011]. The Panola site was chosen to perform analyses with the proposed BEq solver. It lies within the Panola Mountain Research Watershed (PMRW), located about 25 km southeast of Atlanta, Georgia, USA, in the southern Piedmont. The site is of particular interest because a detailed survey was carried out to determine the topography of the bedrock, as distinguished from the topography of terrain surface, shown in Figure 7. The surface topography of the study hillslope is approximately planar while the bedrock topography is very irregular, resulting in highly variable soil depth ranging from 0 to 1.86 m with an average value of 0.63 m. This was shown by *Tromp-van Meerveld and McDonnell* [2006] to be the cause of the complexity of the subsurface storm flow discharge generated.

The site has a slope angle of 13°, is 28 m wide and 48 m long. Soil depths have been measured on a regular 2x2 m grid and linearly interpolated to a 1x1 m digital elevation model for a total of about 1815 cells. The downslope boundary of the Panola hillslope is formed by a 20 m wide trench. The upper boundary of the study hillslope is formed by a small bedrock outcrop. The soil is a sandy loam, without discernible structure and overlain by a 0.15 m deep organic-rich horizon [*Hopp and McDonnell*, 2009]. All other details are described by *Tromp-van Meerveld and McDonnell* [2006], *Meerveld and Weiler* [2008] and we refer the reader to those papers for further information.

Overland flow is uncommon at the Panola site and is observed only during very intense thunderstorms after extended dry periods. Even during these storms, overland flow was restricted to small areas and re-infiltrated within several meters. A constant water-table recharge rate, Q (see Equation (1)), of two millimeters per hour (2 mm/hr) for 48 hours was assumed on the basin. This is coherent with the magnitude to the event of March 6-7,1996, reported in *Hopp and McDonnell* [2009]. Simulations were performed assuming hydraulic conductivity, K_S= 0.1 m/hr (2.78 10^{-5} m/s) and completely dry initial conditions (null water thickness $h = 0$).

Due to the irregular bedrock, very soon after the beginning of the rainfall event, flow creates irregular water table levels along the hillslope which cannot be simulated with one dimensional models of flow; these are clearly evident after 24 hours, as shown in Figure 8. Variable zones of null water table depth also appear and, after the end of the rainfall event, small, disconnected, perched water tables remain in the domain. For comparison, Figure 9 reports the behavior of a purely planar hillslope of 13° slope under the same conditions. It is easily understood that the flow is absolutely symmetric and trivial.

The irregularities of the bedrock also affect the discharge at the toe of hillslope, as collected at the trench position, and shown in Figure 10. The most evident feature is an increase of the mean transit time of water, with a consequent decrease of the discharge peak by approximately one fourth.

However, since the recharge is constant and synchronous everywhere on the bedrock, filling and spilling phenomena (i.e. the production of multiple peaks) [*Tromp-van Meerveld and McDonnell*, 2006] are not present. This supports the idea that filling and spilling are due to the irregular arrival time of water infiltrating to the different depths implied by the irregular distance between terrain surface and bedrock.

5.5. Comparison with the GEOtop distributed hydrological model

In order to better comprehend the capabilities of the proposed numerical method for solving the Boussinesq Equation with irregular topography, a preliminary comparison with the distributed hydrological model GEOtop is here presented. The GEOtop model solves the 3D Richards' Equation and extends it to the case of saturated soils [*Zanotti et al.*, 2004; *Rigon et al.*, 2006; *Bertoldi et al.*, 2006, 2010; *Dall'Amico et al.*, 2011; *Endrizzi and Gruber*, 2012]. GEOtop is an open source free software available on www.geotop.org. However, GEOtop is not completely compatible with BEq: by construction GEOtop resolves vertical infiltration, while BEq does not. A proper comparison would require coupling BEq with an infiltration module, which is beyond the scope of the present paper. Nevertheless, we effected the comparison as we believe it to be instructive to the reader. Regarding computational time, given equivalent grid sizes, BEq is much faster than GEOtop. This is because GEOtop is 3D, rather than 2D, and it includes many other processes, such as surface runoff and runoff re-infiltration that BEq does not consider. The comparison

is made with the application of the two models to the Panola hillslope,already used and described above.

The hillslope terrain is planar whereas the bedrock topography is irregular; average soil thickness is reduced to 0.5 m to minimize the effects of infiltration. The GEOtop simulations are performed with the build 1.225-9. During the simulations, a constant precipitation rate of 10 mm/hr is applied uniformly over the whole hillslope for 48 hours. Analogously with the case described in the previous section, the simulations were performed assuming hydraulic conductivity, K_S= 0.1 m/hr (2.78 10^{-5} m/s), and completely dry initial conditions (corresponding to null water thickness). This means that soil water pressure head is initially uniformly distributed and equal to $-\infty$ (in practice, it is equal to a relatively high negative value). In the presented simulations with the Boussinesq Equation, the soil water retention curve is modeled as a step function (i.e. it is equal to the soil porosity in saturated zones and 0 in unsaturated zones). On the other hand, GEOtop models the soil water retention curve according to *VanGenuchten* [1980]'s formula with the following parameters: α_{VG}=10 m^{-1}, n=3 and m=0.667, typical values for a sandy soil. However, *VanGenuchten*'s parameters are set such that the retention curves for the two models are very similar and GEOtop's numerical convergence is guaranteed.

In GEOtop, the water-table thickness can be obtained by observing the growth of saturated soil layers over the bedrock for each point of the basin. However, for the purposes of this paper, we are not interested in the 3D water profile in the vadose zone. Therefore, it is simply estimated from the values of pressure head just above the bedrock, assuming a slope-normal hydrostatic equilibrium profile (e.g. *Cordano and Rigon*, 2008's equation 10):

$$\psi = (z - d)\cos\alpha \tag{48}$$

where ψ is the soil water pressure head obtained by GEOtop, α is the slope degree of the Panola hillslope terrain which is about 13 degrees, z is here a slope-normal downward vertical coordinate and d is the depth of water-table.

When the pressure head over the bedrock is positive, a perched water-table occurs. In this case d is calculated by inverting (48) and the water thickness is obtained from the difference with the local soil thickness.

Figure 11 illustrates the dynamic behaviors of the vertical water-table thickness over the Panola topography, simulated with the Boussinesq Equation solver on the left and GEOtop on the right.

The pattern needs to be read after having weighed the effects of infiltration. While in BEq all the precipitation is immediately provided as "recharge" over the bedrock, in GEOtop, water needs to "infiltrate" downwards (sometimes "precipitation" and "water table recharge" are used as synonyms in groundwater literature but they are different). Therefore in BEq simulations a perched water table is formed from the first time instant of simulation, and water begins to flow downhill immediately. In GEOtop, on the other hand, water first needs to infiltrate across the vadose zone and form a water-table before moving downhill. This depends on the water retention curve chosen for the simulation, but it can typically take up to 48 hours. Therefore, the soil water thickness patterns from the two simulations are very similar after 48, 240 and 480 hours (corresponding to 1, 10 and 20 days) from the beginning of the precipitation; during the initial 48 hours, however, the two simulations are not similar. Also as a consequence of missing infiltration, the water

thickness values obtained with the BEq are on average greater than the ones obtained by GEOtop, which, however, stores water in the vadose zone. Some exceptions are clarified below. Unlike Figure 8 and Figure 9, Figure 11 illustrates water thickness stored within the soil thickness (i.e. surface water is not taken into account in these simulations).

Besides the visual comparison shown in Figure 11 a scatterplot of BEq versus GEOtop water-table depth is reported in Figure 12. During the initial timesteps, there is not a good correlation between the two models. Surprisingly, there is a considerable number of points where there is a higher water table in GEOtop than in BEq. This is not completely intuitive but can be explained as follows: inspection of the points on the upper left quadrant (of the top left plot) shows that these are all located close to the divide where water in BEq flows away proportionally to saturated hydraulic conductivity and the local gradient of bedrock topography, while in GEOtop it is still infiltrating. This is confirmed in the top left scatterplot of Figure 13, where the total volume of water, including unsaturated water volume per unit area, are estimated for each pixel. In particular, going back to the points close to the divides, the water simulated in the BEq experiment, has already flowed away, whereas the water simulated by GEOtop has just reached the bedrock and forms a perched water-table.

As the time increases the number of points where GEOtop water storage is larger than BEq decreases and, as expected, most of the points have a lower water table thickness in GEOtop than in BEq. However, there is a good correlation between data from the two models, with a coefficient greater than 0.95. It can also be observed that many of the points accumulate on the x-y plane bisector: they mostly represent the parts of the basin in which the soil is completely saturated.

Figure 13 shows the comparison of water volume per unit area for each pixels in GEOtop and BEq. The scatterplots of Figure 13 show a better general better agreement between the two models than those based on the water table thickness. GEOtop gives larger values of stored water volumes in the lower range of volumes, for the same phenomenology described above to explain the water table dynamics of points close to the divides. The differences between the results of the two models tend to decrease, exponentially after 10 and 20 days from the beginning, even if the delay in the GEOtop simulation caused by infiltration is still evident.

6. Conclusion

A new two-dimensional numerical solver of the Boussinesq Equation has been presented. The solver derives from a finite-volume mass budget for each element of the domain. The Boussinesq equation is reduced to a non-linear system composed of three terms, where the known term corresponds to the initial condition and the external forcing. The unknowns appear in a non-linear term, which is the water volume stored in each cell, and a linear term deriving from the fluxes of water between cells.

The method is innovative with respect to other two-dimensional solvers [e.g. *Harman and Sivapalan*, 2009] and other widely used models [e.g. *Harbaugh et al.*, 2000a; *Painter et al.*, 2008], in that it intrinsically preserves mass (even for large integration time steps, where accuracy is lost) and properly accounts for wetting and drying of the water-table without the introduction of *ad hoc* internal iteration schemes. The solver can properly reproduce simple drainage problems that have analytical solutions, and it performs competitively with non-linear analytic solutions [*Song et al.*, 2007]. The solver also performs well with the HsB model [*Troch et al.*, 2003], at least for the simplified setting proposed in the

literature, despite that it works with two-dimensional water table patterns as opposed to the one-dimensional patterns of the HsB model.

Simulations in complex topography, as those for the Panola site, show the capabilities of the BEq solver to describe the complex water flow generated in simulations of water table above rugged bedrock.

A comparison with GEOtop [*Rigon et al.*, 2006; *Endrizzi and Gruber*, 2012], a model solving the 3D Richards' equations, was carried out, despite some limitations. The main obstacles to a proper simulation comparison are: (i) the absence of an integrated vertical infiltration module within the Boussinesq Equation; and (ii), because of the GEOtop code, the impossibility of introducing a direct water water table recharge source in each part of the domain into the GEOtop model itself. In fact, solving either problem would require a big effort on the source codes of both models, which goes beyond the scope of this paper. Nevertheless, the results show consistent behaviour and encourages one to think that, once the appropriate infiltration module is created, the results given by BEq would be credible, and fit well to real case studies.

Therefore, it is clear that the BEq algorithm can be successfully be integrated into rainfall-runoff models of large areas if a detailed, two-dimensional, forecast of the water table position is necessary, especially if the runoff model is integrated with an appropriate (even simplified) infiltration model. It is also clear that the BEq algorithm could exploit the information contained in soil depth distribution maps, when available, to simulate complex patterns of soil moisture and runoff. Obviously, the model can be successfully used in all the traditional applications related to two-dimensional unconfined aquifers without any modification.

Acknowledgments.

This work is partially sponsored by the projects MORFEO and HydroAlp (University of Trento), ace-sap, ENVIROCHANGE and IDROCLIMA (Fondazione Edmund Mach). The presented numerical algorithm for a numerical solution of BEq is coded in C (the BEq code) and freely available on request to the authors. The analytical solutions used for the comparisons of the BEq code are implemented as an R package called "boussinesq" and freely available under GPL license on CRAN (Comprehenisive R Archive Network) at http://cran.r-project.org/web/packages/boussinesq/index.html. GEOtop is coded in C/C++ and freely available under GPL3 license at http://www.geotop.org. The elaborations of GEOtop results are performed with the R package "geotopbricks" freely available under GPL on CRAN website http://cran.r-project.org/web/packages/geotopbricks/ . The authors thank Eng. Joseph Tomasi and Eng. Dr. Cristiano Lanni for helpful suggestions, Prof. Peter Troch for making the HsB code available, the associate editor and the anonymous reviewers for helpful comments and suggestions, and Dr. Stefano Endrizzi for the help and the suggestions on the GEOtop simulations.

Appendix A: The structure of the numerical solver utilized

As derived in section 3, the spatial and temporal discretization method consists in reducing the free-surface hydrodynamic problem to an algebraic system of the following form:

$$\vec{V}\left(\vec{\zeta}\right) + \mathbf{T}\cdot\vec{\zeta} = \vec{b} \tag{A1}$$

where $\overrightarrow{\zeta} = \left[\zeta_1, \ldots, \zeta_i, \ldots, \zeta_{N_p}\right]^T$ is the array of the unknown quantities (one for each of the N_p grid cells), $\overrightarrow{b} = \left[b_1, \ldots, b_i, \ldots, b_{N_p}\right]^T$ is the array of known parameters, and $\overrightarrow{V}(\overrightarrow{\zeta}) = \left[V_1(\zeta_1), \ldots, V_i(\zeta_i), \ldots, V_{N_p}(\zeta_{N_p})\right]^T$ are the values of the field conserved quantity, i.e. the water volume stored in the i-th cell. All of these "vectors" are denoted by the symbol $\overrightarrow{\cdot}$, or *harpoon*, to distinguish them from space vectors, denoted by $\vec{\cdot}$. $\mathbf{T}$ is a $N_p \times N_p$ matrix which satisfies one of the following properties [*Brugnano and Casulli*, 2008]:

- **T1** : a Stieltjes matrix, i.e., a symmetric M-matrix [e.g., *Horn and Johnson*, 1991];
- **T2**: a symmetric positive semidefinite matrix such that $T_{i,j} \leq 0$ for each $i \neq j$ and $\sum_{i=1}^{N_p} T_{i,j} = 0$ [*Casulli*, 2009] ;

System (A1) can also be written with the following index notation:

$$V_i(\zeta_i) + \sum_{j=1}^{N_p} T_{ij}\zeta_j = b_i \tag{A2}$$

for every i-th cell of the domain. This notation highlights that the i-th component, V_i, of the conserved quantity vector, $\overrightarrow{V}$, is solely a function of the component ζ_i and, in the case analyzed in this paper, related to the i-th cell itself.

If the following residual function is defined:

$$\overrightarrow{R}(\overrightarrow{\zeta}) := \overrightarrow{V}(\overrightarrow{\zeta}) + \mathbf{T} \cdot \overrightarrow{\zeta} - \overrightarrow{b} \tag{A3}$$

solving (A1) corresponds to seeking the zeros of the residual function $\overrightarrow{R}(\overrightarrow{\zeta})$. Furthermore, when the Jacobian matrix of the residual $\overrightarrow{R}(\overrightarrow{\zeta})$ is locally a continuous, non-singular,

Lipschitz matrix around the solution $\vec{\zeta}$ [e.g. *Kelley*, 2003], then the zeros of the residual function (i.e. the solution of (A1)) can be found with a Newton-like iterative method:

$$\vec{\zeta}^{;m} = \vec{\zeta}^{;m-1} - \mathbf{J_R^{-1}}(\vec{\zeta}^{;m-1}) \cdot \vec{R}\,(\vec{\zeta}^{;m-1}) \tag{A4}$$

where $\mathbf{J_R}$ is the Jacobian matrix of the residual function, defined as:

$$J_{R_{lk}}^{;m} := \frac{\partial R_l}{\partial \zeta_j}\Bigg]^{;m} \tag{A5}$$

where $l, k = 1, \cdots, N_p$, and m (preceded by a semicolon) is the iteration level of Newton's method. An explicit calculation shows that $\mathbf{J_R}$ is the sum of $\mathbf{T}$, which is symmetric and positive by definition, and the Jacobian matrix of $\vec{V}(\vec{\zeta})$, i.e.:

$$\mathbf{J_R} = \mathbf{T} + \mathbf{P} \tag{A6}$$

with

$$P_{lk} := \frac{\partial V_l}{\partial \zeta_j}|^{;m} \tag{A7}$$

where ":=" indicates a definition (rather than an equality).

If the volume $V_i(\zeta_i)$ (the conserved quantity) of a generic i-th grid element is a non-decreasing function of the unknown variable ζ_i, and does not depend on the values of ζ in neighboring cells, then it can be shown that $\mathbf{P}$ is a diagonal matrix with non-null entries that are all positive, which correspond to the horizontal wet area of each cell, as will be shown in the next section. In practical applications, it is not computationally convenient

to use (A4) and then find the inverse of the Jacobian matrix, whose storage in memory can be overwhelming and time-expensive. Thus, equation (A4) is usually solved by finding the solution for the associated linear system:

$$\mathbf{J_R}(\vec{\zeta}^{;m_N-1}) \cdot \left[\vec{\zeta}^{;m_N-1} - \vec{\zeta}^{;m_N}\right] = \vec{R}\,(\vec{\zeta}^{;m_N-1}) \tag{A8}$$

where the sparse Jacobian matrix, $\mathbf{J_R}$, can be used in a, so called, matrix-free implementation that is much less demanding, both computationally and on storage. Given the symmetry of $\mathbf{J_R}$, the linear system (A8) can be efficiently solved with a preconditioned conjugate gradient method [e.g. *Schewchuk*, 1994]. Under the conditions described above, the solution of (A1) is unique and it can be proved that (A4) converges to such a solution with few iterations. In particular, when $\mathbf{T}$ is irreducible and satisfies the **T2** property, the following condition needs to be satisfied [*Casulli*, 2009]:

$$\sum_{i=1}^{N_p} b_i = \sum_{i=1}^{N_p} V_i\,(\zeta_i) > 0 \tag{A9}$$

which means that no more water mass can be abstracted through sinks than is present in the domain [*Brugnano and Casulli*, 2008]. If $\mathbf{T}$ is reducible (i.e. not irreducible, the "wet" domain is decomposed into disconnected parts) and satisfies the **T2** property, then (A9) must be changed into the following scalar product [*Brugnano and Casulli*, 2008]:

$$\vec{v} \cdot \vec{b} = \sum_{i=1}^{N_p} v_i\, b_i > 0 \tag{A10}$$

for each $\vec{v}$, eigenvector of $\mathbf{T}$, giving a null eigenvalue:

$$\mathbf{T} \cdot \overline{v} = 0 \tag{A11}$$

Appendix B: The analytical one-dimensional linearized solution of the Boussinesq equation

From Section 5, Equation (33) is rewritten as (41):

$$\frac{\partial}{\partial x}\left[K_S\,\eta_M \frac{\partial \eta}{\partial x}\right] = s\frac{\partial \eta}{\partial t} \tag{B1}$$

where K_S and η_M are two suitable constants, and the following boundary conditions must be imposed:

$$\eta = \eta_1 \qquad x = 0 \tag{B2}$$

$$\eta = \eta_2 \qquad x = L \tag{B3}$$

$$\eta = \eta_2 \qquad t = 0 \tag{B4}$$

To standardize the solution of the problem, a non-dimensional form of (B1) is usually applied. Consequently, a new variable w is introduced:

$$w = \frac{\eta - \eta_2}{\eta_1 - \eta_2} \tag{B5}$$

so that (41) (or (B1)) is modified and further simplified to a constant-coefficient linear equation, which is the classical form of *heat* equation:

$$D\frac{\partial^2 w}{\partial x^2} = \frac{\partial w}{\partial t} \tag{B6}$$

where

$$D := \frac{K_S\,\eta_M}{s} \tag{B7}$$

The boundary and initial conditions (B2),(B3) and (B4) are rewritten with the new variable w to obtain respectively:

$$w = 1 \qquad x = 0 \tag{B8}$$

$$w = 0 \qquad x = L \tag{B9}$$

$$w = 0 \qquad t = 0 \tag{B10}$$

Finally, the exact solution is [e.g. *Rozier-Cannon*, 1984]:

$$w = \frac{L-x}{L} + \sum_{n=1}^{\infty} w_n \exp\left(-n^2\pi^2\,\frac{D\,t}{L^2}\right)\sin\left(\frac{n\pi x}{L}\right) \tag{B11}$$

where w_n is defined for each n (from 1 to ∞) so that:

$$\frac{L-x}{L} + \sum_{n=1}^{\infty} w_n \sin\left(\frac{n\pi x}{L}\right) = 0 \qquad 0 < x \leq L \tag{B12}$$

and then, by Fourier series decomposition, it is:

$$w_n = -\frac{1}{L}\int_0^{2L}\left(1-\frac{x}{L}\right)\sin\left(\frac{n\pi x}{L}\right)\,dx = -\frac{2}{\pi\,n} \tag{B13}$$

In conclusion, by assembling (B5),(B11) and (B13), the explicit form of the solution to (B1) is:

$$\eta = \eta_2 + \frac{\eta_1 - \eta_2}{L}(L - x) - \frac{2(\eta_1 - \eta_2)}{\pi} \sum_{n=1}^{\infty} \frac{1}{n} \exp\left(-n^2\pi^2 \frac{D\,t}{L^2}\right) \sin\left(\frac{n\pi x}{L}\right) \quad \text{(B14)}$$

References

Akylas, E., and A. D. Koussis (2007), Response of sloping unconfined aquifer to stage changes in adjacent stream. i. theoretical analysis and derivation of system response functions, *Journal of Hydrology*, *338*(1-2), 85–95.

Barenblatt, G., V. Entov, and V. M. Ryzhik (1990), *Theory of fluid flows through natural rocks*, Dordrecht: Kluwer Academic Publishers.

Barling, R. D., I. D. Moore, and R. B. Grayson (1994), A quasi-dynamic wetness index for characterizing the spatial distribution of zones of surface saturation and soil water content, *Water Resour. Res.*, *30*(4), 1029–1044.

Bear, J. (1972), *Dynamics of fluids in porous media*, American Elsevier Publisher, New York.

Bertoldi, G., R. Rigon, and T. M. Over (2006), Impact of watershed geomorphic characteristics on the energy and water budgets, *Journal of Hydrometeorology*, *7*(3), 389–403, doi:10.1175/JHM500.1.

Bertoldi, G., C. Notarnicola, G. Leitinger, S. Endrizzi, M. Zebisch, S. Della Chiesa, and U. Tappeiner (2010), Topographical and ecohydrological controls on land surface temperature in an alpine catchment, *Ecohydrology*, *3*(2), 189–204, doi:10.1002/eco.129.

Beven, K. J., and M. J. Kirkby (1979), A physically based, variable contributing area model of basin hydrology / un modèle àbase physique de zone d'appel variable de l'hydrologie du bassin versant, *Hydrological Sciences Bulletin*, *24*(1), 43–69.

Boussinesq, J. (1877), Essai sur la theorie des eaux courantes, *Mem. Acad. Sci. Inst. Fara.*, *23*(1), 252–260.

Brugnano, L., and V. Casulli (2008), Iterative solution of piecewise linear systems, *J. Sci. Comput.*, *30*(1), 463–472.

Brutsaert, W. (1994), The unit response of groundwater outflow from a hillslope, *Water Resour. Res.*, *30*(10), 2759–2764.

Casulli, V. (2009), A high-resolution wetting and drying algorithm for free-surface hydrodynamics, *International Journal for Numerical Methods in Fluids*, *60*(4), 391–408, doi:10.1002/fld.1896.

Casulli, V., and R. A. Walters (2000), An unstructured grid, three-dimensional model based on the shallow water equations, *International Journal for Numerical Methods in Fluids*, *32*(3), 331–348, doi:10.1002/(SICI)1097-0363(20000215)32:3¡331::AID-FLD941¿3.0.CO;2-C.

Cayar, M., and M. L. Kavvas (2009), Symmetry in nonlinear hydrologic dynamics under uncertainty: Ensemble modeling of 2d boussinesq equation for unsteady flow in heterogeneous aquifers, *Journal of Hydrologic Engineering*, *14*(10), 1173–1184, doi: http://dx.doi.org/10.1061/(ASCE)HE.1943-5584.000011.

Celia, M. A., E. T. Bouloutas, and R. L. Zarba (1990), A general mass-conservative numerical soluton for the unsaturated flow equation, *Wat. Resour. Res.*, *26*(7), 1483–1496.

Childs, E. C. (1971), Drainage of groundwater resting on a sloping bed, *Water Resour. Res.*, *7*(5), 1256–1263.

Chirico, G. B., R. B. Grayson, and A. W. Western (2003), On the computation of the quasi-dynamic wetness index with multiple-flow-direction algorithms, *Water Resour. Res.*, *39*(5).

Cordano, E. (2011), *boussinesq: Analytic Solutions for (ground-water) Boussinesq Equation*, r package version 1.0.

Cordano, E., and R. Rigon (2008), A perturbative view on the subsurface water pressure response at hillslope scale, *Water Resour. Res.*, *44*, 5.

Cormen, T. H., C. E. Leiserson, R. L. Rivest, and C. Stein (2001), *Introduction to Algorithms*, ISBN 0262032937, MIT Press and McGraw-Hill.

Dagan, G. (1989), *Flow and Transport in Porous Formations*, Springer-Verlag, Berlin New York.

Dall'Amico, M., S. Endrizzi, S. Gruber, and R. Rigon (2011), A robust and energy-conserving model of freezing variably-saturated soil, *The Cryosphere*, *5*(2), 469–484, doi:10.5194/tc-5-469-2011.

Davis, T. C. (2006), *Direct Methods for Sparse Linear Systems*, SIAM, Philadelphia, PA,USA.

Dehotin, J., R. F. Vázquez, I. Braud, S. Debionne, and P. Viallet (2011), Modeling of hydrological processes using unstructured and irregular grids: 2d groundwater application, *Journal of Hydrologic Engineering*, *16*(2), 108–125, doi:DOI:10.1061/(ASCE)HE.1943-5584.0000296.

Dietrich, W. E., and D. Montgomery (1994), A physically based model for the topographic control on shallow landsliding, *Water Resour. Res.*, *30*(4), 1153–1171.

D'Odorico, P., S. Fagherazzi, and R. Rigon (2005), Potential for landsliding: Dependence on hyetograph characteristics, *J. Geophys. Res.*, *110*(F1), doi:10.1029/2004JF000127.

Doherty, J. (2001), Improved calculations for dewatered cells in modflow, *Ground Water*, *39*(6), 863–869.

Don, N. C., H. Araki, H. Yamanishi, and K. Koga (2005), Simulation of groundwater flow and environmental effects resulting from pumping, *Environmental Geology*, *47*, 361–374, 10.1007/s00254-004-1158-1.

Endrizzi, S., and S. Gruber (2012), Investigating the effects of lateral water flow on spatial patterns of ground temperature, depth of thaw and ice content, in *Proceedings of the 10th International Conference on Permafrost*, pp. 91–96, Salekhard, Russia.

Fan, Y., and R. L. Bras (1998), Analytical solutions to hillslope subsurface storm flow and saturation overland flow, *Water Resour. Res.*, *34*(4), 921–927.

Hantush, M. S. (1967), Flow of groundwater in relatively thick leaky aquifers, *Water Resour. Res.*, *3*(2), 583–590.

Harbaugh, A., E. Banta, M. Hill, and M. MacDonald (2000a), *MODFLOW-2000, The U.S. Geological Survey Modular Ground-Water Model-User Guide to Modularization Concepts and the Ground-Water Flow Process*, U.S. Geological Survey, Reston, VA, USA, open-file report 00-92 ed.

Harbaugh, A., E. Banta, M. Hill, and M. McDonald (2000b), Modflow 2000, the u.s. geological survey modular ground-water model—user guide to modularization concepts and the ground-water flow process, *USGS Open File Report 00-92*.

Harman, C., and M. Sivapalan (2009), Effects of hydraulic conductivity variability on hillslope-scale shallow subsurface flow response and storage-discharge relations, *Water*

Resour. Res., *45*(1), doi:10.1029/2008WR007228.

Hilberts, A. G., P. A. Troch, and C. Paniconi (2005), Storage-dependent drainable porosity for complex hillslopes, *Water Resour. Res.*, *41*, W06,001, doi:10.1029/2004WR003725.

Hilberts, A. G. J., P. A. Troch, C. Paniconi, and J. Boll (2007), Low-dimensional modeling of hillslope subsurface flow: Relationship between rainfall, recharge, and unsaturated storage dynamics, *Water Resour. Res.*, *43*(3), doi:10.1029/2006WR004964.

Hjerdt, K. N., J. J. McDonnell, J. Seibert, and A. Rodhe (2004), A new topographic index to quantify downslope controls on local drainage, *Water Resour. Res.*, *40*(5).

Hopp, L., and J. J. McDonnell (2009), Connectivity at the hillslope scale: Identifying interactions between storm size, bedrock permeability, slope angle and soil depth, *Journal of Hydrology*, *376*(3-4), 378–391.

Horn, R. A., and C. R. Johnson (1991), *Topics in Matrix Analysis*, Cambridge University Press, New York.

Iverson, R. (2000), Landslide triggering by rain infiltration, *Water Resour. Res.*, *36*(7), 1897–1910.

Kelley, C. (2003), *Solving Nonlinear Equations with Newton's Method*, SIAM Society of Industrial and Applied Mathematics, Philadelphia,PA,USA.

Kim, D.-J., and M.-J. Ann (2001), Analytical solutions of water table variation in a horizontal unconfined aquifer: Constant recharge and bounded by parallel streams, *Hydrological Processes*, *15*(13), 2691–2699, doi:10.1002/hyp.495.

Kollet, S. J., and R. M. Maxwell (2006), Integrated surface-groundwater flow modeling: A free-surface overland flow boundary condition in a parallel groundwater flow model, *Adv. in Wat. Resour.*, *29*, 945–958.

Lanni, C., J. McDonnell, and R. Rigon (2011), On the relative role of upslope and downslope topography for describing water flowpath and storage dynamics: a theoretical analysis, *Hydrological Processes*, pp. n/a–n/a, doi:10.1002/hyp.8263.

Leveque (2002), *Numerical Methods for Conservation Laws*, Birkhauser.

Lockington, D. A., J. Y. Parlange, M. B. Parlange, and J. Selker (2000), Similarity solution of the boussinesq equation, *Advances in Water Resources*, *23*(7), 725–729.

Manglik, A., and S. N. Rai (2000), Modeling of water table fluctuations in response to time-varying recharge and withdrawal, *Water Resources Management*, *14*, 339–347, 10.1023/A:1011154903100.

Meerveld, I. T.-v., and M. Weiler (2008), Hillslope dynamics modeled with increasing complexity, *Journal of Hydrology*, *361*(1-2), 24–40.

Painter, S., H. Basagaoglu, and A. Liu (2008), Robust representation of dry cells in single-layer modflow models, *Ground Water*, *46*(6), 873–881.

Panday, S., and P. S. Huyakorn (2004), A fully coupled physically-based spatially-distributed model for evaluating surface/subsurface flow, *Adv. in Wat. Resour.*, *27*, 361–382.

Paniconi, C., P. A. Troch, E. E. van Loon, and A. G. J. Hilberts (2003), Hillslope-storage boussinesq model for subsurface flow and variable source areas along complex hillslopes: 2. intercomparison with a three-dimensional richards equation model, *Water Resour. Res.*, *39*(11), doi:10.1029/2002WR001730.

Parlange, J.-Y., W. L. Hogarth, R. S. Govindaraju, M. B. Parlange, and D. Lockington (2000), On an exact analytical solution of the boussinesq equation, *Transport in Porous Media*, *39*, 339–345, 10.1023/A:1006504527622.

Pruess, K., C. M. Oldenburg, and C. Moridis (1999), *TOUGH2 User's Guide Version 2*, Lawrence Berkeley National Laboratory, paper lbnl-43134. retrieved from: http://www.escholarship.org/uc/item/4df6700h ed.

Rai, S. N., A. Manglik, and V. S. Singh (2006), Water table fluctuation owing to time-varying recharge, pumping and leakage, *Journal of Hydrology*, *324*(1-4), 350–358.

Rigon, R., G. Bertoldi, and T. Over (2006), A Distributed Hydrological Model with Coupled Water and Energy Budgets, *Journal of Hydrometeorology*, *7*(3), 371–388.

Rocha, D., J. Feyen, and A. Dassargues (2007), Comparative analysis between analytical approximations and numerical solutions describing recession flow in unconfined hillslope aquifers, *Hydrogeology Journal*, *15*, 1077–1091, 10.1007/s10040-007-0170-4.

Rozier-Cannon, J. (1984), *The One-Dimensional Heat Equation*, Addison-Wesley Publishing Company, Menlo Park, California, encyclopedia of Mathematics and its applications.

Schewchuk, J. R. (1994), An introduction to the conjugate gradient method without the agonizing pain, *Tech. rep.*, School of Computer Science, Carnegie Mellon University, Pittsburgh, Pennsylvania, USA, Carnagie Mellon University Pittsburgh, PA 15213, USA.

Sokrut, N., K. Werner, and H. J. (2007), Integrated surface- subsurface water flow modeling of the laxemar area. application of the hydrological model, ecoflow, *Sweden: Svenska Karnbranslehantering AB, Swedish Nuclear Fuel and Waste Management Co.*

Song, Z.-y., L. Li, and L. David (2007), Note on barenblatt power series solution to boussinesq equation, *Applied Mathematics and Mechanics*, *28*, 823–828, 10.1007/s10483-007-0612-x.

Stelling, G., and S. Duynmeyer (2003), A staggered conservative scheme for every froude number in rapidly varied shallow water flows, *Internat. J. Numer. Methods Fluids*, *43*, 1329–1354.

Telyakovskiy, A. S., G. A. Braga, S. Kurita, and J. Mortensen (2010), On a power series solution to the boussinesq equation, *Advances in Water Resources*, *33*(9), 1128 – 1129, doi:10.1016/j.advwatres.2010.06.017.

Troch, P. A., C. Paniconi, and E. Emiel van Loon (2003), Hillslope-storage boussinesq model for subsurface flow and variable source areas along complex hillslopes: 1. formulation and characteristic response, *Water Resour. Res.*, *39*(11), doi: 10.1029/2002WR001728.

Troch, P. A., A. H. van Loon, and A. G. J. Hilberts (2004), Analytical solution of the linearized hillslope-storage boussinesq equation for exponential hillslope width functions, *Water Resour. Res.*, *40*(8), doi:10.1029/2003WR002850.

Tromp-van Meerveld, H. J., and J. J. McDonnell (2006), Threshold relations in subsurface stormflow: 2. the fill and spill hypothesis, *Water Resour. Res.*, *42*(2).

VanGenuchten, M. T. (1980), A closed-form equation for predicting the hydraulic conductivity of unsaturated soils., *Soil Sci. Soc. Am. Jour.*, *44*, 892–898.

Werner, A., M. Gallaghar, and S. Weeks (2006), Regional-scale, fully coupled modeling of stream-aquifer interaction in a tropical catchment, *Journal of Hydrology*, *238*(3-4), 497–510.

Western, A. W., and R. B. Grayson (1998), The Tarrawarra data set: Soil moisture patterns, soil characteristics, and hydrological flux measurements, *Water Resour. Res.*, *34*(10), 2765–2768, doi:10.1029/98WR01833.

Zanotti, F., S. Endrizzi, G. Bertoldi, and R. Rigon (2004), The geotop snow module, *Hydrological Processes*, *18*(18), 3667–3679, doi:10.1002/hyp.5794.

Figure 1. Graphical representation of the one-dimensional problem used for the comparison between numerical and linearized analytical solutions of BEq. The soil is bounded by two reservoirs where water surface elevations are η_1 and η_2 at $x = 0$ and $x = L$ respectively. An intermediate dynamical state is represented

Figure 2. Graphical representation of the one-dimensional problem used for the comparison between numerical and *Song et al.*'s analytical solutions of BEq. The problem is a wetting process on an initially dry bedrock ($\eta_2 = 0$), which is a substantially different from the case depicted in Figure 1. At $x = 0$ the water surface level suddenly increases to η_1 at the beginning of the simulation. To obtain the analytical solution L is taken $\to \infty$

Figure 3. Water surface profiles, BEq solution compared to the linearized (p=0 p=0.5 and p=1, see equation (42)) and analytic solutions after 1,5,10 and 20 days from instant $t = 0$. The porosity, s, is 0.4 and the saturated hydraulic conductivity K_S is 10^{-4} m/s in blue, 10^{-3} m/s in green, 10^{-2} m/s in red, 10^{-1} m/s in black. Solid lines refer to the numerical solution; dashed lines to the linearized solution with p=0; dotted lines to the solution with p=0.5; dot-dashed lines to the solution with p=1. The furthest right black dashed line refers to the analytical asymptotic (steady-state) solution.

Figure 4. Water surface profiles, the BEq solution against *Song et al.*'s analytical solution after 1,5,10 and 20 days from the instant $t = 0$. The porosity s is 0.4 and the saturated hydraulic conductivity K_S is 10^{-4} m/s in blue, 10^{-3} m/s in green, 10^{-2} m/s in red, 10^{-1} m/s in black. Solid lines refer to the numerical solution. Dashed lines to the analytical one.

Figure 5. Map of the bedrock elevation of the analyzed hillslopes: uniform (A), convergent(B),divergent(C)

Figure 6. Water-table thickness, h, evaluated along the principal direction of the hillslopes, simulated for hillslopes A, B, and C with our BEq model and the HsB model (dotted lines) after 1, 5, and 20 days from the beginning of the simulation.

Figure 7. On the left: map of the Panola bedrock elevation expressed in meters. The horizontal line marks the outlet where the water recharge is plotted in figure 10. On the right: map of the 13-degree planar slope elevation used as comparison (expressed in meters).

Figure 8. Figure Map of Panola water thickness (expressed in meters) after a rainfall event with 2 mm/hr water-table recharge rate, and duration of 48 hr. The maps are referred to 24,48,120,240,360 and 480 hours since the beginning of the rainfall event. Soil drainable porosity is $s = 0.4$ and saturated hydraulic conductivity is K_S= 0.1 m/hr (2.78 10^{-5} m/s)

Figure 9. Figure Map of water thickness (expressed in meters) over the 13-degree steep planar slope after a rainfall event with 2 mm/hr water-table recharge rate and duration 48 hr. The maps are referred to 24,48,120,240,360 and 480 hours since the beginning of the rainfall event. Soil drainable porosity is $s = 0.4$ and saturated hydraulic conductivity is K_S= 0.1 m/hr (2.78 10^{-5} m/s)

Figure 10. Hydrograph (Water discharge vs time) at the bottom of the Panola hillslope (solid line) and 13-degree planar slope (dotted line) after an event with recharge rate of 2 mm/hr and duration 48 hr

Figure 11. Figure Map of BEq-generated (left) and GEOtop-generated (right) Panola water thickness (expressed in meters) after a rainfall event with 10 mm/hr water-table recharge rate/rainfall , and duration of 48 hr. The maps are referred to 48,240 and 480 hours since the beginning of the rainfall event. Soil drainable porosity is $s = 0.4$ and saturated hydraulic conductivity is K_S= 0.1 m/hr (2.78 10^{-5} m/s)

Figure 12. Comparison between GEOtop-generated and BEq-generated Panola water-table thicknesses. See the corresponding spatial patterns shown in Fig. 11 for the time instant: 48,240 and 480 hours.

Figure 13. Comparison between GEOtop-generated and BEq-generated Panola water volume in a soil column per unit area. In the case of GEOtop, these plots include also the water stored in the vadose zone.

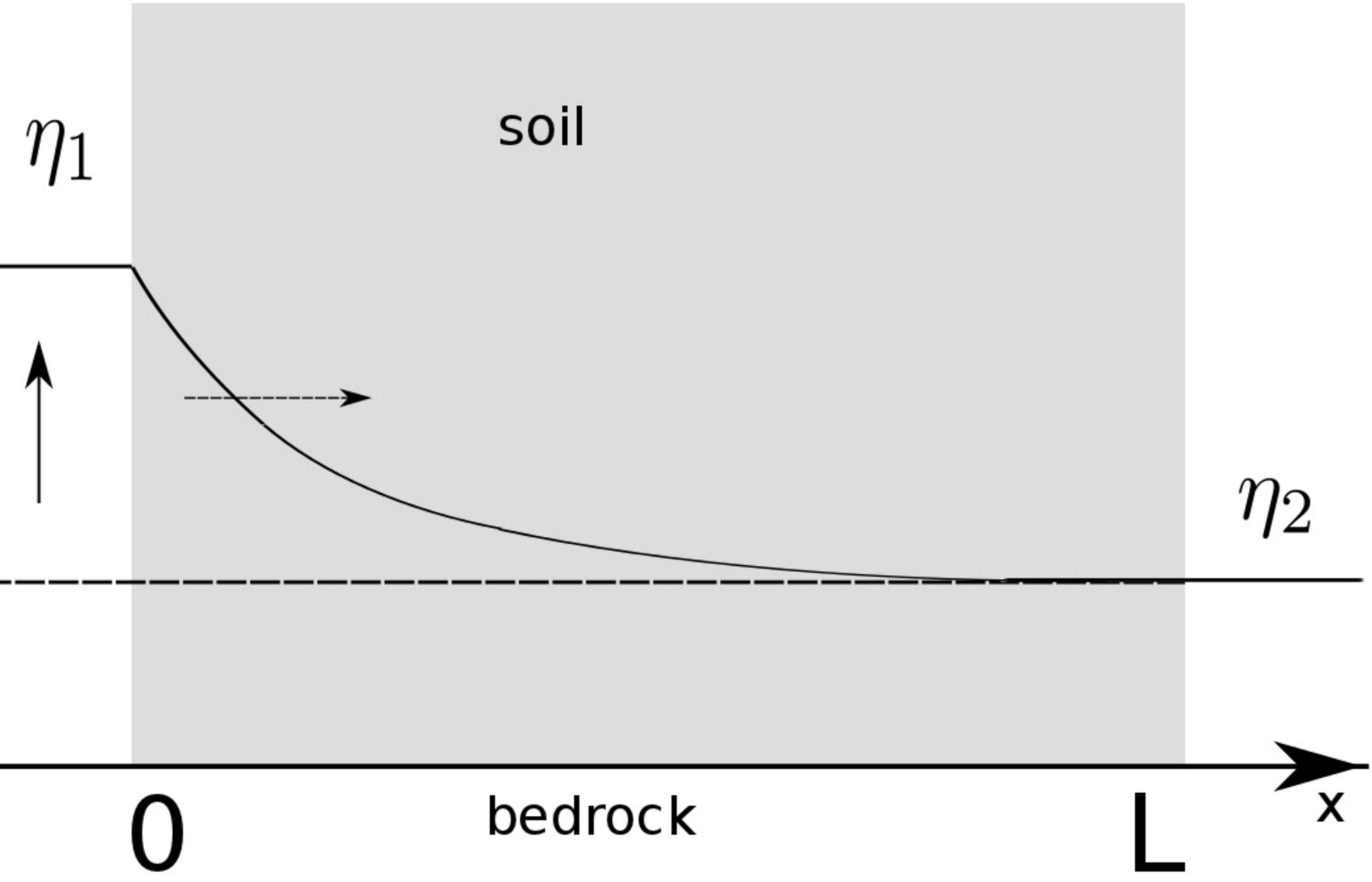
soil
η_1
η_2
0
bedrock
L
x

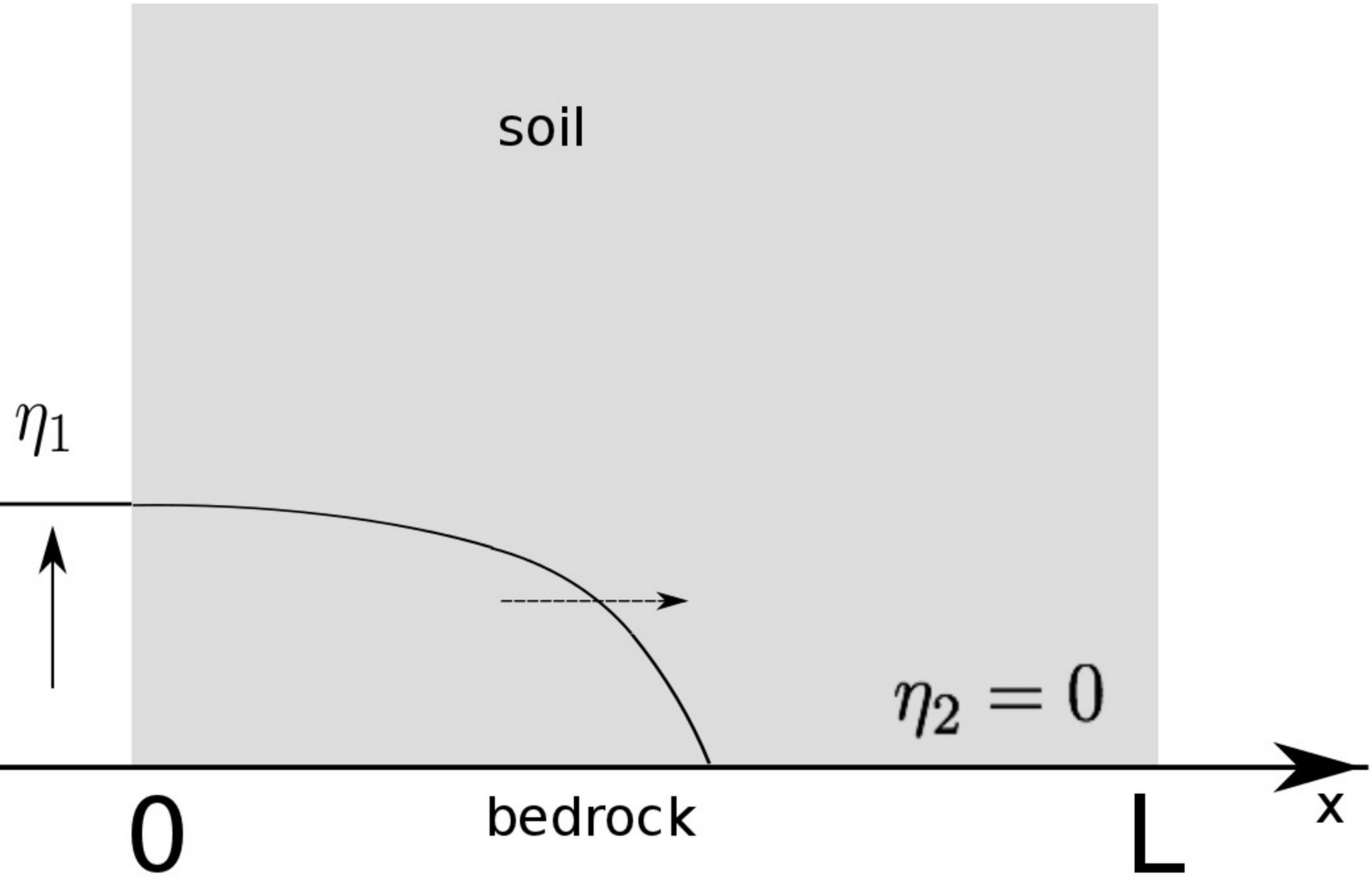
soil
η_1
$\eta_2 = 0$
0
bedrock
L
x

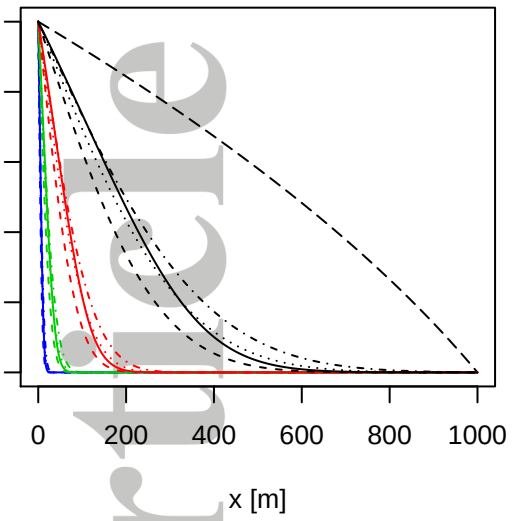

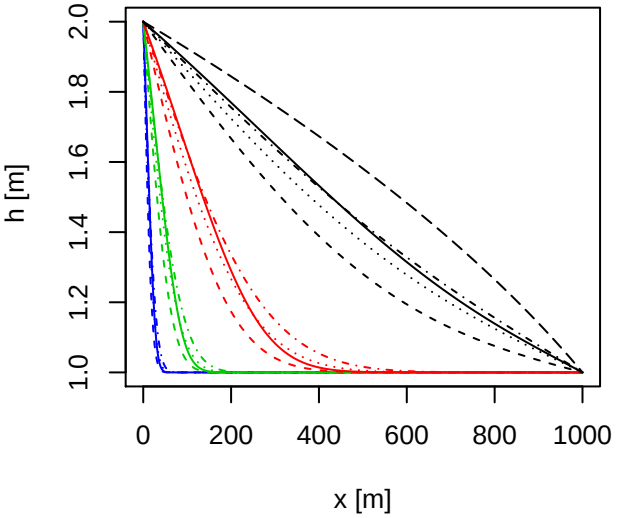

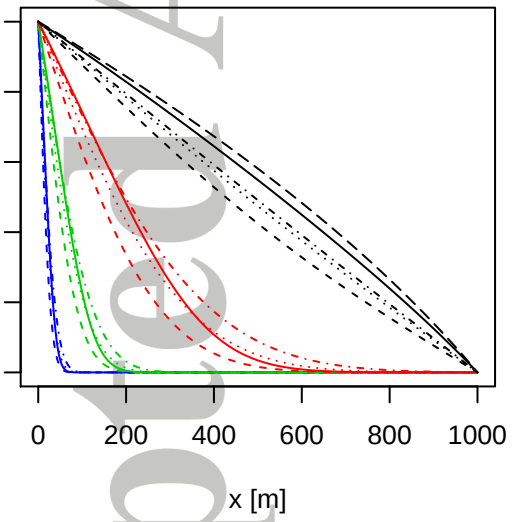

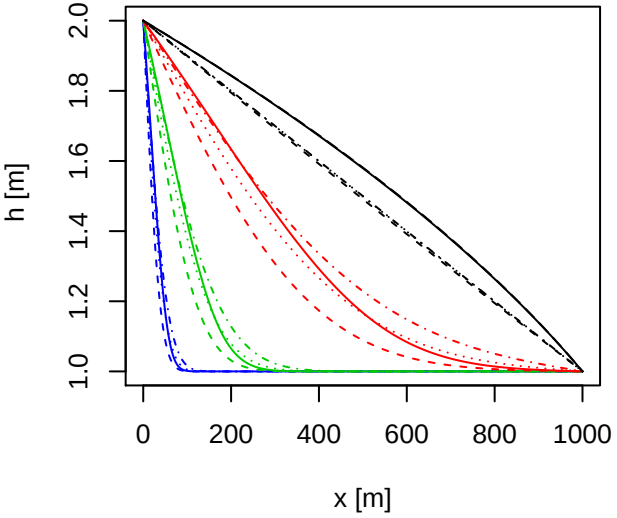

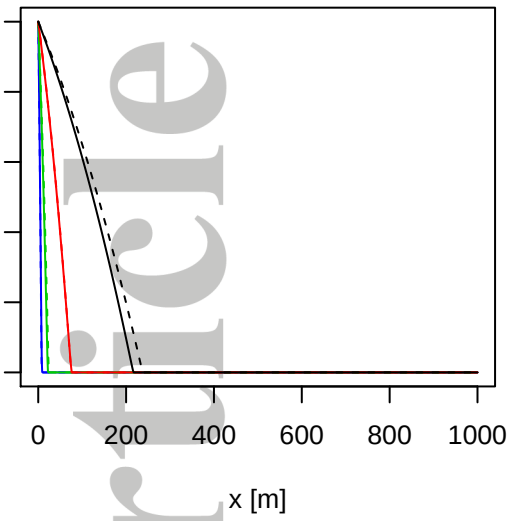

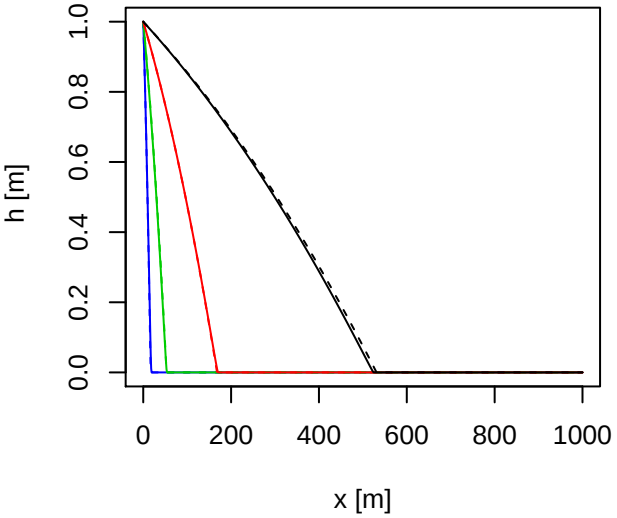

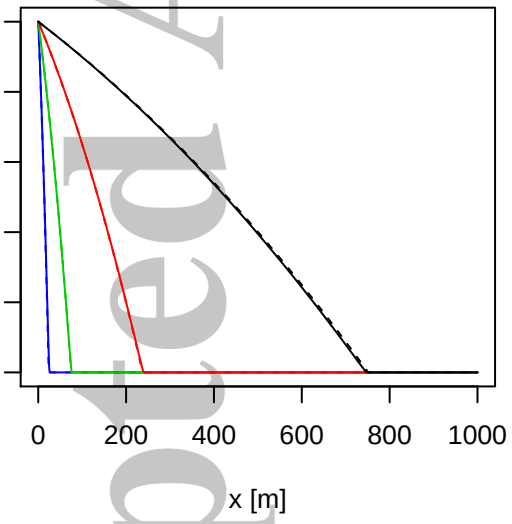

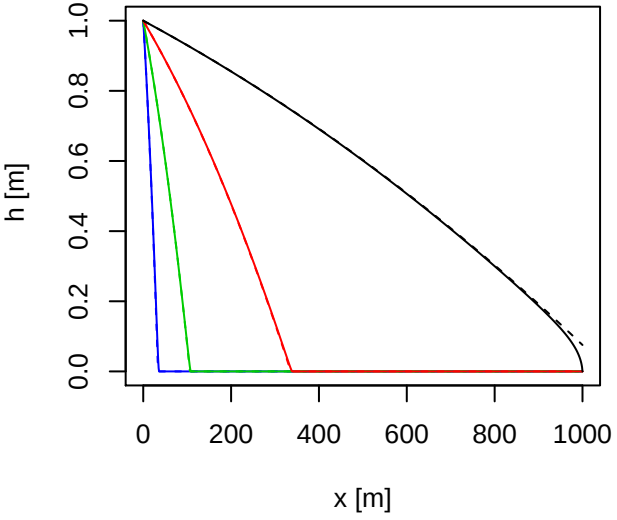

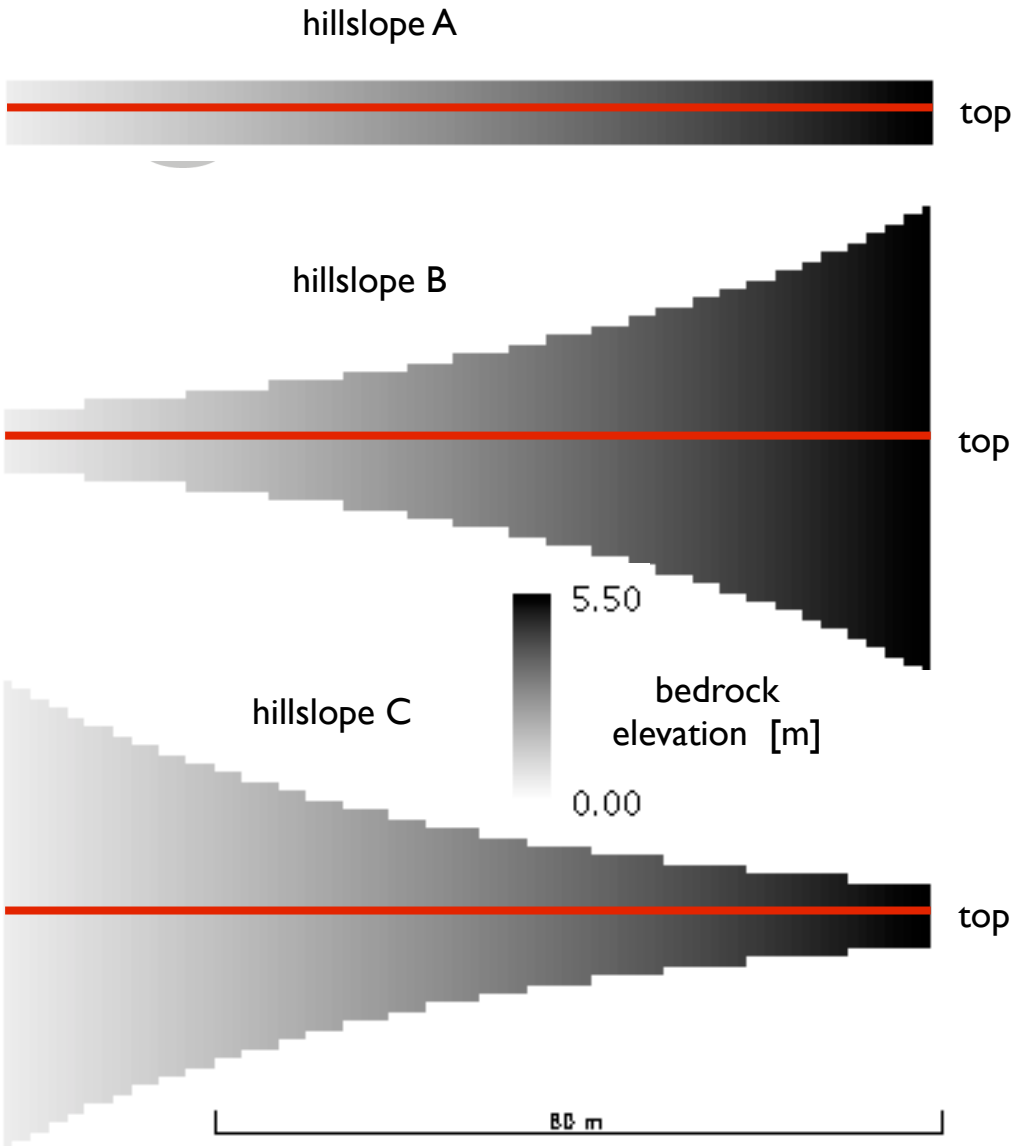
hillslope A
top
hillslope B
top
5.50
bedrock
elevation [m]
hillslope C
0.00
top
80 m

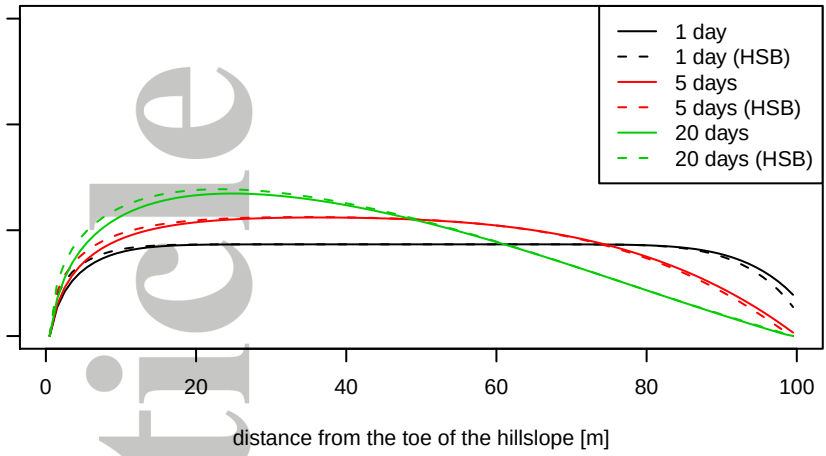

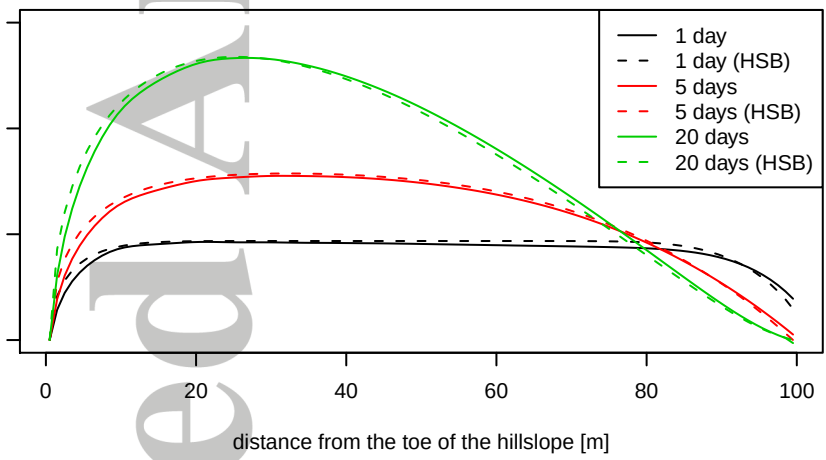

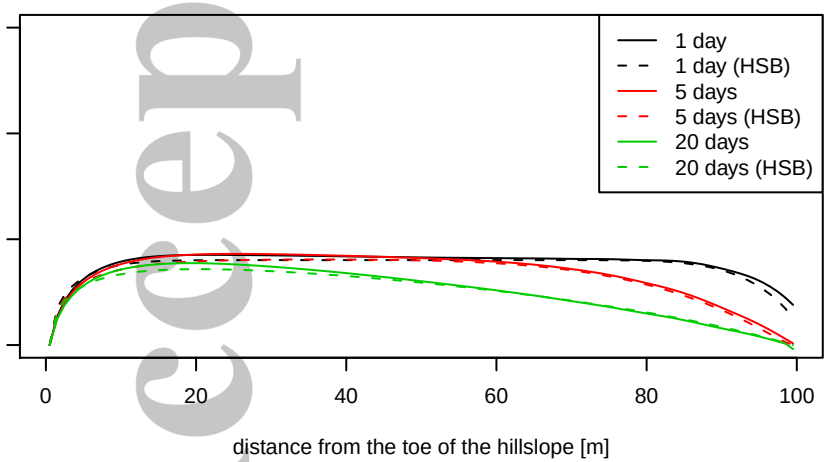

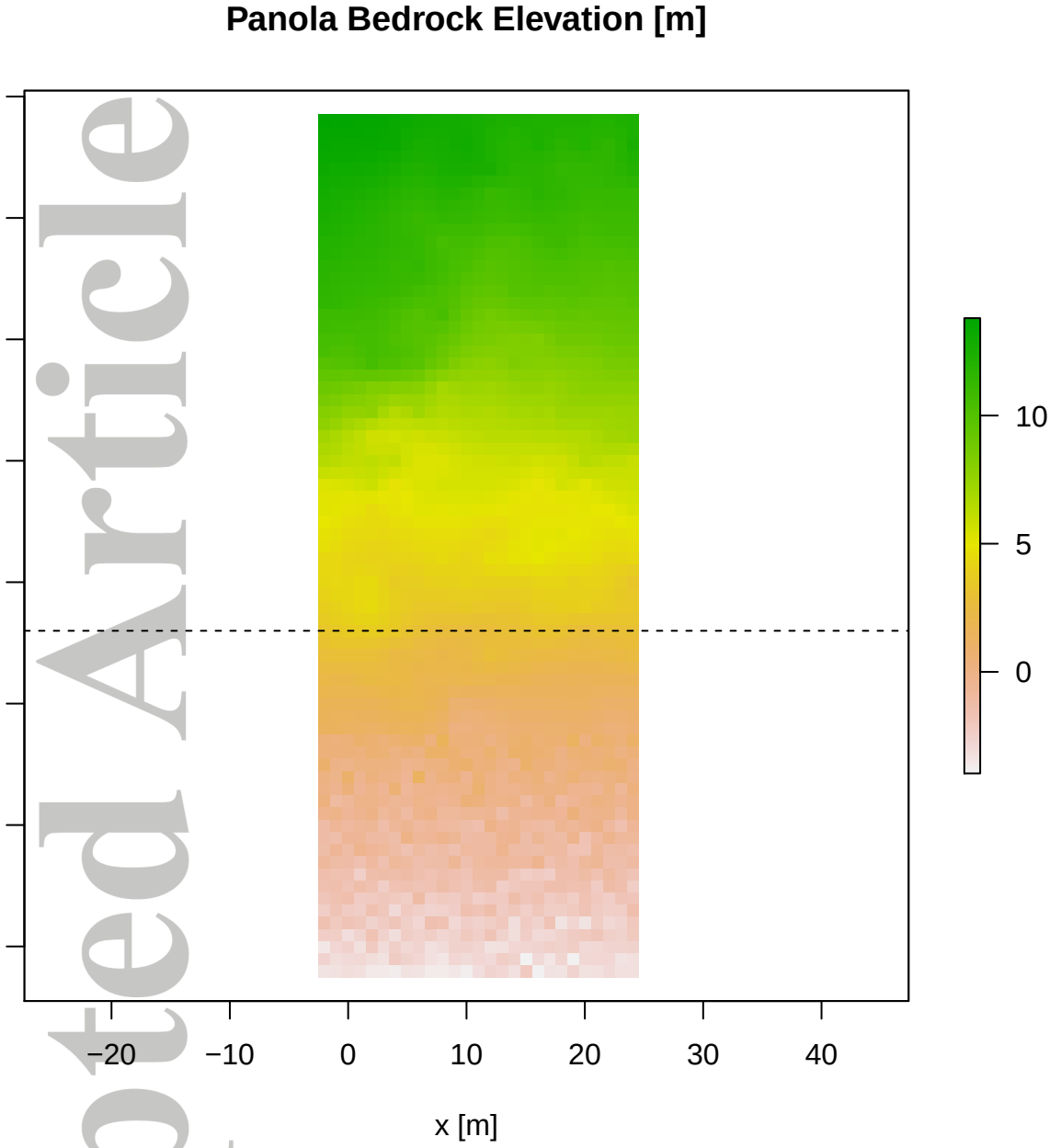

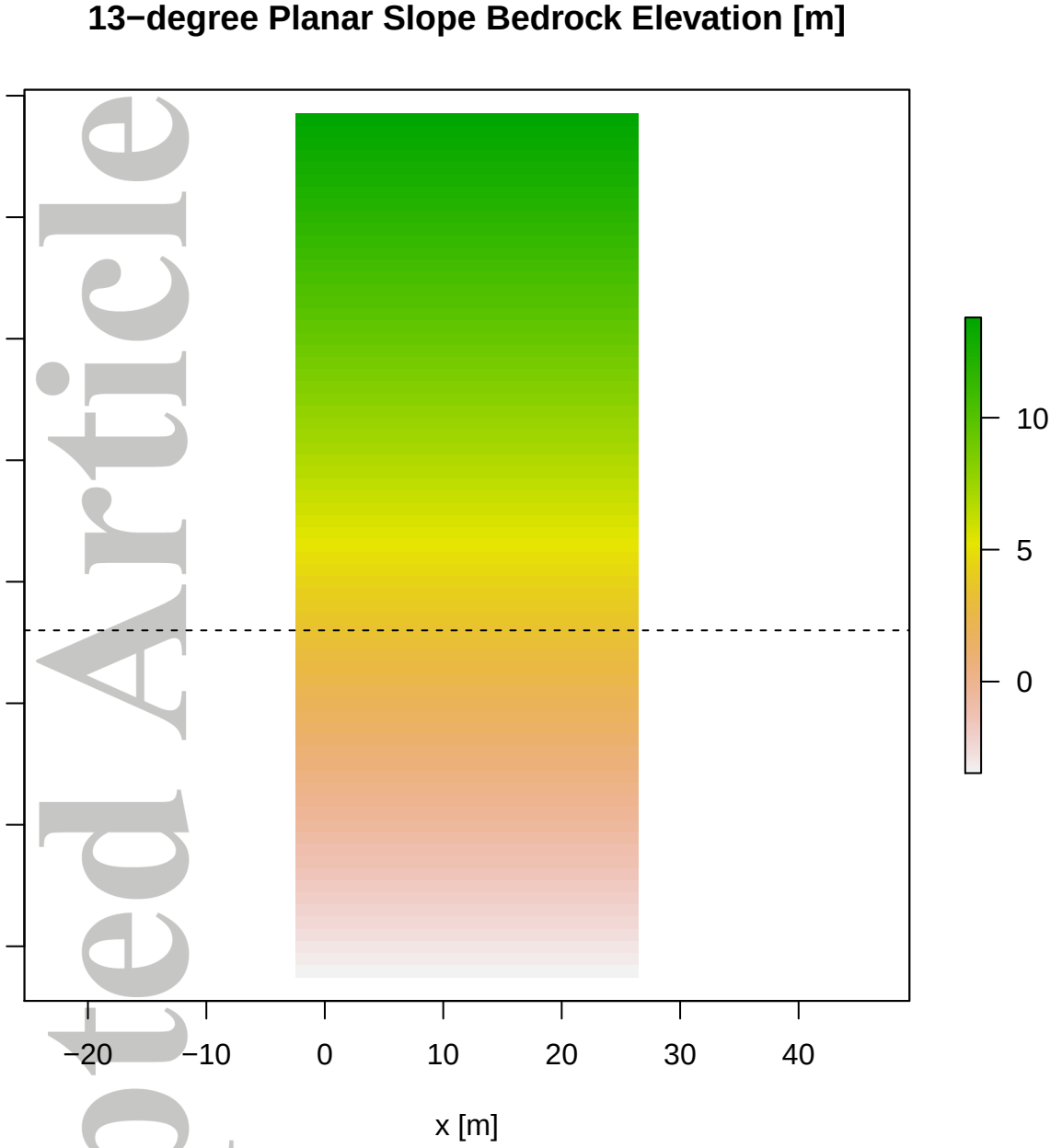

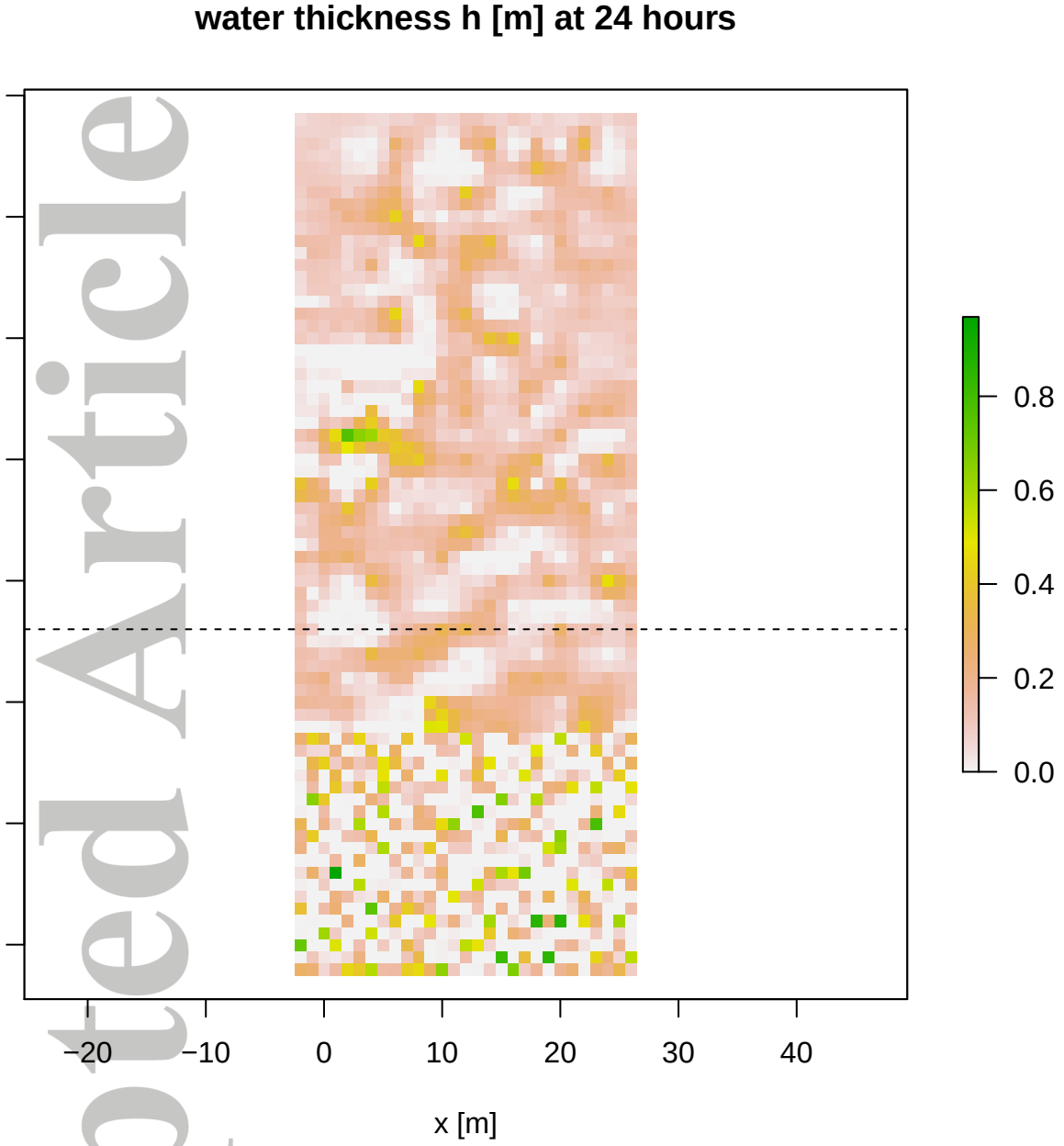

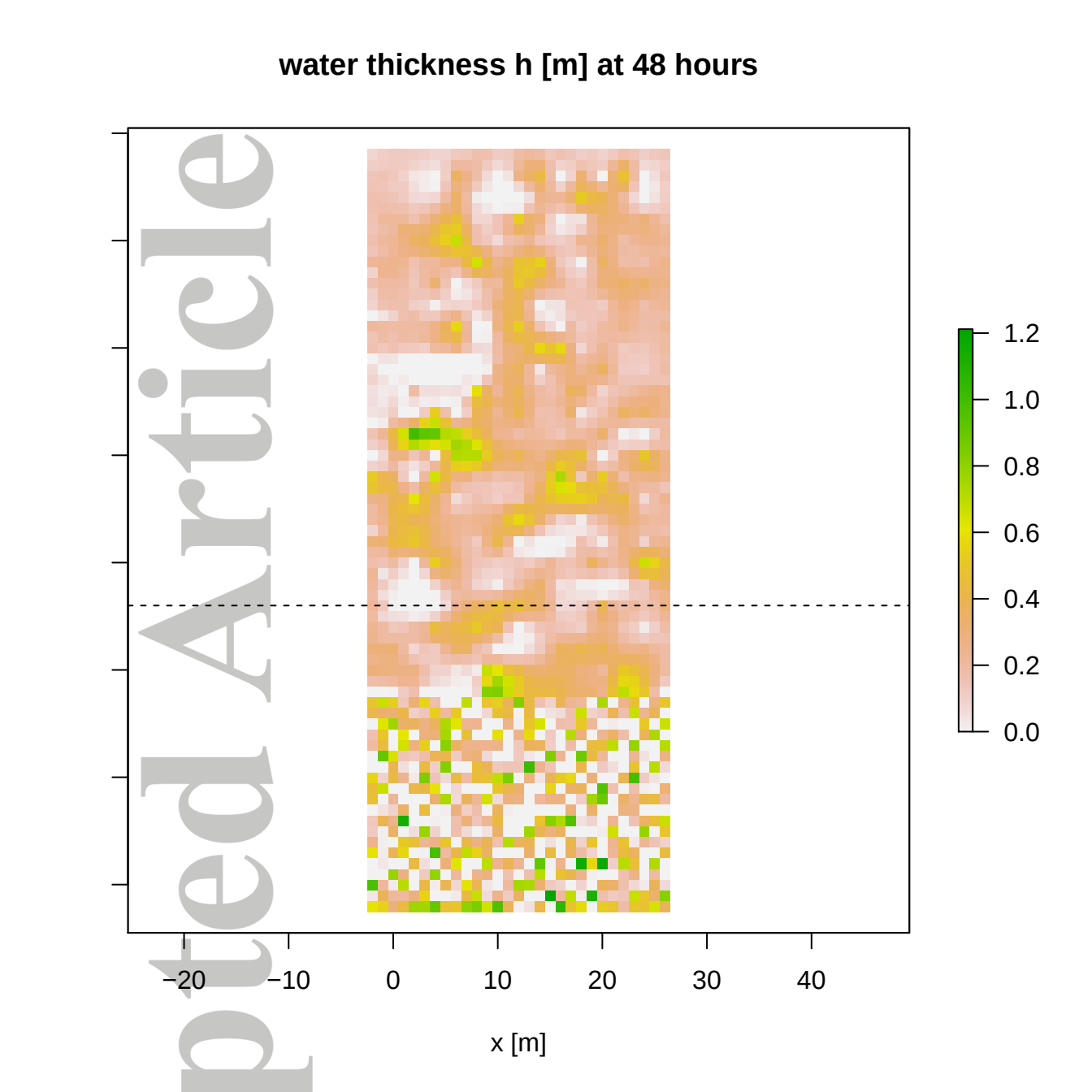

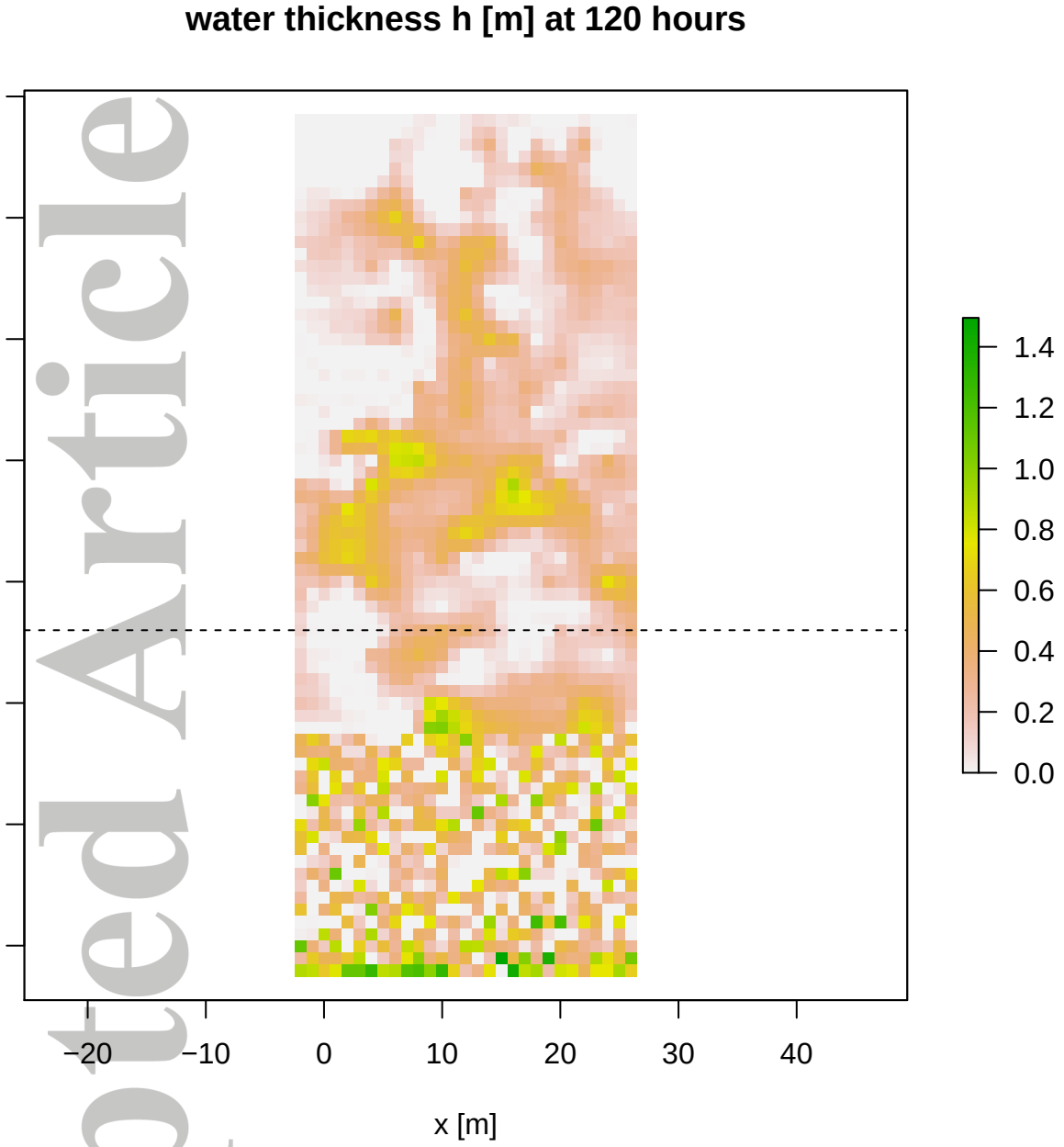

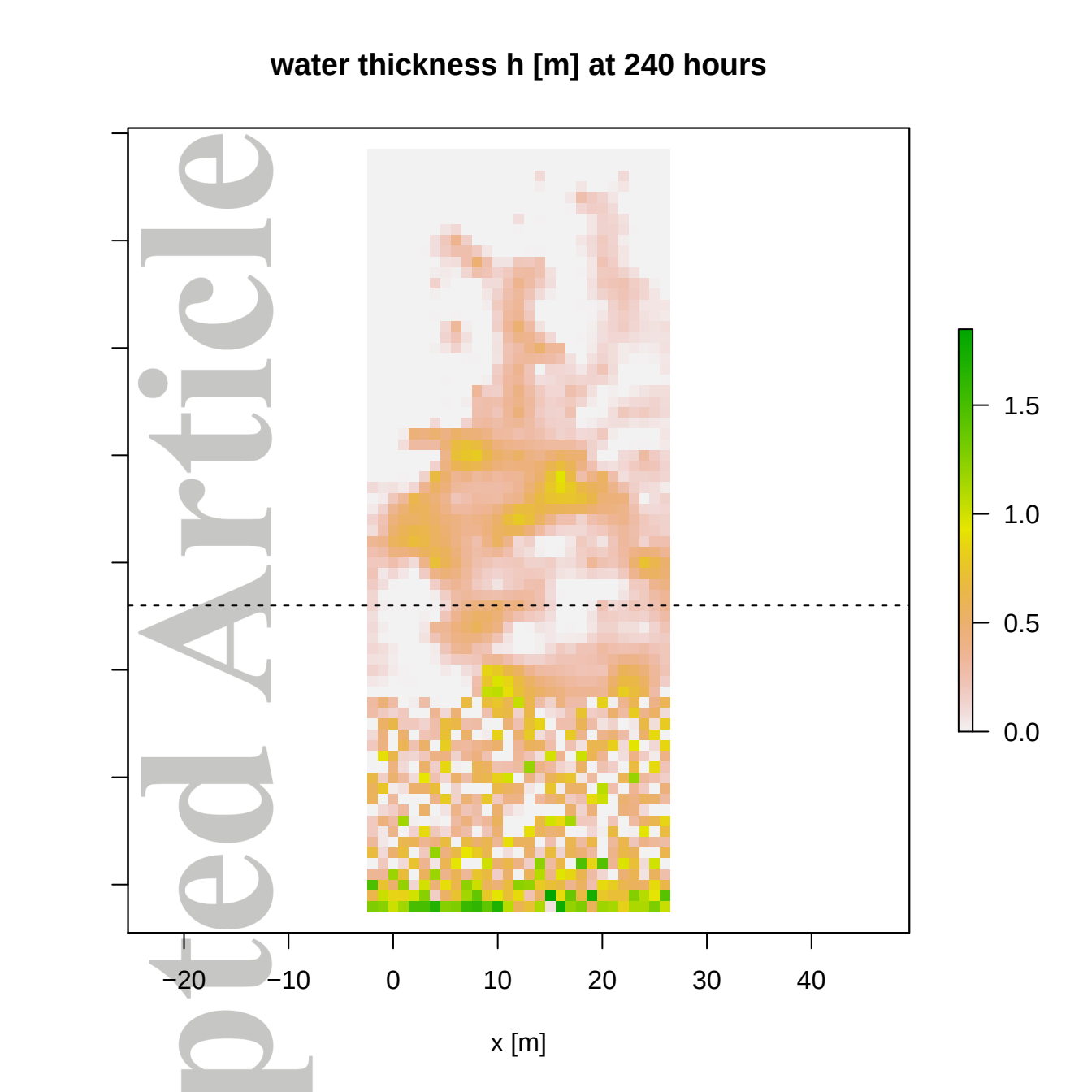

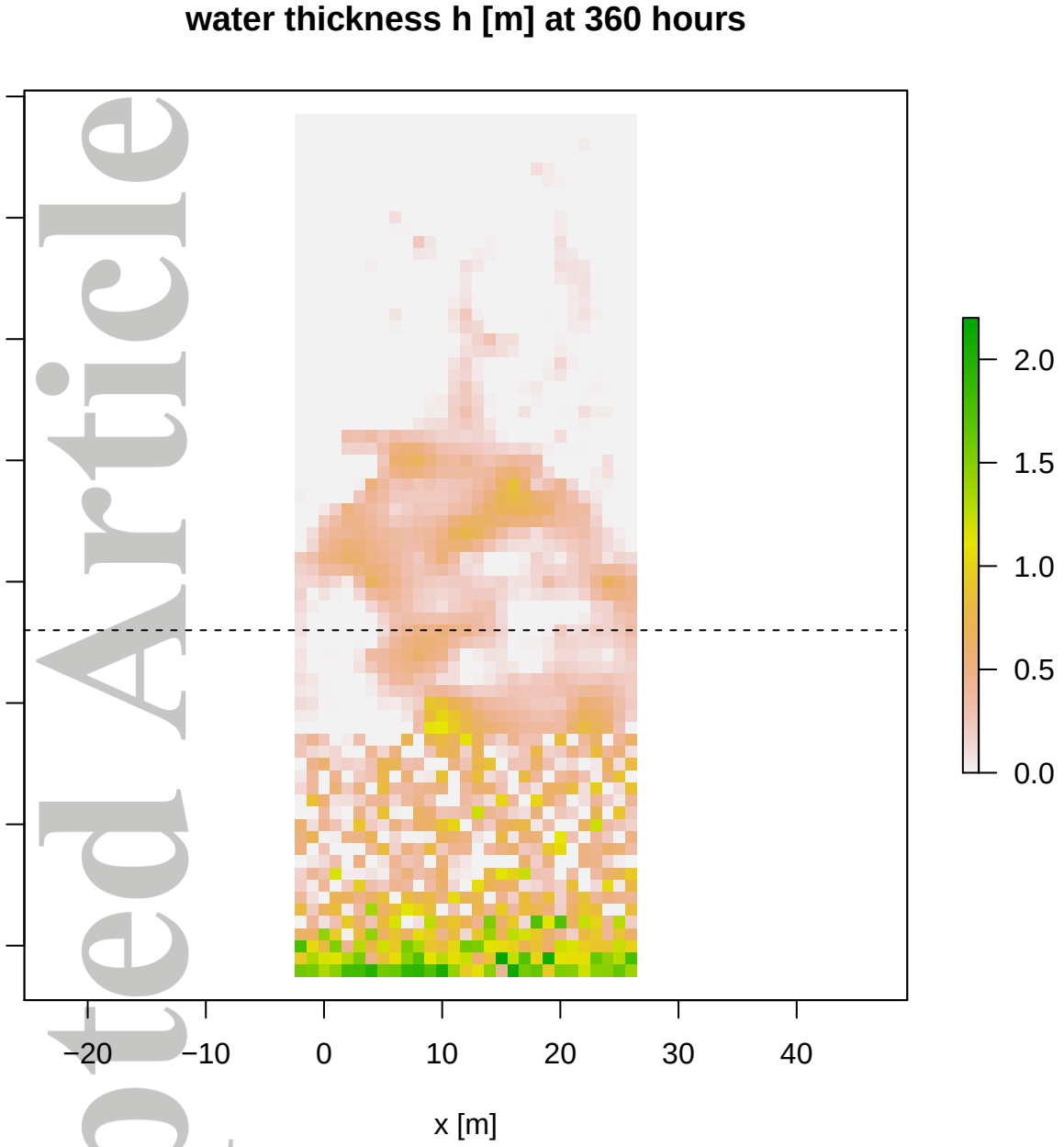

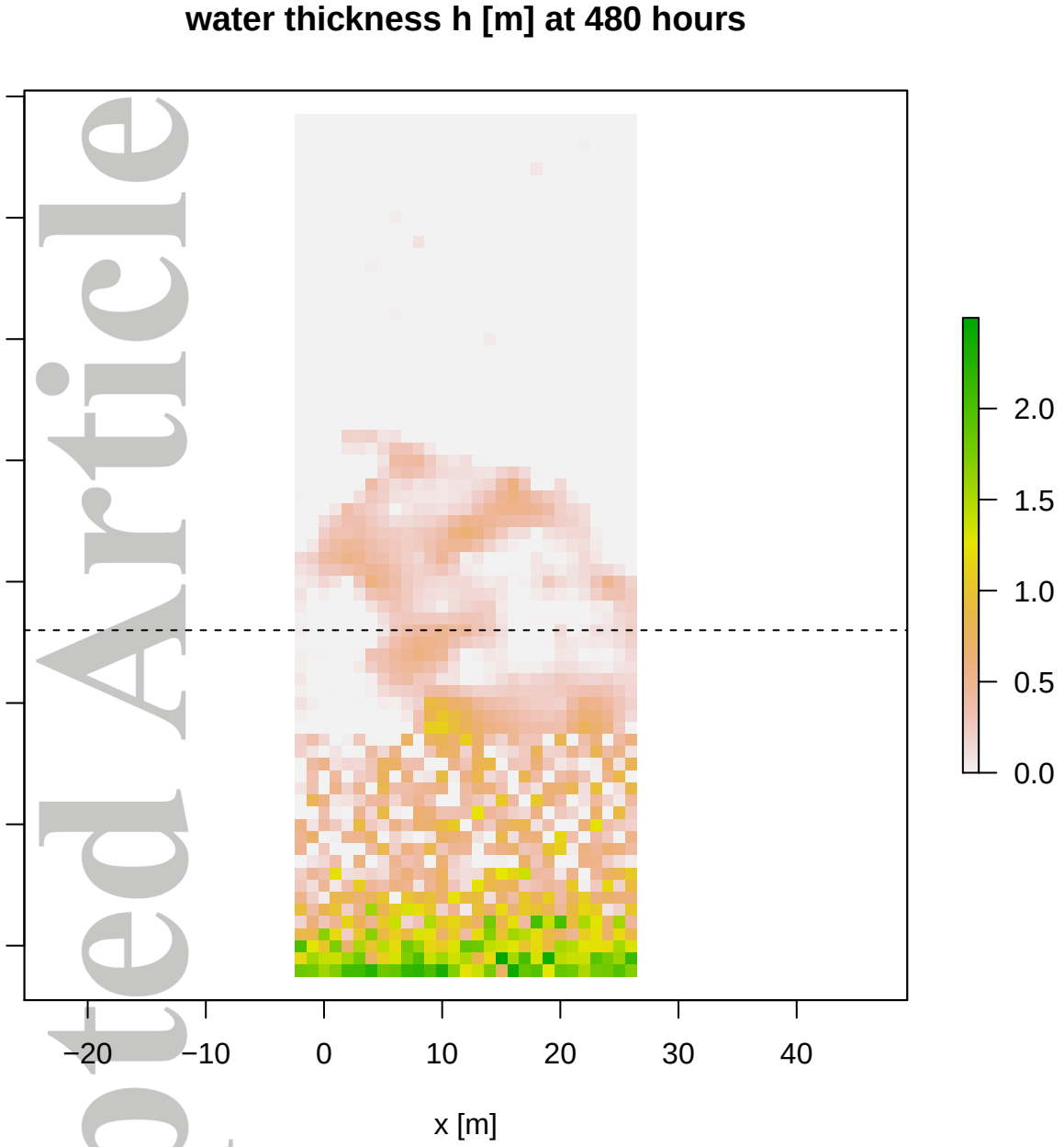

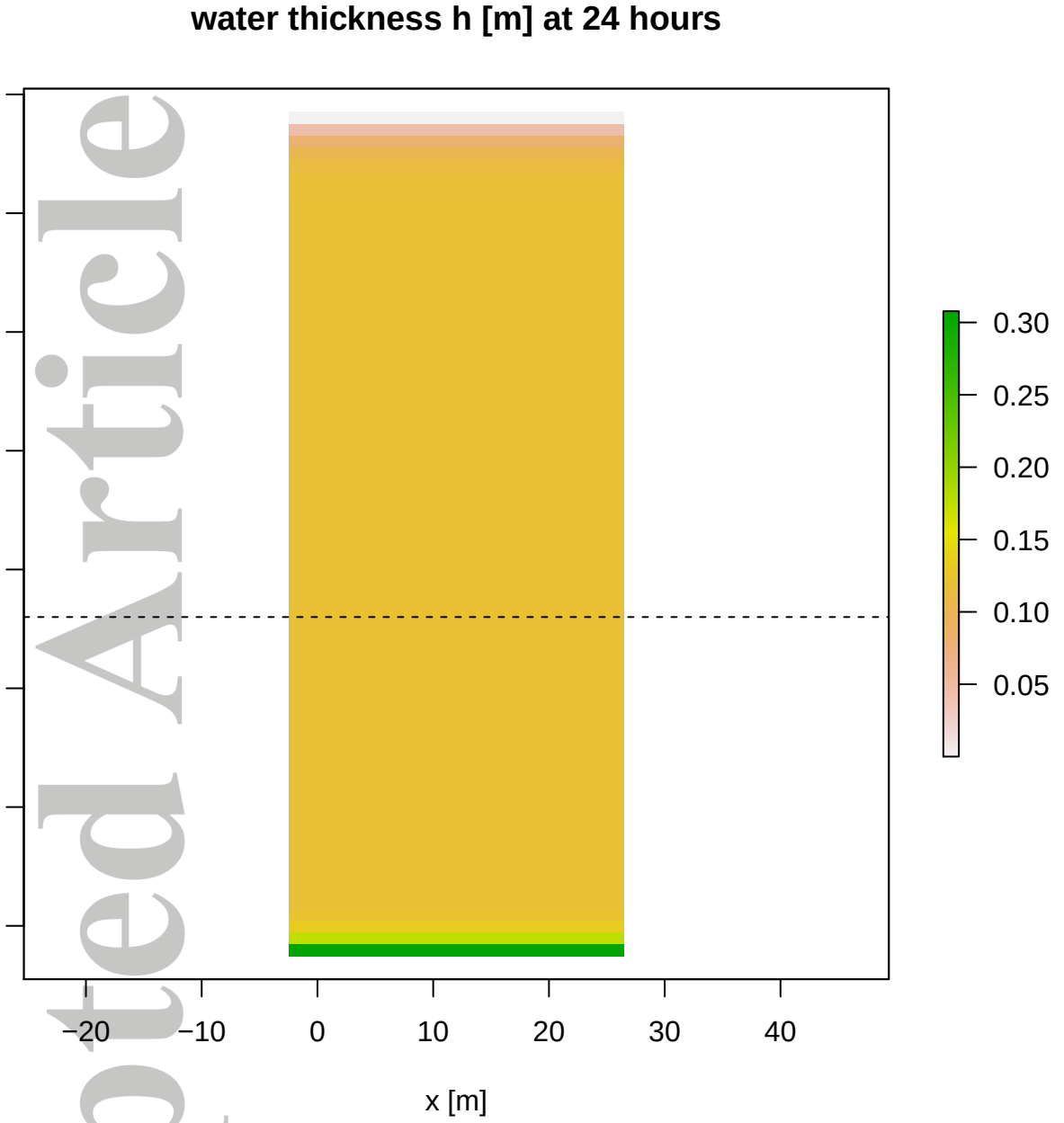

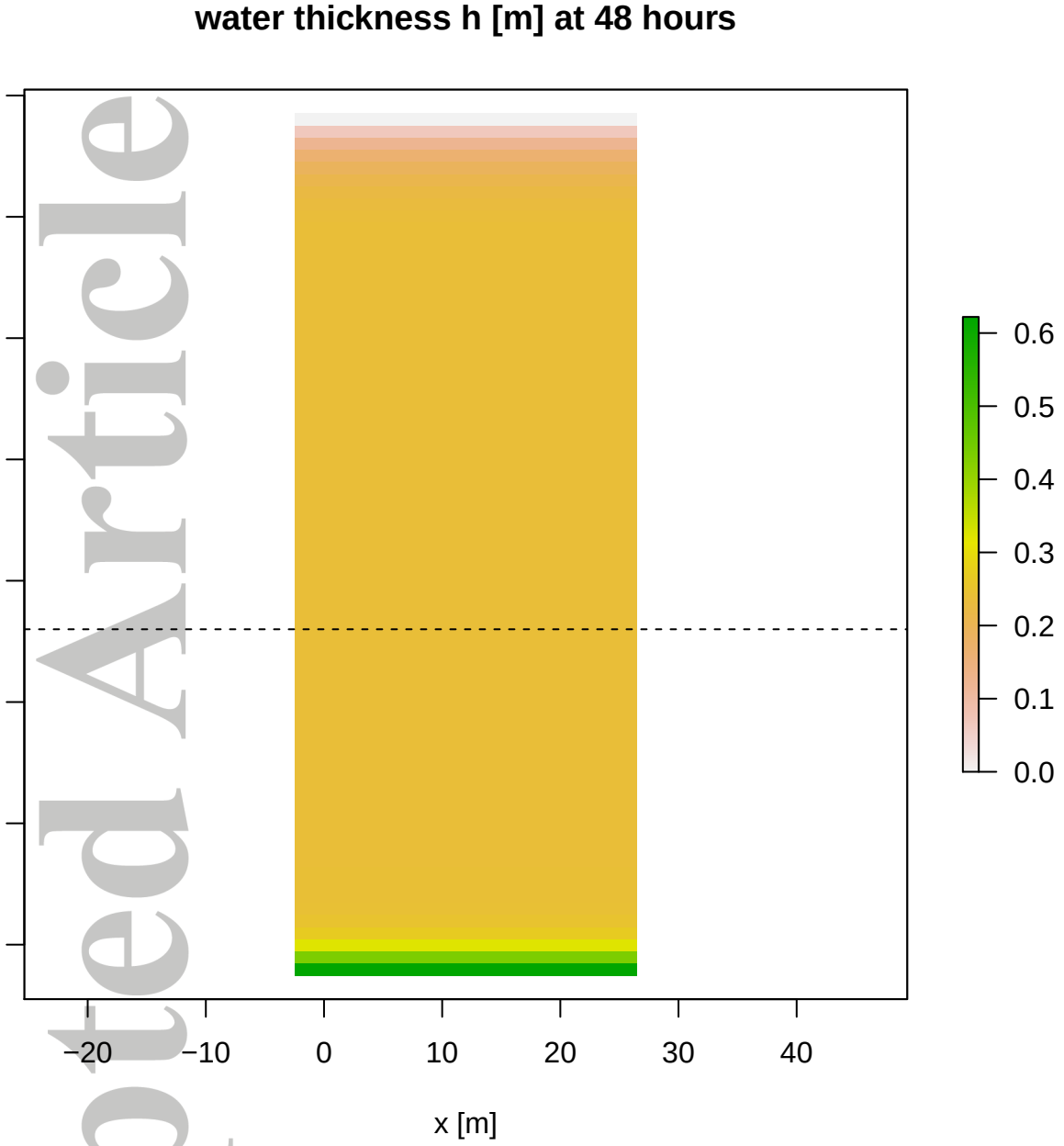

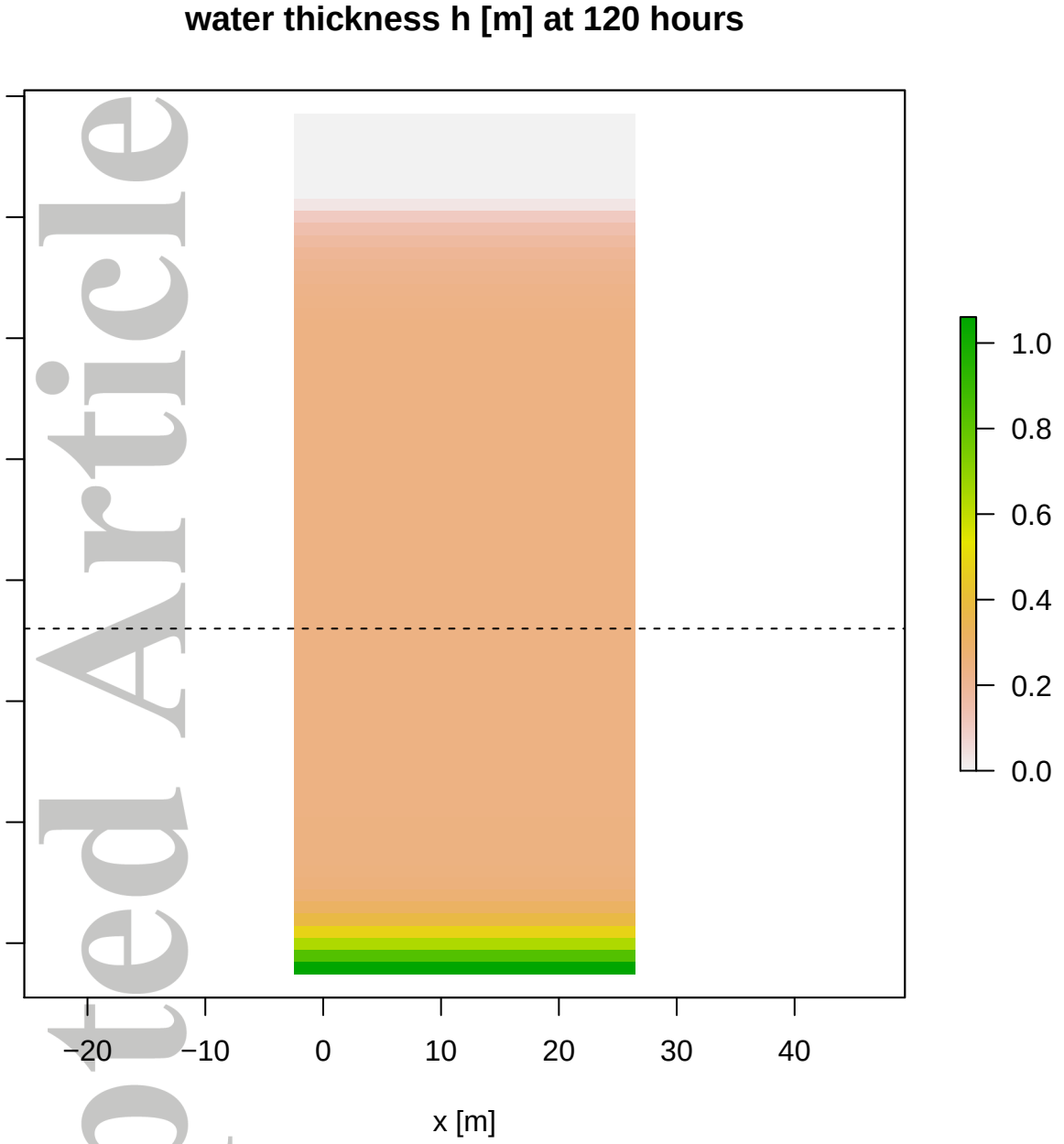

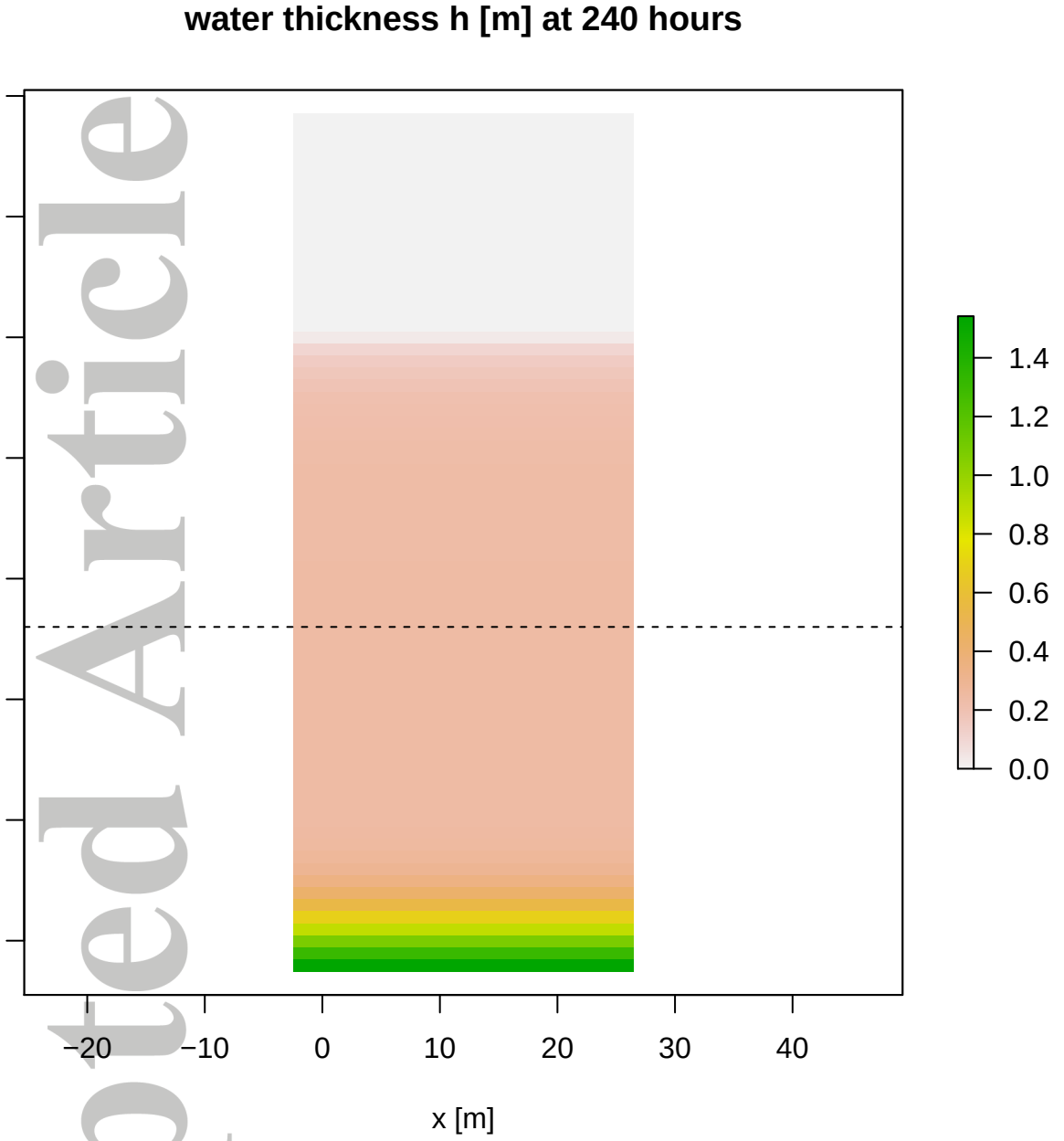

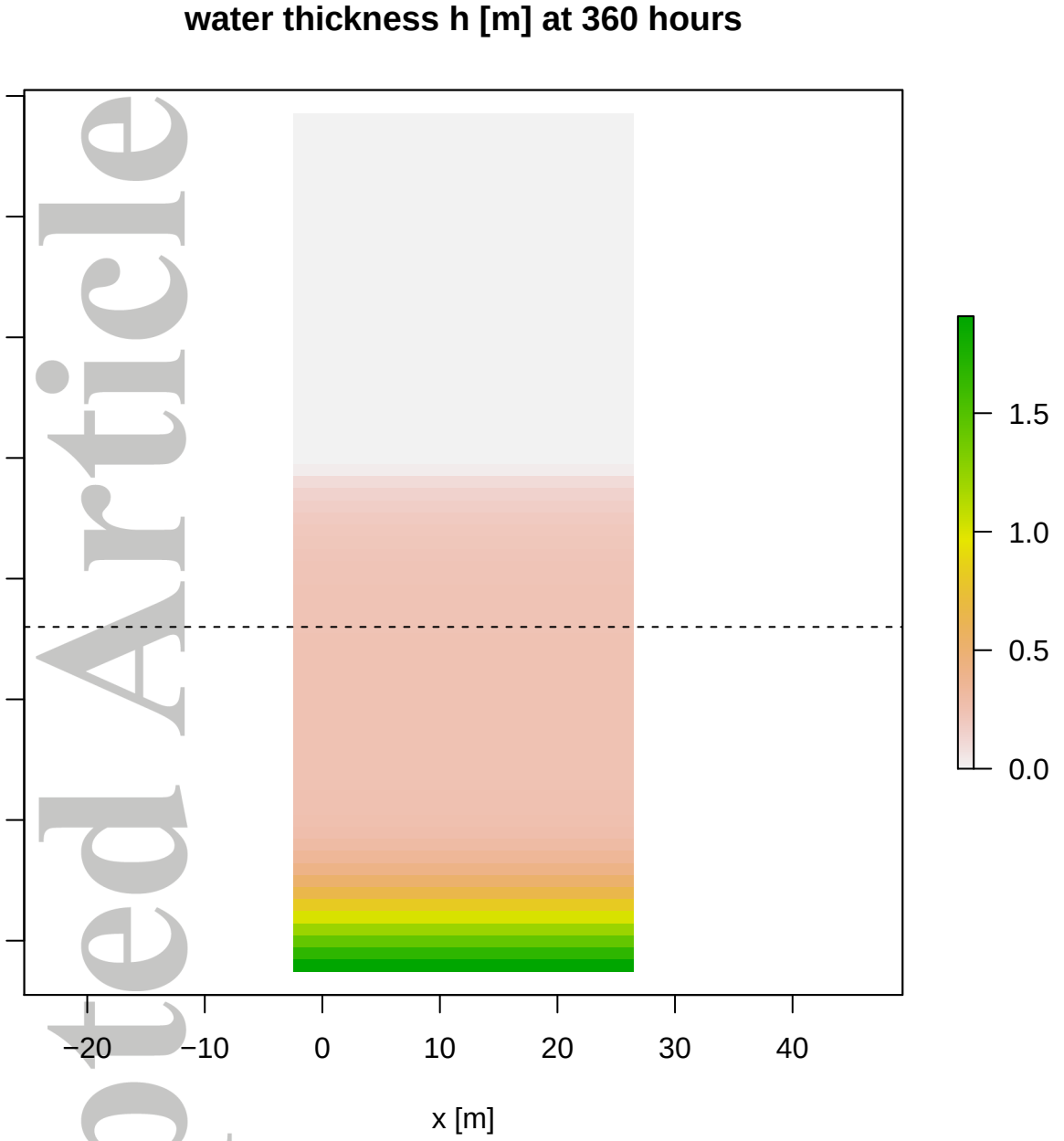

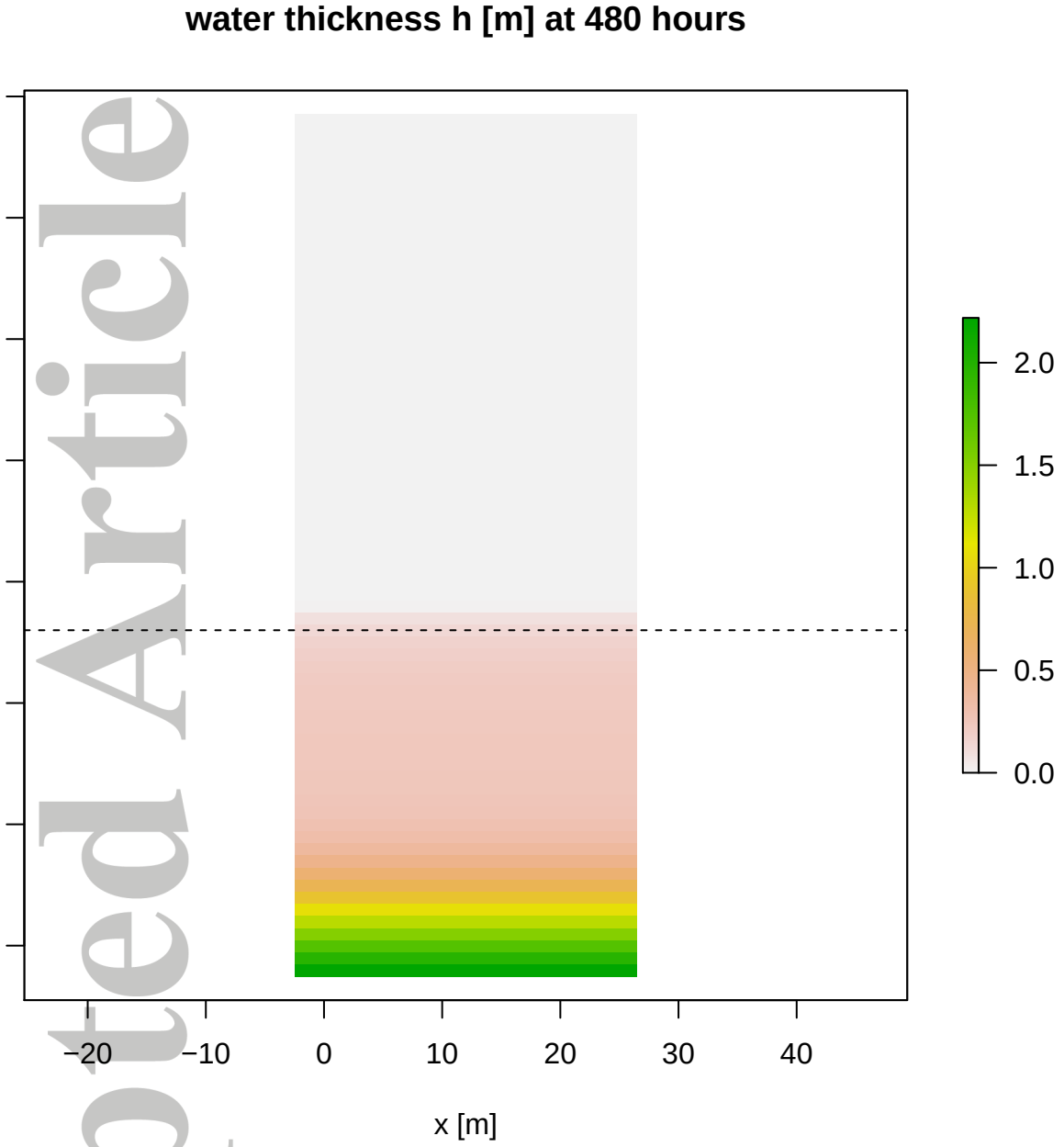

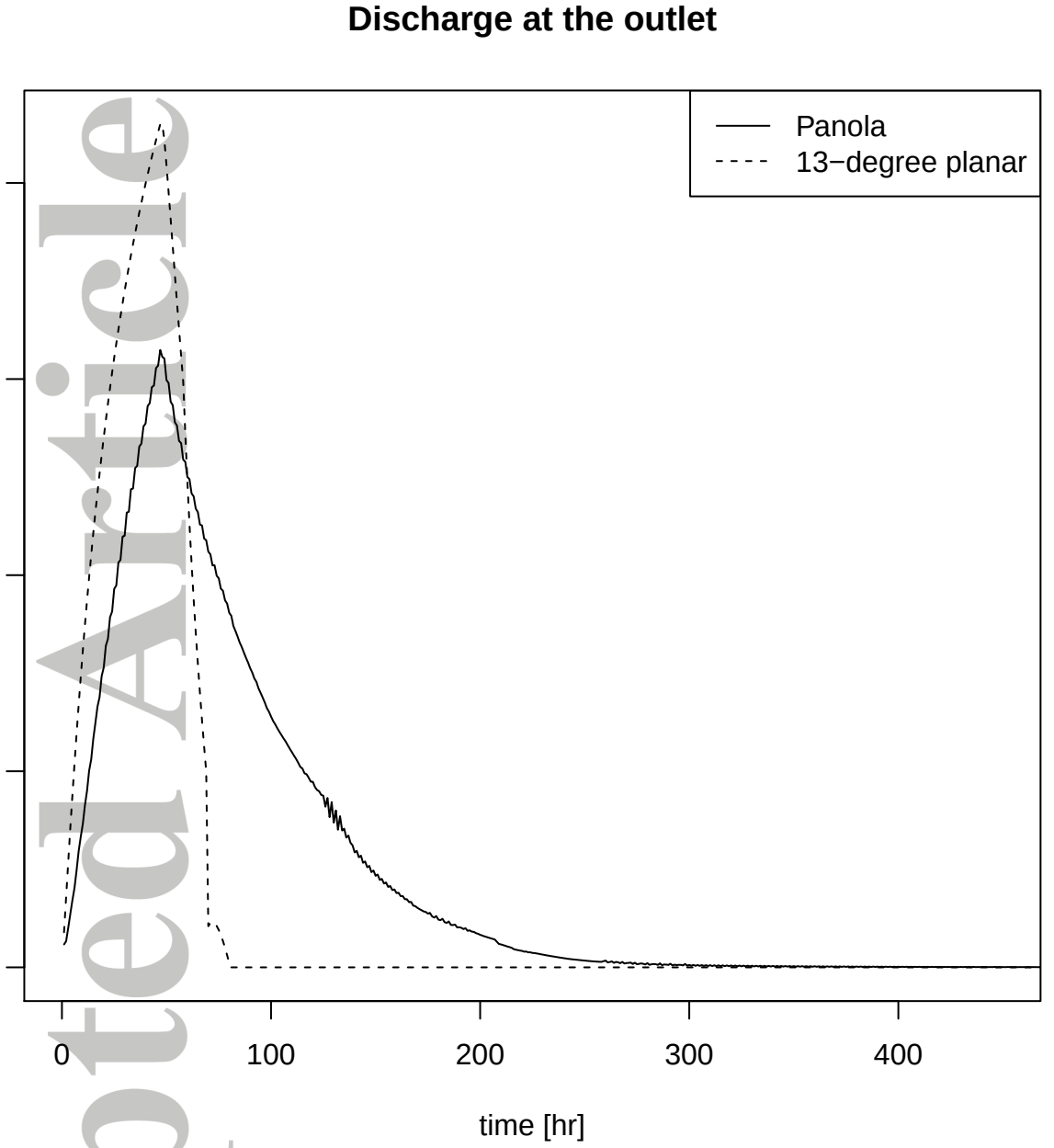

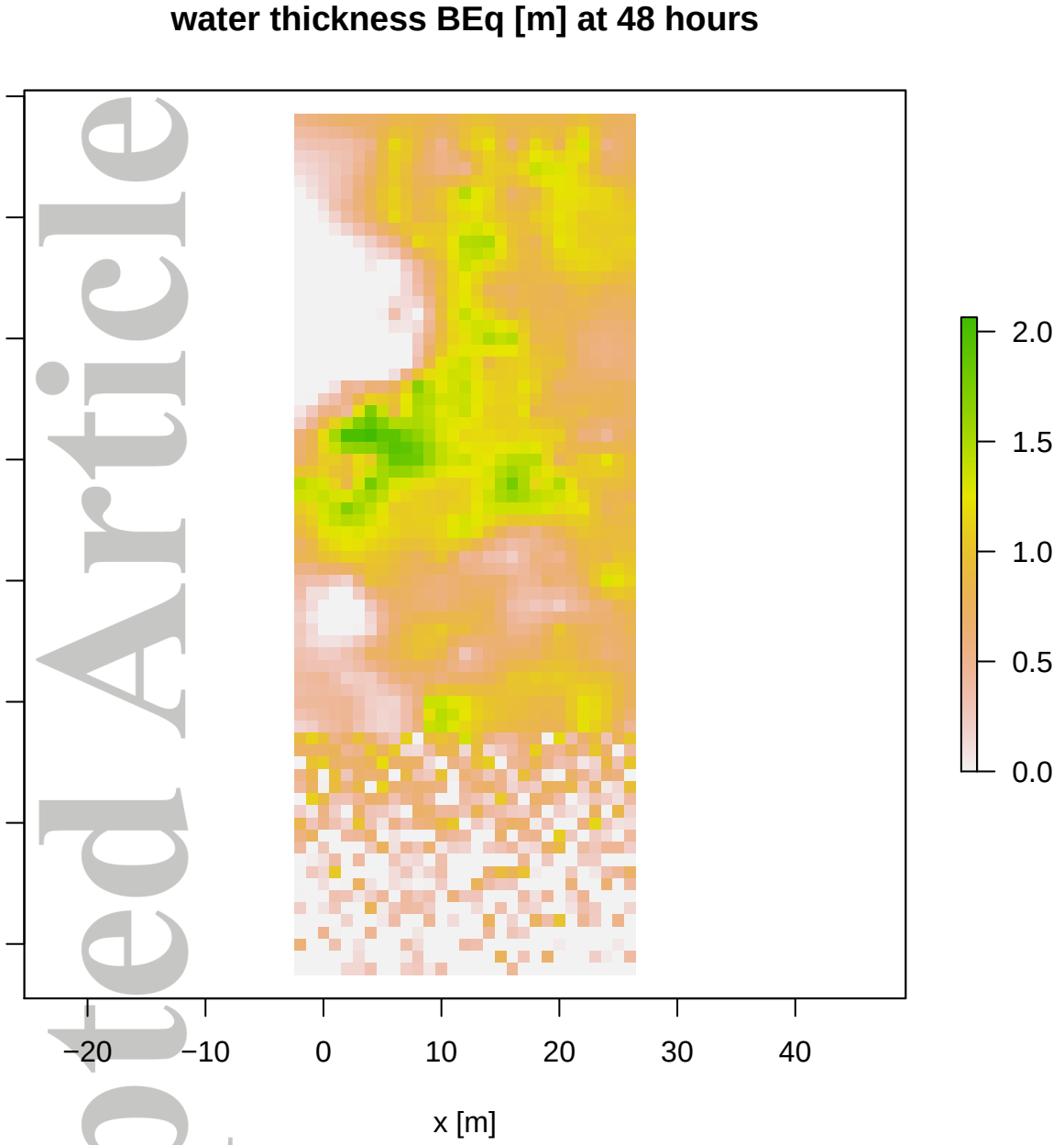

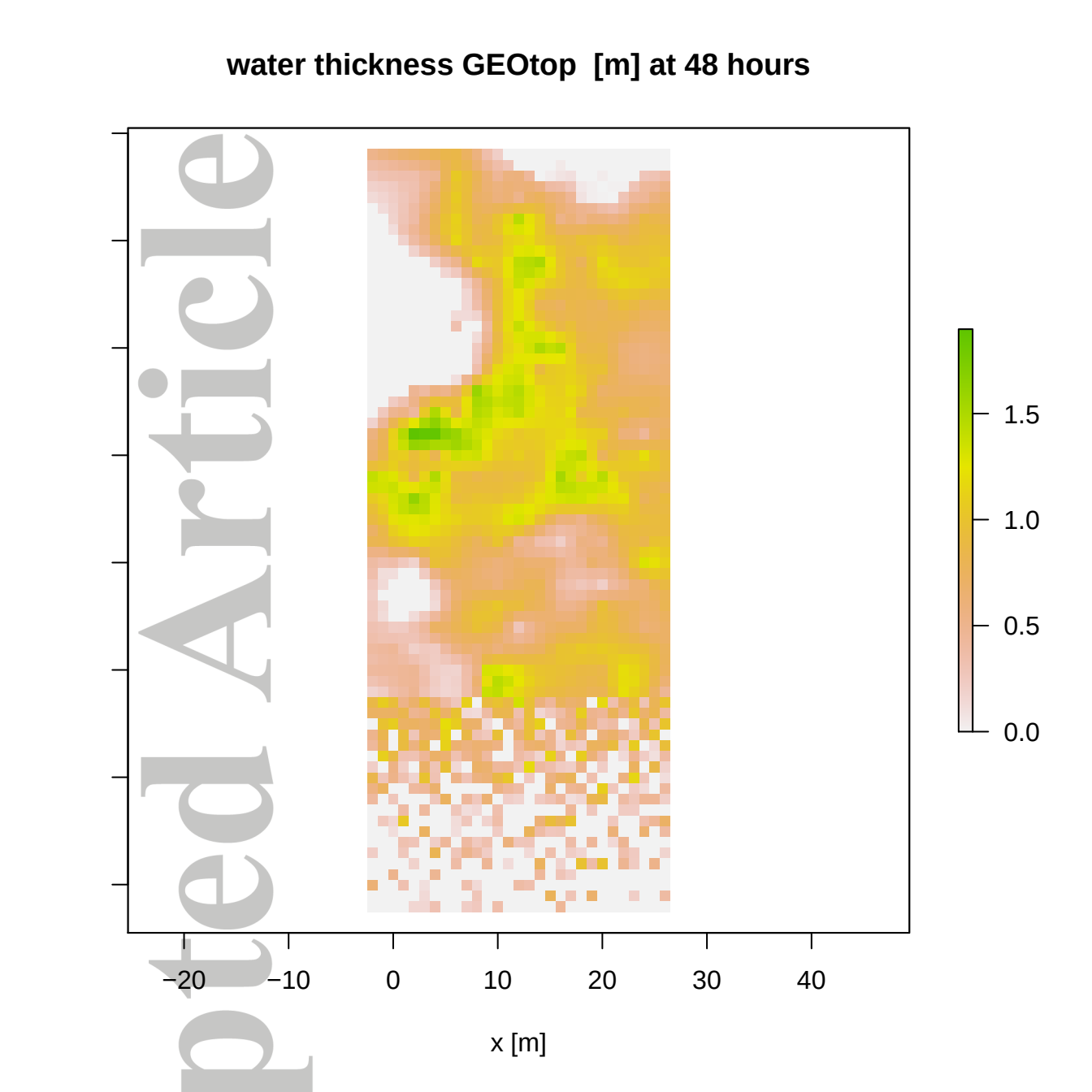

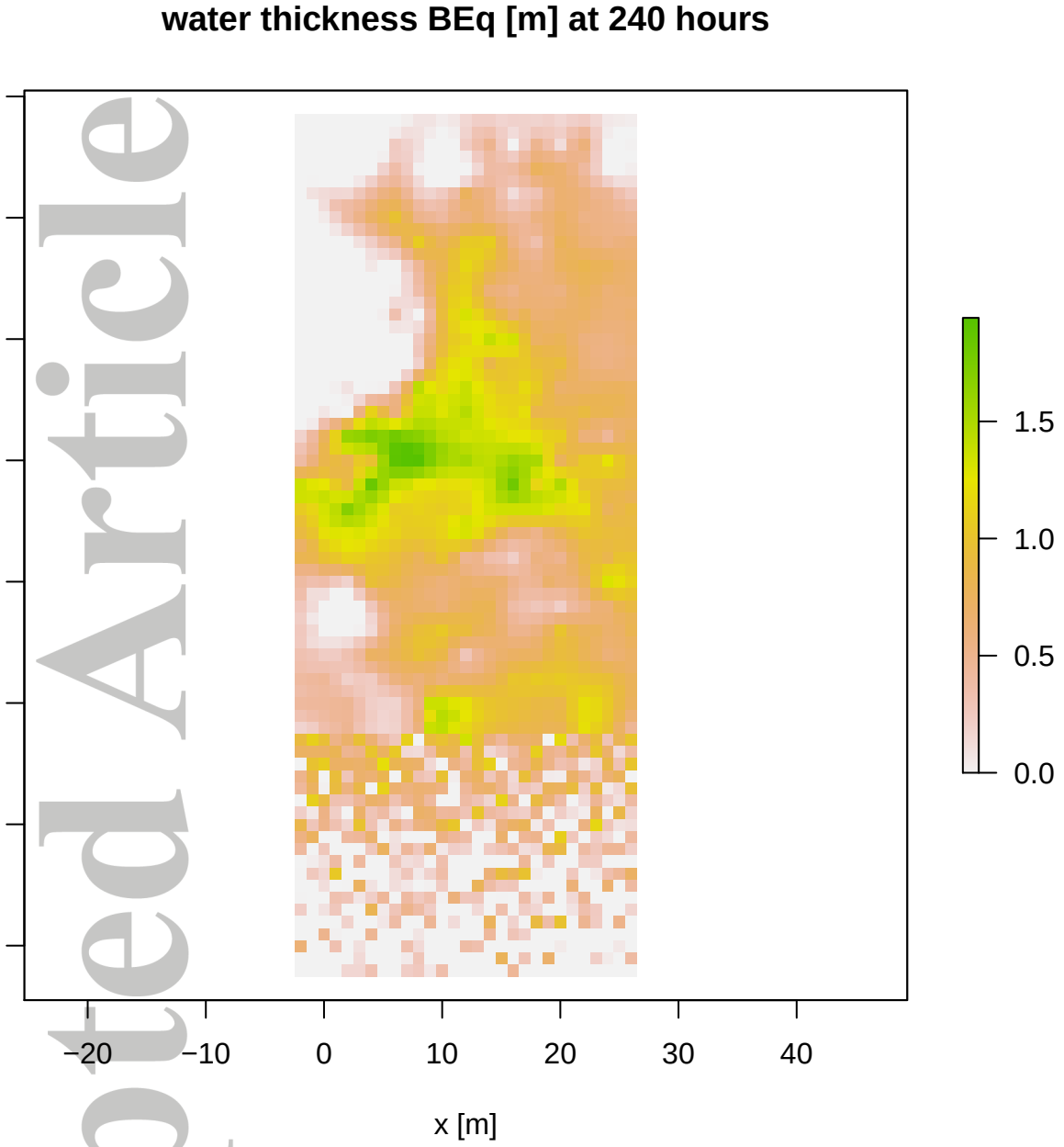

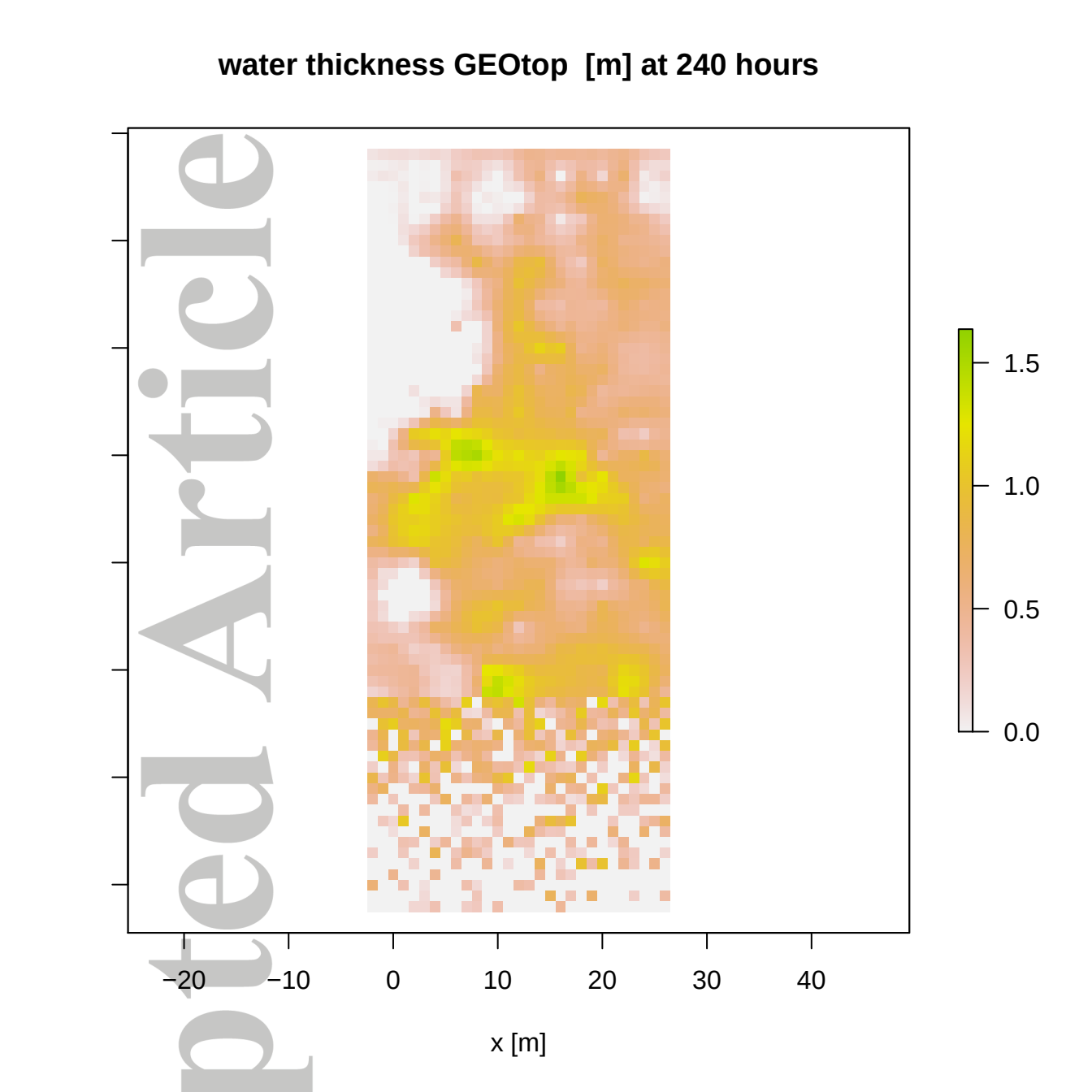

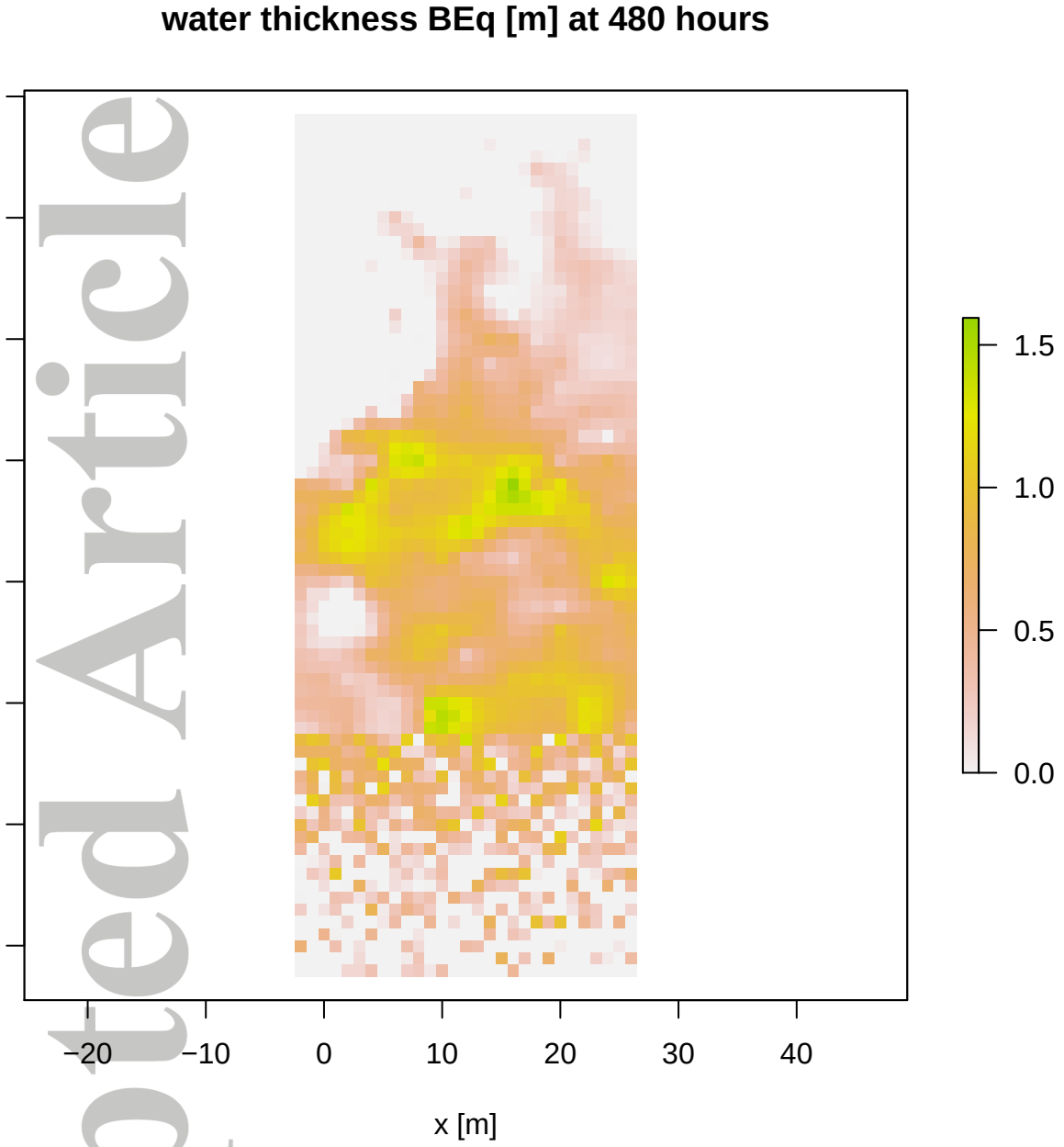

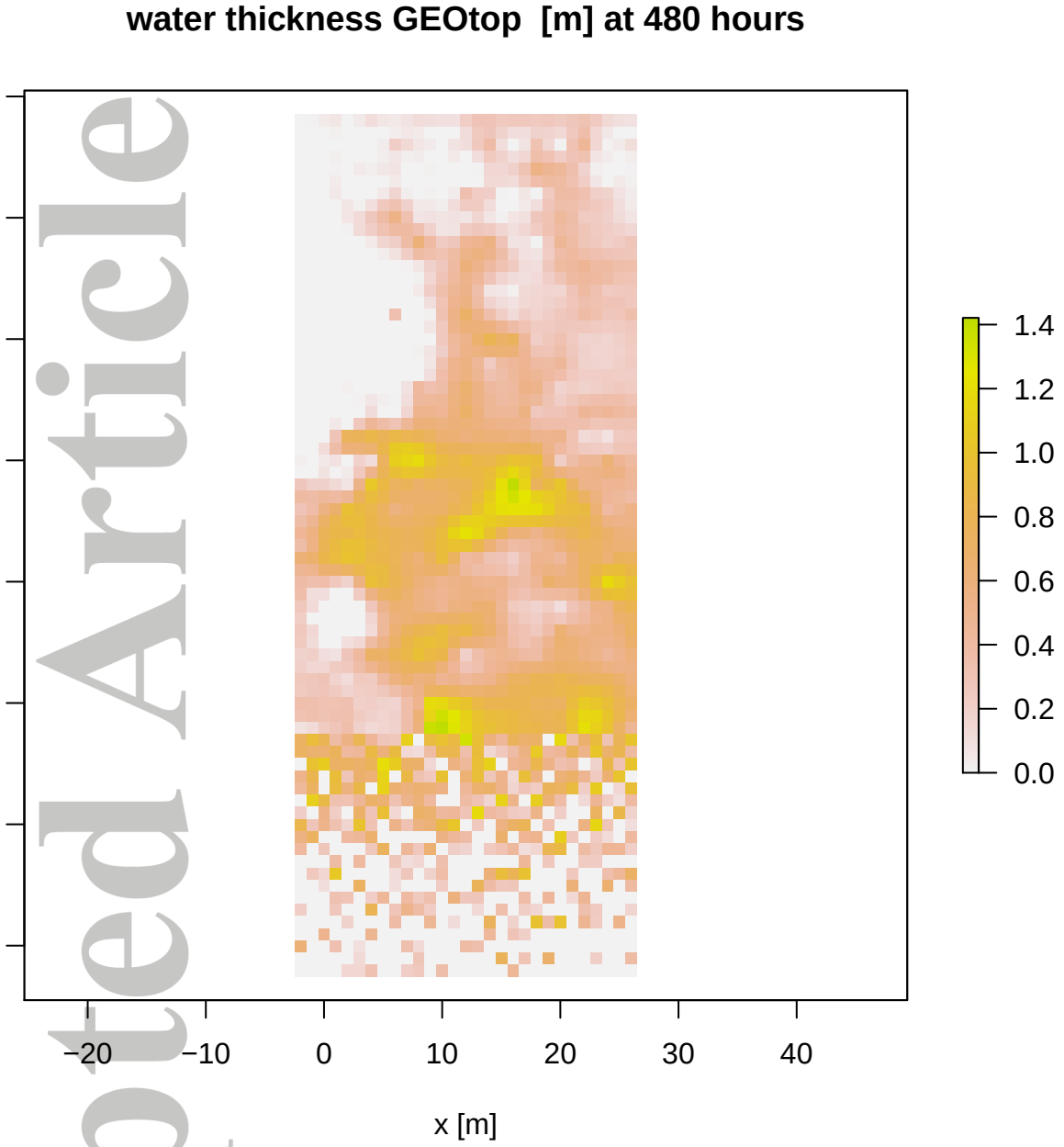

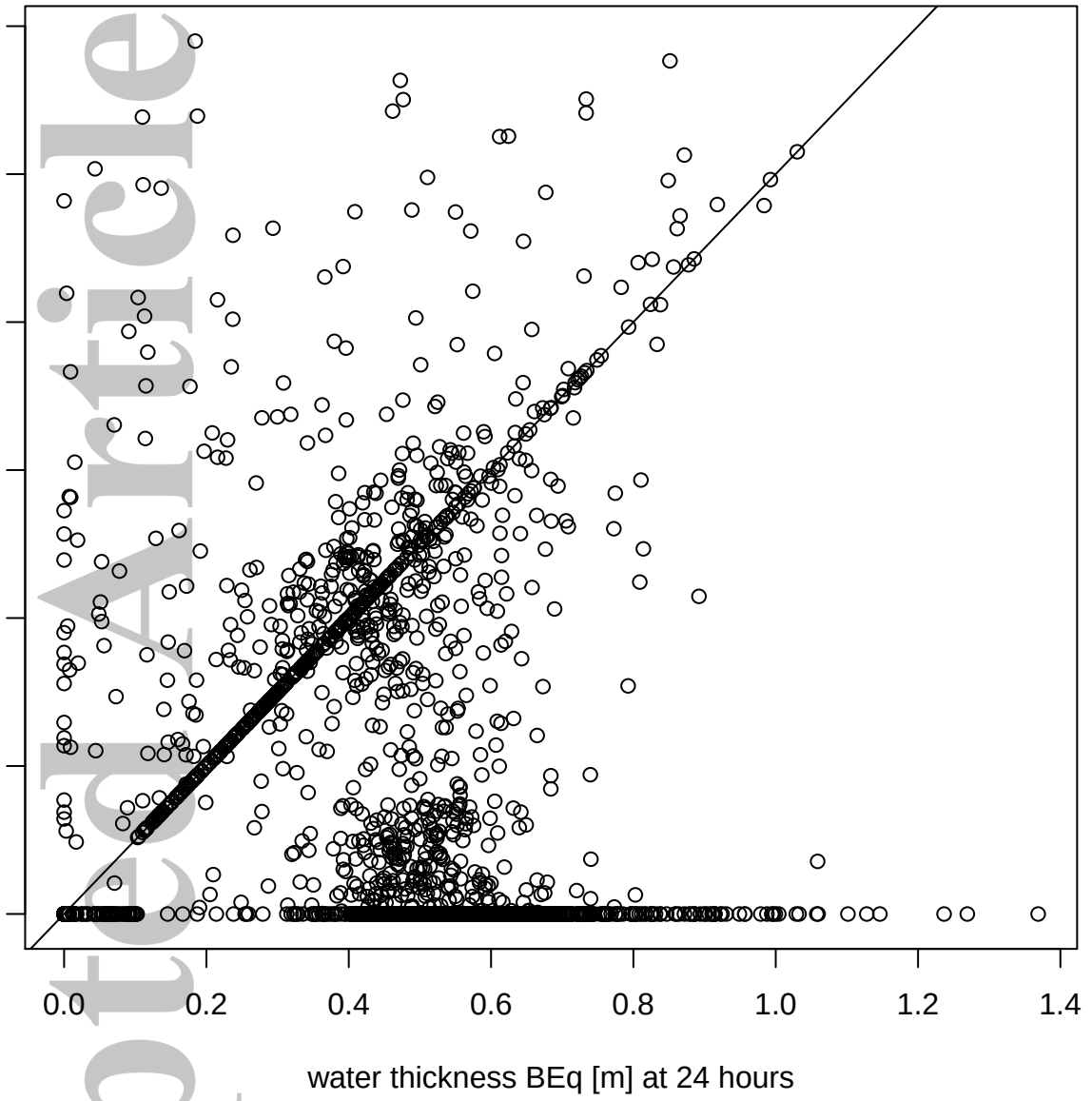

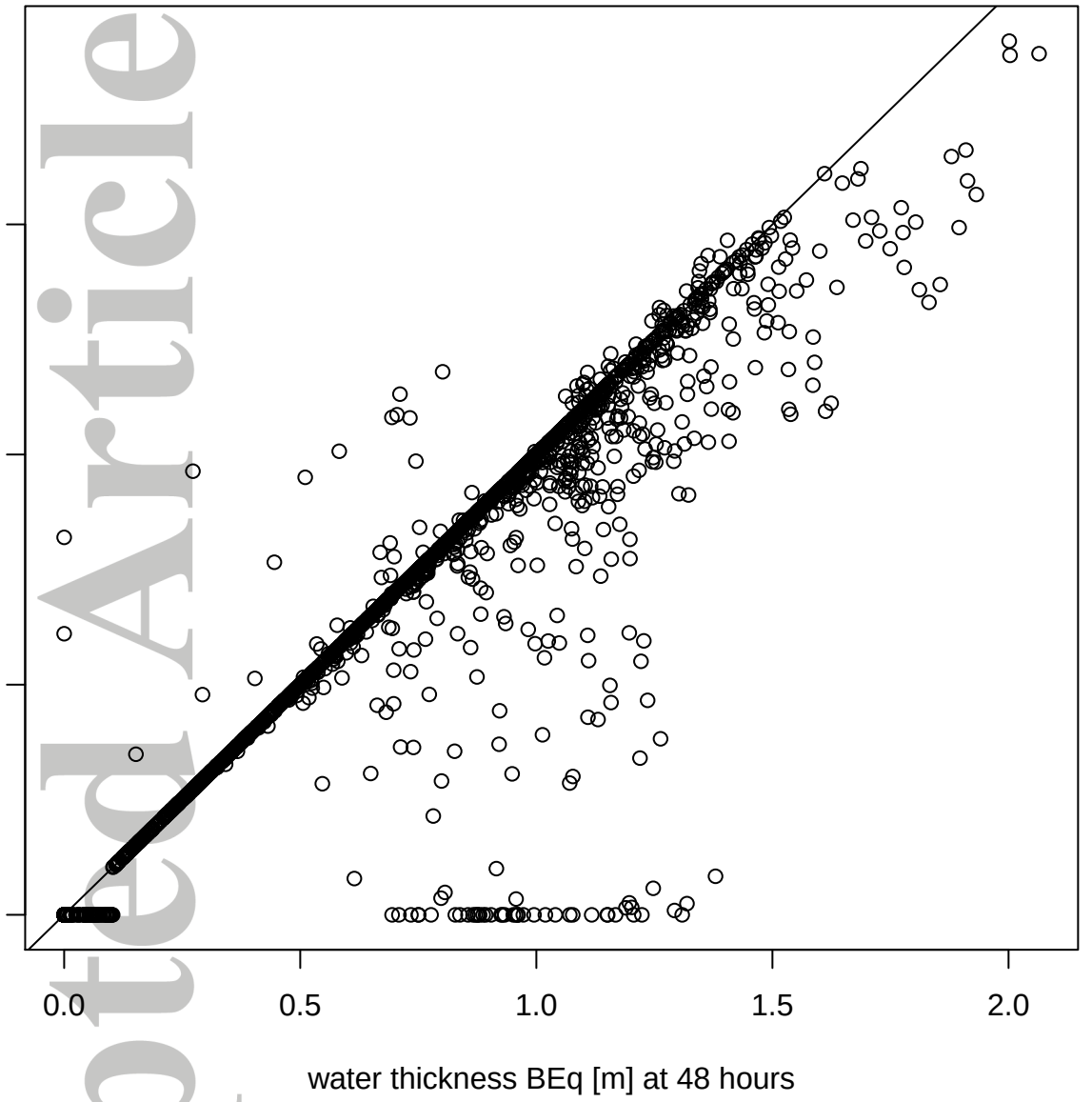

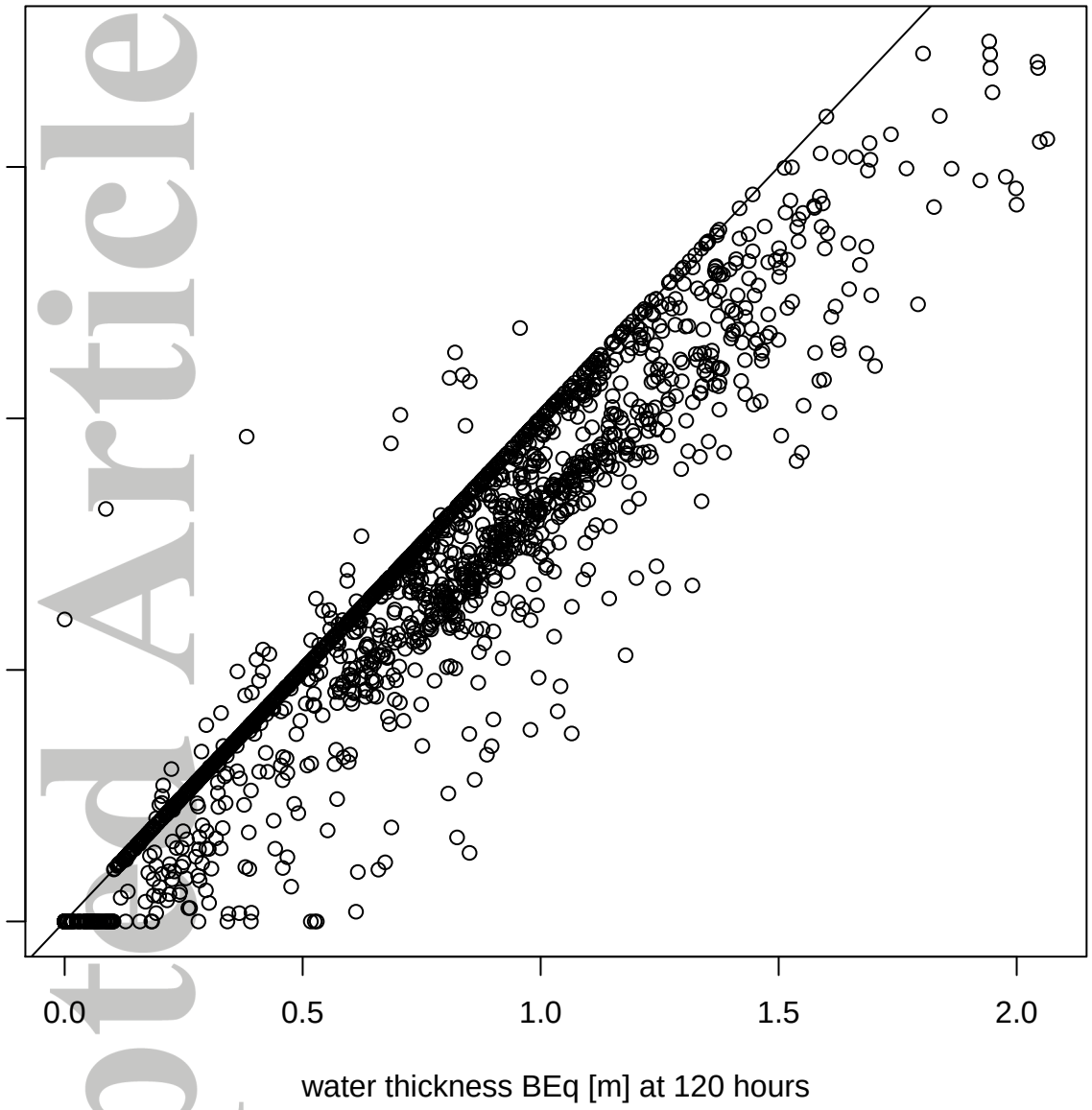

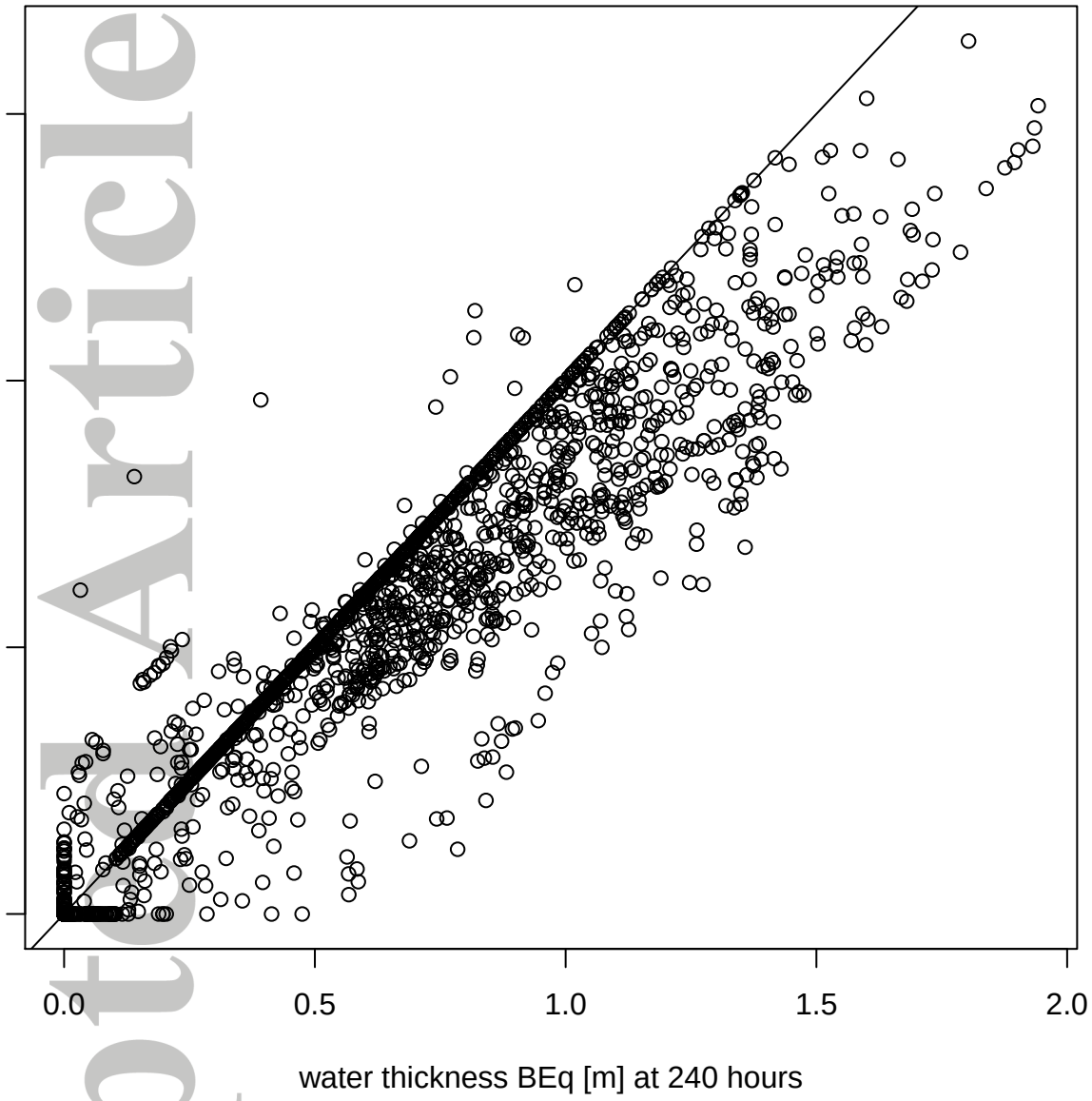

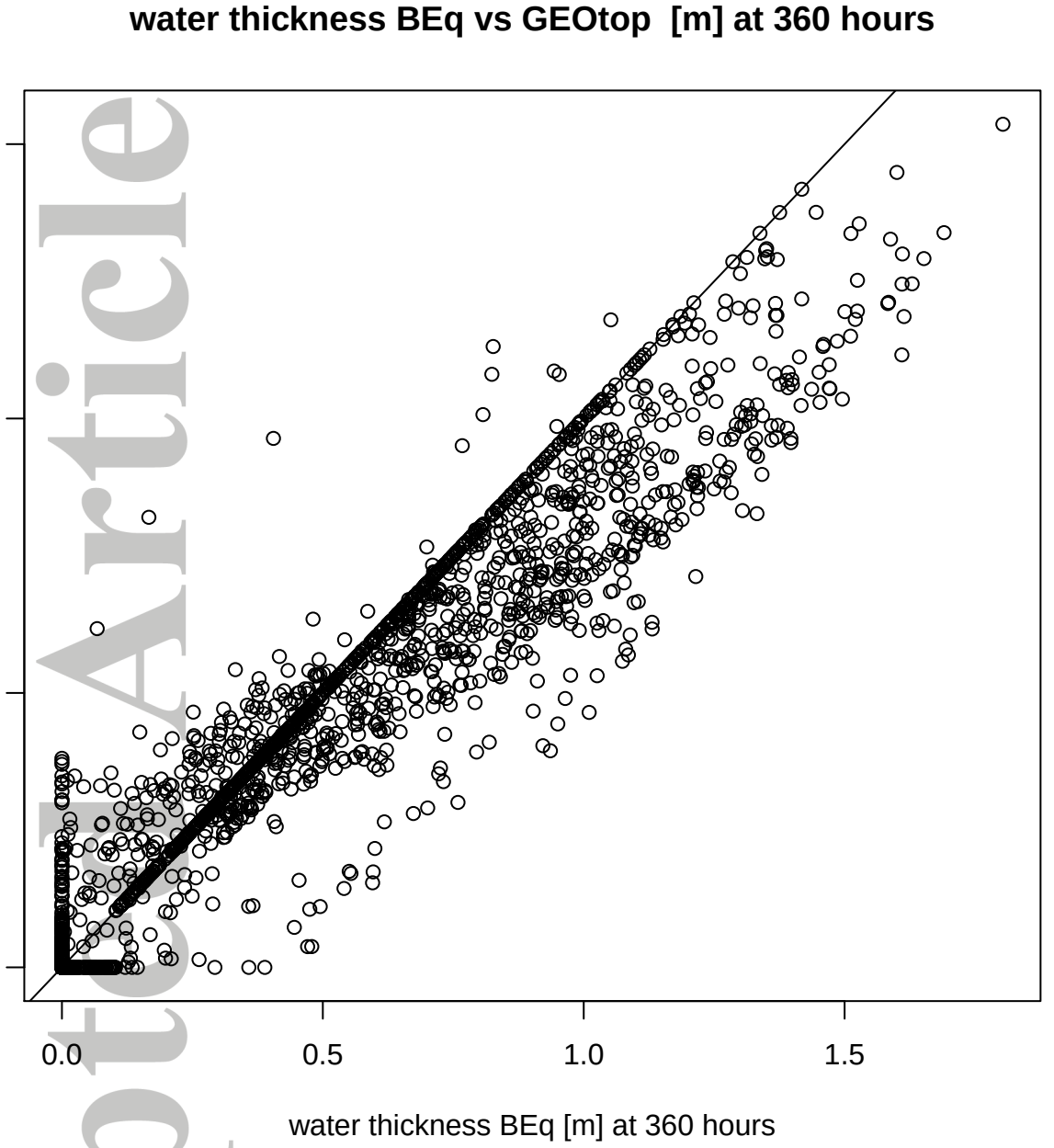

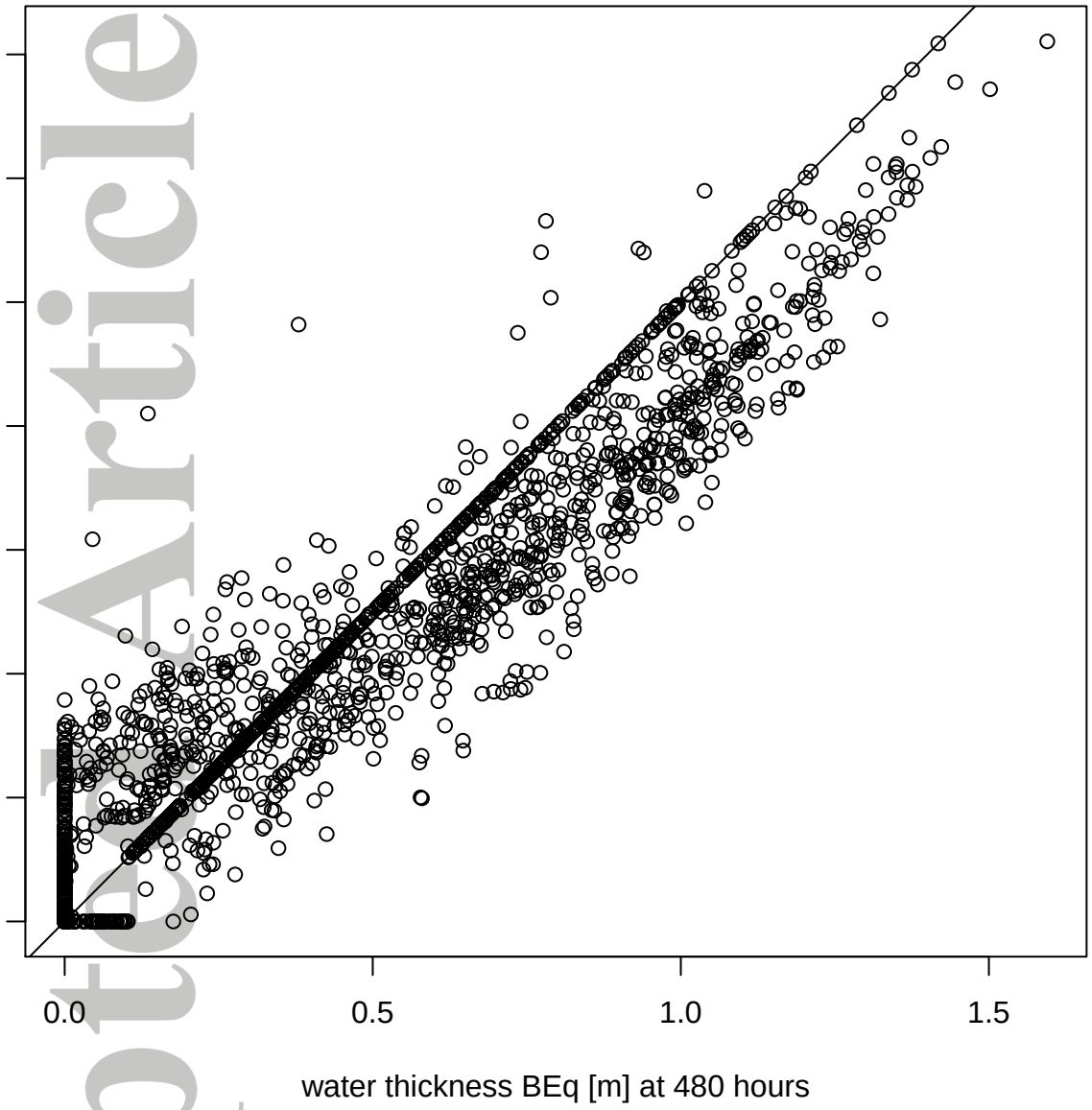

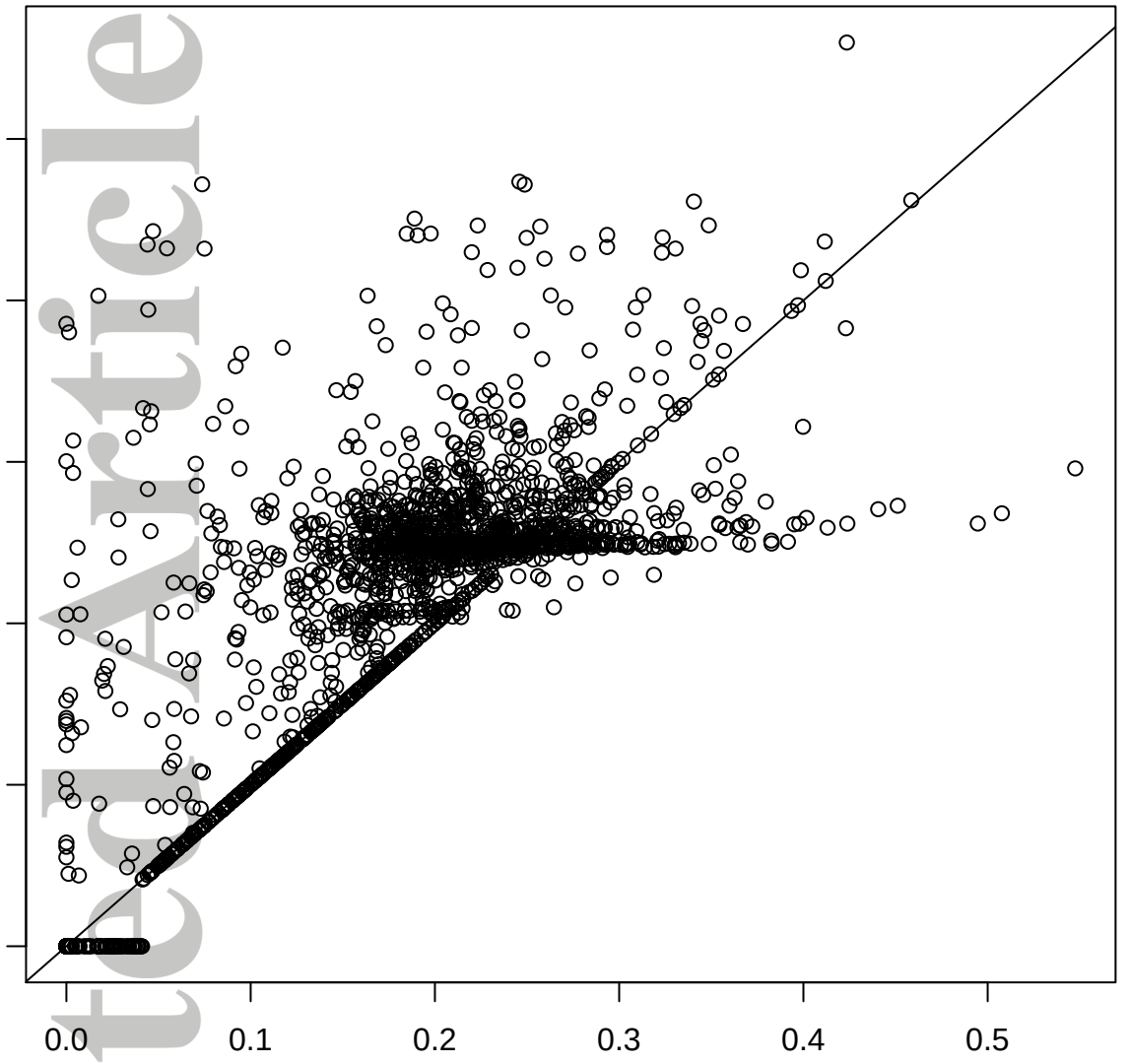

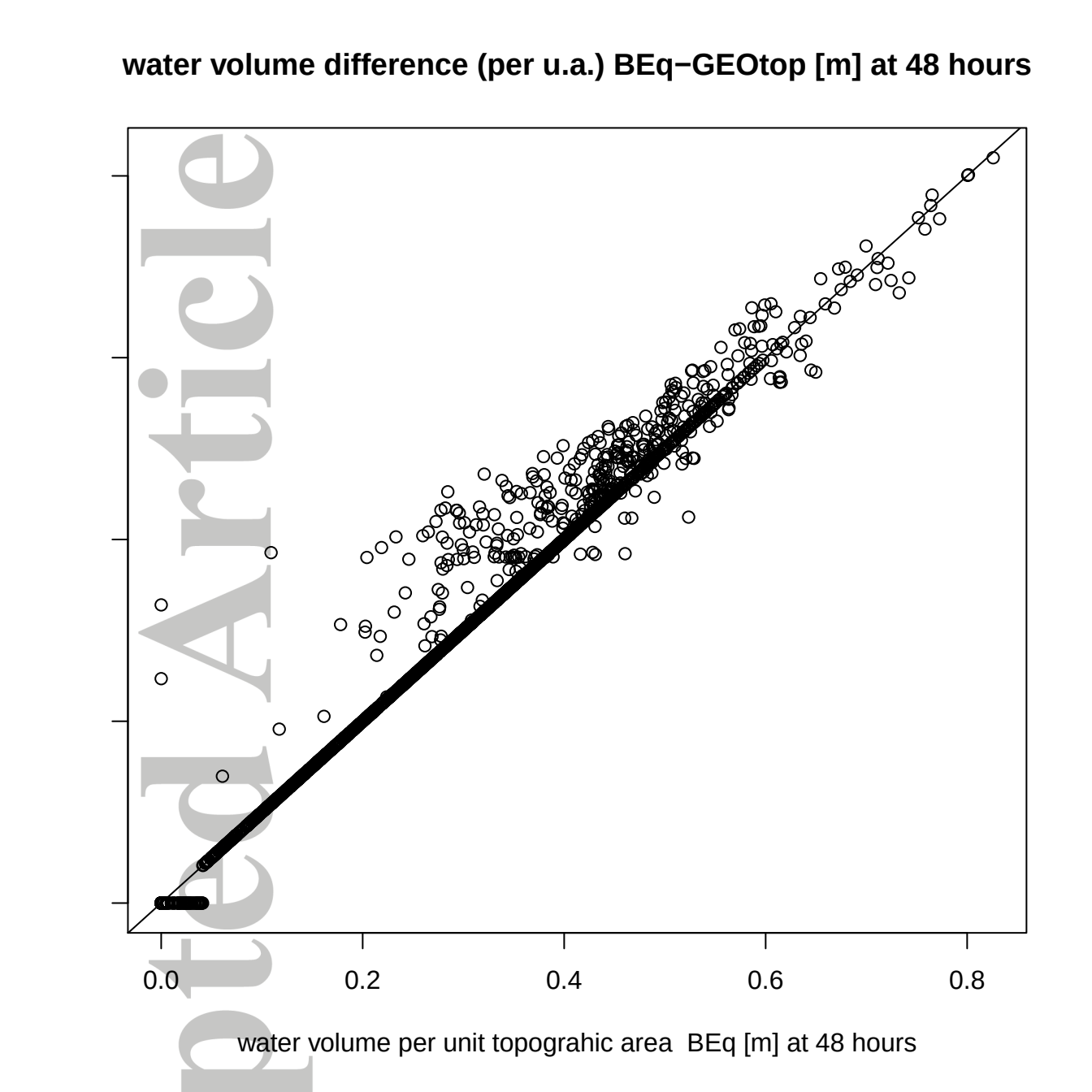

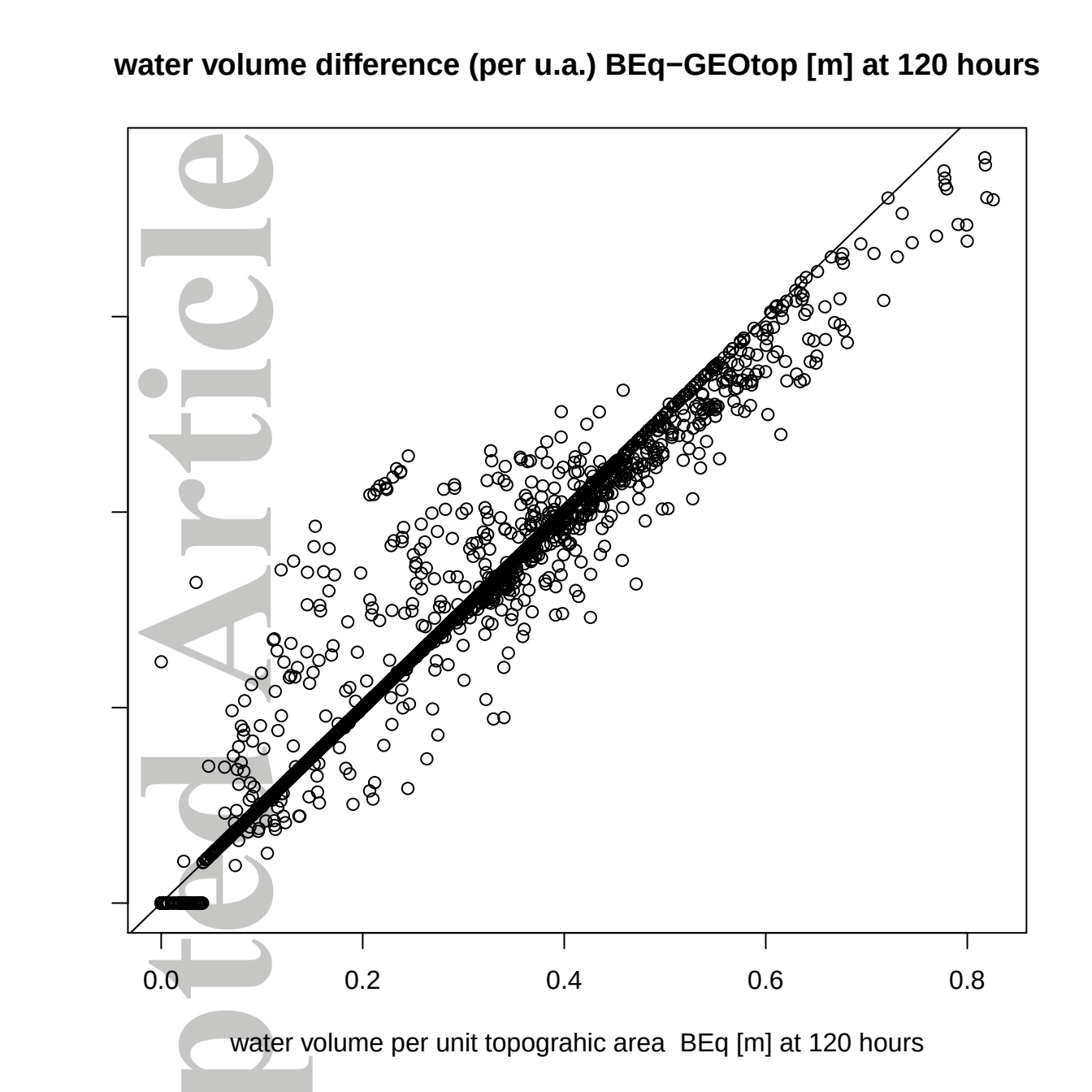

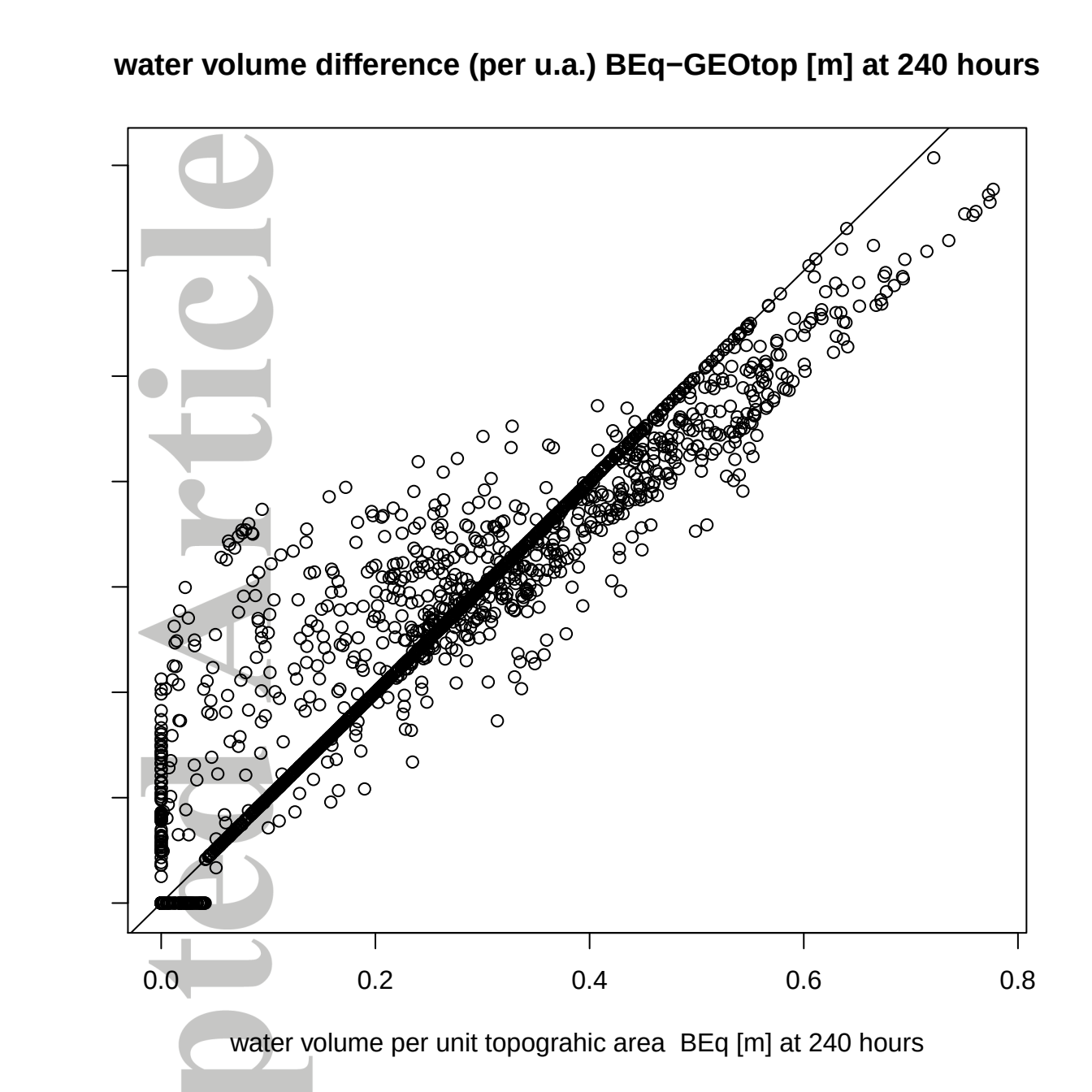
water volume difference (per u.a.) BEq−GEOtop [m] at 240 hours
0.0
0.2
0.4
0.6
0.8
water volume per unit topograhic area BEq [m] at 240 hours

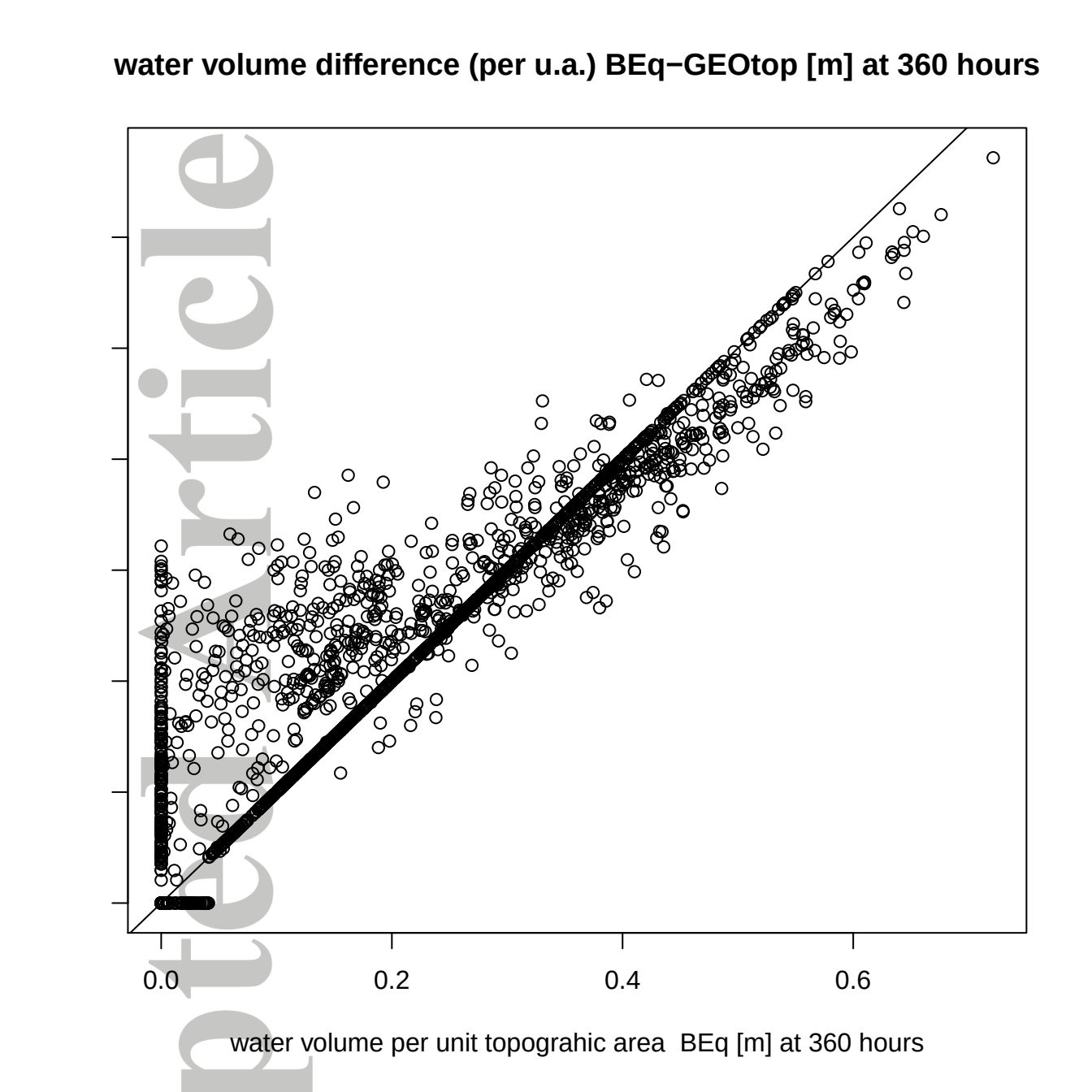
water volume difference (per u.a.) BEq−GEOtop [m] at 360 hours
0.0
0.2
0.4
0.6
water volume per unit topograhic area BEq [m] at 360 hours

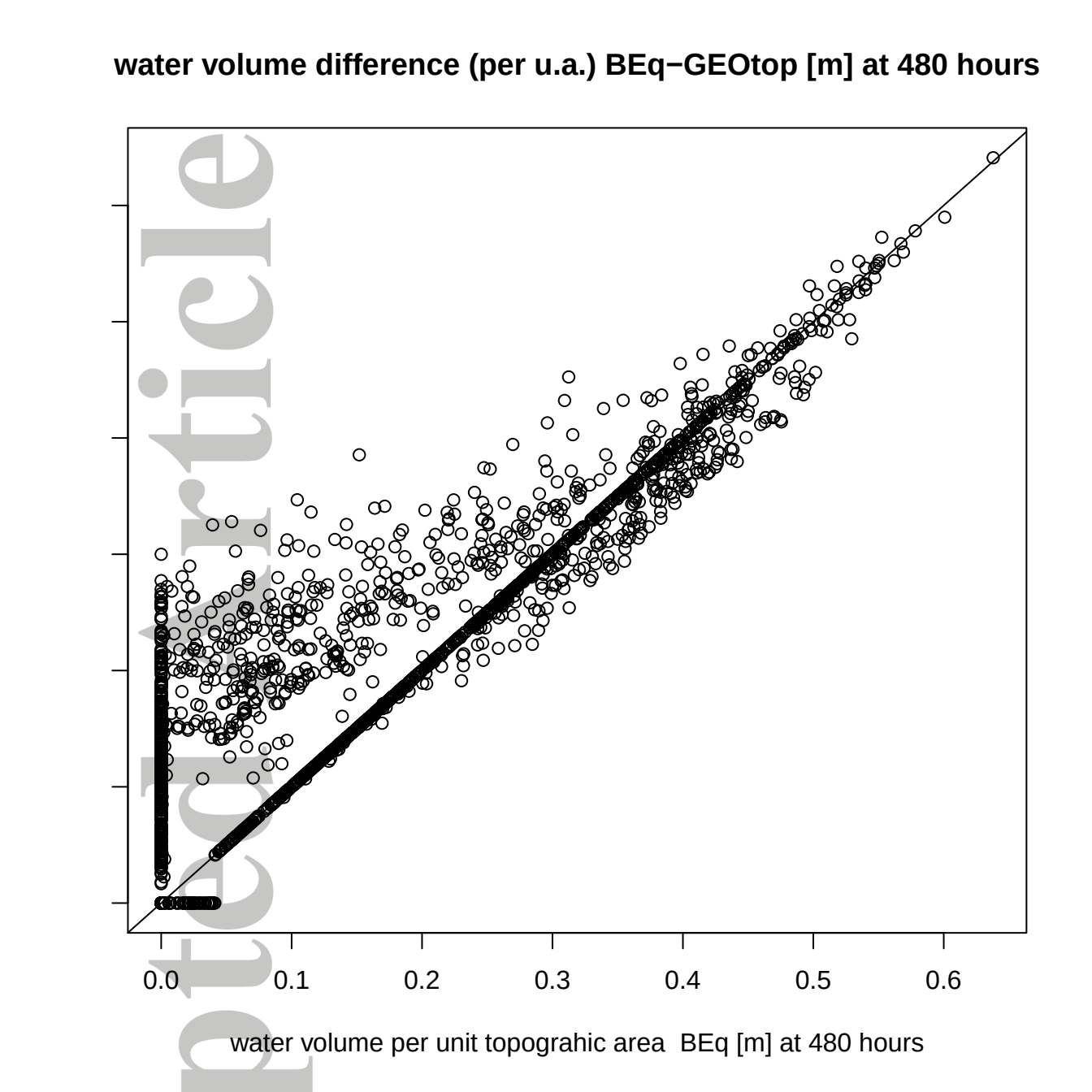
water volume difference (per u.a.) BEq−GEOtop [m] at 480 hours
0.0
0.1
0.2
0.3
0.4
0.5
0.6
water volume per unit topograhic area BEq [m] at 480 hours